



TECHNISCHE  
UNIVERSITÄT  
WIEN

Vienna University of Technology

# Diplomarbeit

## LEARNING PARADIGMS IN LARVAL ZEBRAFISH AND BRAIN-WIDE IMAGING OF NEURONAL DYNAMICS

ausgeführt zum Zwecke der Erlangung des akademischen Grades eines  
Diplom-Ingenieurs

unter der Leitung von

Univ.Prof. Dipl.-Phys. Dr.med. Hans Ulrich Dodt  
E362 - Institut für Festkörperelektronik

eingereicht an der Technischen Universität Wien

**Fakultät für Maschinenwesen und Betriebswissenschaften**

von

Magdalena Helmreich  
0504863  
Schulgasse 5, 3950 Gmünd

Wien, am \_\_\_\_\_

\_\_\_\_\_  
Unterschrift



---

# Abstract

One of the intended goals in current neuroscience research is to gain detailed knowledge about cognitive processes that underlie processing of sensory stimuli and the execution of appropriate actions in the vertebrate brain. For this purpose it is required to simultaneously record a large population of neurons of awake and behaving animals. Rapidly developing imaging technologies as well as the introduction of the zebrafish as a favourable animal model in neuroscience in diverse respects opened up new possibilities to get specific insights of neuronal dynamics during behaviour and learning. Especially the larval form of the zebrafish represents a good compromise between system complexity and practical simplicity and is therefore well-suited to investigate coherencies between neuronal activity and behaviour.

So far the neurocognitive capability of larval zebrafish is relatively unexplored. Hence, the establishment of robust and reliable learning paradigms in zebrafish is of high interest in order to investigate their ability of learning.

In this thesis, the extend of learning ability was examined by the development of various conditioning assays for awake, restrained zebrafish larvae. The data presented herein show a clear behavioural progress during operant conditioning. A large fraction of the animals showed a significant increase in learning performance across the training trials.

Furthermore, the work presented in this thesis involved the development of further conditioning assays in order to investigate other types of learning, such as classical conditioning. A definite success in classical conditioning could not be obtained but indications for possible improvements are given.

In order to gain insights of neuronal activity during conditioning, it is required to combine the established assays with an appropriate whole-brain imaging technique. Preliminary results of whole-brain imaging by light-field microscopy are presented and it is demonstrated how the established assay is coupled with LFM, with the aim to lay a foundation for further investigations on neural circuits during behaviour.





---

# Kurzfassung

Eines der derzeit angestrebten Ziele im Forschungsfeld der Neurowissenschaften ist die Erlangung von detailliertem Wissen über kognitive Vorgänge im Gehirn von Mensch und Tier, die der Verarbeitung von sensorischen Stimuli sowie dem Ablauf der dadurch ausgelösten Reaktionen zugrunde liegen. Zu diesem Zweck ist es erforderlich, die Aktivität einer Vielzahl von Neuronen im lebenden Organismus während bestimmter Verhaltensabläufe zeitgleich zu erfassen. Aufgrund der laufenden Entwicklung neuer bildgebender Verfahren und der Entdeckung des Zebrafährlings als ein in jeglicher Hinsicht zweckdienlicher Modellorganismus in den Neurowissenschaften, ergeben sich neue Möglichkeiten, genaueres Verständnis über die neuronale Dynamik während Verhaltensabläufen und Lernprozessen zu erlangen.

Speziell die Larvenform des Zebrafährlings stellt einen guten Kompromiss zwischen Komplexität des Systems und Einfachheit in praktischer Anwendbarkeit dar und eignet sich daher in besonderer Weise, Zusammenhänge zwischen neuronaler Aktivität und Verhalten zu untersuchen.

Bislang ist die neurokognitive Fähigkeit der Zebrafährchen noch weitestgehend unerforscht. Für die Untersuchung der Lernfähigkeit von Zebrafährchen ist somit die Entwicklung von robusten und zuverlässigen Lernparadigmen von großem Interesse.

In dieser Arbeit wurden verschiedene Konditionierungsabläufe für lebende, allerdings bewegungseingeschränkte Larven entwickelt, um das Ausmaß ihrer Lernfähigkeit zu testen. Während der operanten Konditionierung konnte eine eindeutige Verhaltensentwicklung der Tiere beobachtet werden, ein großer Anteil der Fische wies sogar einen signifikanten Anstieg in ihrer Lernleistung während des Trainings auf.

Außerdem beinhaltet die Arbeit die Erläuterung weiterer entwickelter Konditionierungsabläufe, um andere Arten des Lernens, wie etwa die klassische Konditionierung, bei Zebrafährchen zu untersuchen. Ein eindeutiger Lernerfolg während klassischer Konditionierung konnte zwar nicht beobachtet werden, allerdings werden mögliche Verbesserungsvorschläge diskutiert.

Um Einblicke in neurologische Vorgänge während der Konditionierung zu erhalten, müssen die entwickelten Konditionierungsabläufe mit einem kompatiblen Abbildungsverfahren entsprechend kombiniert werden. Das gesamte Gehirn der Zebrafährchen konnte durch die Verknüpfung des zur Konditionierung entwickelten Set-ups mit Lichtfeldmikroskopie, einem dreidimen-

sionalen Bildgebungsverfahren, während des Lernprozesses erfasst werden. Diese Arbeit beinhaltet sowohl die entsprechende Vorgangsweise als auch erste Resultate der Gehirnaufnahmen, mit dem Ziel, damit eine Grundlage für weitere Untersuchungen von neuronalen Netzwerken während Verhaltensabläufen zu schaffen.

---

# Acknowledgements

*"Everybody is a genius. But if you judge a fish by its ability to climb a tree, it will live its whole life believing that it is stupid."*

- Albert Einstein

I would like to thank Alipasha Vaziri to give me the opportunity to work within his group at IMP/MFPL and to carry out this exciting project. Thank you for continuous feedback and suggestions during my work.

Thank you to Friederike Schlumm for sharing her knowledge in biological questions and constantly providing me with zebrafish larvae. Thank you also for valuable comments on my thesis. Thank you to Robert Prevedel for helping me with questions about optics during the development of my setup. Thanks to Michael Taylor for language advice. Thanks to all group members for providing a pleasant atmosphere at work.

Thank you to Hans Ulrich Dodt for supervision and constructive feedback.

Finally, I want to thank my family, especially my parents, for their patience and motivation as well as their financial support during my entire studies.



---

# Contents

<b>1</b>	<b>Introduction</b>	<b>1</b>
<b>2</b>	<b>Theoretical Background</b>	<b>3</b>
2.1	Zebrafish: A Promising Model Organism . . . . .	3
2.2	Learning in Zebrafish . . . . .	5
2.2.1	Types of Learning . . . . .	5
2.2.2	Existing Associative Learning Paradigms in Zebrafish . . . . .	8
2.3	Imaging of Neuronal Activity . . . . .	11
2.3.1	Basics of Neuroanatomy & Neuronal Activity . . . . .	11
2.3.2	Whole-Brain Imaging Techniques . . . . .	15
2.3.3	Light Field Microscopy Technique . . . . .	16
<b>3</b>	<b>Materials &amp; Methods</b>	<b>21</b>
3.1	Animals and Procedures . . . . .	21
3.2	Experimental Setup . . . . .	21
3.3	Automated Tail Tracking . . . . .	24
3.4	Operant Conditioning Paradigm . . . . .	31
3.4.1	Conditioning Protocol . . . . .	31
3.4.2	Experimental Realization . . . . .	35
3.4.3	Conditioning with Additional Odor Stimulation . . . . .	36
3.5	Classical Fear Conditioning Paradigm . . . . .	38
3.5.1	Conditioning Protocol . . . . .	38
3.5.2	Experimental Realization . . . . .	40
3.6	Imaging Experiments . . . . .	45
<b>4</b>	<b>Results</b>	<b>47</b>
4.1	Operant Conditioning Experiments . . . . .	47
4.1.1	Experiments with Additional Odor Stimulation . . . . .	54
4.2	Classical Fear Conditioning Experiments . . . . .	59

4.3 Preliminary Results of Imaging Experiments . . . . .	63
<b>5 Discussion &amp; Outlook</b>	<b>69</b>
<b>List of Figures</b>	<b>73</b>
<b>List of Tables</b>	<b>75</b>
<b>A Setup Components &amp; Preparatory Work</b>	<b>77</b>
<b>B Experimental Procedures</b>	<b>95</b>
<b>C Matlab Codes</b>	<b>101</b>
C.1 Graphical User Interface (GUI) . . . . .	101
C.2 Operant Conditioning Protocol . . . . .	110
C.3 Classical Conditioning Protocol . . . . .	113
<b>D Abbreviations</b>	<b>119</b>
<b>Bibliography</b>	<b>121</b>

---

# Introduction

Cognitive processes in vertebrates are universally complex, even in simple instances of learning and behaviour. Most behaviours, such as generation of motor output induced by sensory input, as well as simple innate reflexes, are mediated by complex neuronal dynamics throughout the brain. Understanding how behaviour in general, and especially learning and decision making, is processed in the vertebrate brain is one of the most fundamental and challenging questions in current neuroscience research.

How do interconnected populations of neurons process information, sensory stimuli and execute appropriate actions? How are adapted behaviours like decision making, learning and memory encoded in the brain? And what do the dynamics of firing patterns of these neurons look like? Aside from limited examples, to date it is still poorly understood how neuronal network activity contributes to all these tasks.

Understanding activity across networks of interconnected neurons in a behaving animal is challenging primarily due to the size and complexity of the vertebrate brain. Also, the limited ability to record the activity of large neuronal populations *in vivo* makes it difficult to get insights into processes that underlie learning and memory.

An animal model that circumvents these problems is the zebrafish, *Danio rerio*. The larval form provides an especially useful system for investigating basic processes on behaviour and learning on account of simpler neural circuits and smaller number of neurons.

Zebrafish were originally used as an animal model in genetics and for studying development and soon aroused interest among neuroscientists focused on learning and memory. It represents a good compromise between system complexity and practical simplicity, and is therefore a promising model in behavioural research.

The model zebrafish possess a rich repertoire of behaviours and an easily accessible brain, such that optical techniques are readily applied to investigating underlying brain functions. Various experimental advantages and a continually improved molecular toolkit for zebrafish increase its popularity in behavioural research, in addition to its frequent application in genetics and biochemistry.

Recent development of non-invasive imaging methods and genetically encoded calcium indicators (GECIs) [6, 23] have opened up the possibility of investigating neural activity of awake, behaving animals. Using a high speed, large scale imaging technique called light field microscopy (LFM), it is possible to simultaneously record activity at single cell resolution in the whole brain of restrained, behaving zebrafish larvae [44, 57]. This is a powerful way to correlate the activation of individual neurons with the execution of particular motor outputs and learning processes (see Section 2.3.2 and 2.3.3).

So far the neurocognitive capability of larval zebrafish is relatively unexplored, and could be limited due to the underdeveloped connectivity in the brain at larval stage. Therefore, it is necessary to establish robust and reliable learning paradigms in zebrafish in order to investigate its capacity to learn and to study its neurological basis. The zebrafish model, especially larvae, still lacks well-established learning protocols and systematic learning characterization. Very few examples of learning paradigms in larval fish exist [5], while most of the paradigms that are being used to study learning are not yet sufficiently refined in large-scale use [17] (see Section 2.2.2). For that reason, it is important to develop experimental assays in which defined stimuli presented to larvae lead to the execution of specific behaviour and in particular to learning effects.

In this thesis I describe the establishment, implementation and use of such learning assays for awake, restrained larval zebrafish coupled with simultaneous recording neuronal activity (Chapter 3).

The main goal of this work was the establishment of an operant conditioning assay for zebrafish larvae, which was based on the unpublished study by Florian Engert (private communication [28]). The data presented in Chapter 4 show a clear behavioural progress during operant conditioning. Furthermore, it is demonstrated how the established assay is coupled with LFM and preliminary results of whole-brain imaging are presented.

The combination of this robust learning assay with light-field microscopy is a powerful way to acquire quantitative measurements of behaviour as well as monitor large populations of neurons throughout the entire brain simultaneously. Such approaches will help to understand the functional basis of neural circuits during behaviour in a vertebrate brain.



## Theoretical Background

### 2.1 Zebrafish: A Promising Model Organism

The zebrafish *Danio rerio* is a tropical freshwater fish and is native to the south-eastern Himalayan region [47] (see Figure 2.1). Besides being an important vertebrate model organism in genetic and development studies, it has been gaining increasing amount of interest among neuroscientists in the last decades. This vertebrate model has been shown to be an attractive system for studying the neural basis of behaviour due to various experimental advantages.

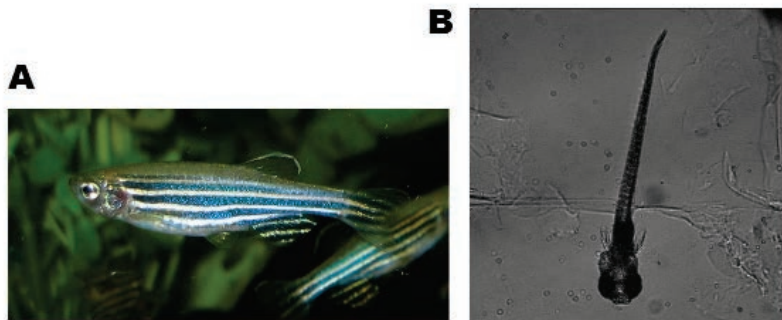


**Figure 2.1: Zebrafish (*Danio rerio*)** (A) An adult specimen of zebrafish (*Danio rerio*). Figure taken from [10]. (B) A 8 day old zebrafish larva.

Among their practical benefits are their easiness to breed, their fast development (5 days from fertilization to free-swimming) and their low cost.

Their popularity in genetic and development studies can be explained by their ease of genetic manipulability and the feasibility of isolating large numbers of mutants [11]. Therefore, this vertebrate model represents an attractive system for studying the development of tissue structures and human diseases [12, 27]. It has physiological similarity to mammals in both genetic compositions and organ structures and is therefore of utmost interest for development studies.

These facts along with their transparency at the larval stage, mainly due to lack of pigments, makes the larval form of zebrafish uniquely suited for neurological investigations as well. Together with their small size, especially their small brain in terms of neuron numbers and physical size (see Section 2.3.1), the exceptional attribute of translucency allows for non-invasive imaging of neural activity throughout the brain.

However, very few learning experiments have been done with the model organism zebrafish to date. These studies demonstrate the ability of learning in zebrafish; a few successful conditioning procedures even exist for the larval form (see Section 2.2.2). Due to abovementioned advantages, this powerful model system has important potential for future research in behavioural neuroscience.

Adult zebrafish possess a rich repertoire of behaviours, most of them in a quite robust and stereotypical manner. Some detailed descriptions of these broad spectrum of innate and other behaviour can be found in ref. [39, 40, 51], including anxiety/fear-related and reward-related behaviour, sleep and sexual behaviour, visually- and olfactory-guided locomotor behaviour, as well as social behaviour [16, 76] and shoaling, a type of group behaviour [29], to mention only a few.

Even larvae already display a wide range of behaviours, like escape behaviour [50], vision and prey capture [13, 52, 53, 54] and many more [21, 30].

These types of behaviours are observed and described in various zebrafish studies and seem to be quite robust and efficient for detailed analysis. However, to date most procedures related to the study of learning in zebrafish are not well refined. For adult zebrafish the ability of learning is known and investigated in different studies, whereas the cognitive capability of zebrafish larvae is still unexplored.

## 2.2 Learning in Zebrafish

### 2.2.1 Types of Learning

Learning is an act of intentional or incidental acquisition of knowledge, skills and behaviour. It can be viewed as progress over time, a process of measureable and enduring change of behaviour due to experience or newly gained cognition. The ability to learn is the foundation of adaption to environmental circumstances and conditions. In physiological sense, learning produces changes in the organism's brain and is relatively permanent, depending on memory power.

Learning is distinguished into two major classifications: non-associative and associative learning (see Figure 2.2).

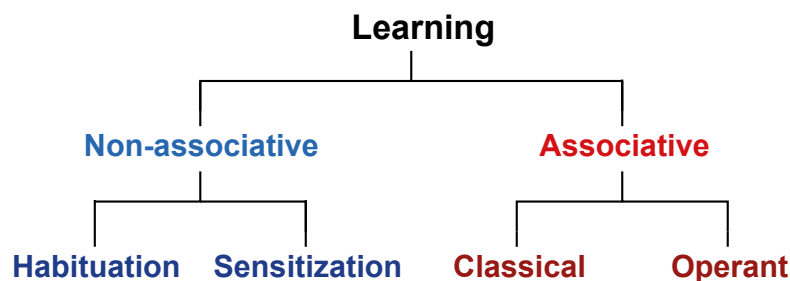


*Figure 2.2: Types of learning. Two major types can be distinguished: Non-associative and associative learning. Figure based on [71, 72].*

### Non-associative Learning

Non-associative learning refers to a progressive change in the strength of response to a stimulus because of preceding repeated presentations of this stimulus. Changes in response due to sensory adaption, motor fatigue or injury do not fall within this definition. This behaviour is stimulus specific and contains two important types, habituation and sensitization.

**Habituation** is the gradual decline of an animal's response to a repeated stimulus of fixed intensity and strength. If the stimulus is neither rewarding nor harmful the response probability is reduced with each repeated exposure.

**Sensitization** is another type of non-associative learning during which the response to an arousing stimulus is amplified following repeated exposure to the commonly painful or noxious stimulus.

Despite the simplicity of these forms of learning, a complete understanding of the underlying neurobiological concepts has not been achieved so far [59].

## Associative Learning

Associative learning is a process in which an animal learns to make an association between two stimuli or between a stimulus and a behaviour. Associating two environmental cues can often be essential for an animal's survival and is therefore a crucial type of learning.

Paradigms in associative conditioning are powerful methods to study the biological basis of learning and memory. To finally understand these underlying processes is a major goal of behavioural neuroscience.

Two forms of associative learning can be distinguished: **classical conditioning**, the association of two stimuli and **operant conditioning**, the correlation of behaviour with its consequences.

### Classical Conditioning

Classical Conditioning refers to an animal's ability of associating a neutral stimulus with a reinforcing stimulus. First described by Pavlov [7], it is also called Pavlovian Conditioning with its most prominent example, the example of Pavlov's dog.

The previously neutral stimulus (conditioned stimulus, or CS) is repeatedly paired with an unconditioned stimulus (US) which elicits a specific response. After successful conditioning the neutral stimulus presented alone will evoke a resembling response, called the conditioned response (CR).

Classical Conditioning is still the most widespread experimentation technique for studying learning in animals and often considered as the most basic and robust type of associative learning.

Depending on the kind of behaviour the unconditioned stimulus is evoking, classical conditioning can be divided into two groups (see Figure 2.3). In contrast to presenting a positive reinforcer as the US, called **appetitive conditioning**, **aversive** or **fear conditioning** occurs, when an aversive stimulus provokes an avoidance behaviour or fear response. Thus, fear conditioning can be described as the ability of an animal to predict an aversive event. This means that at the end of the training the neutral stimulus by itself should lead to a fear response.

Another classification is based on the timing aspect of the two stimuli presentations, the CS and the US (see Figures 2.3 and 2.4).

**Forward Conditioning** is the most common form because it shows the highest learning rate. It means that the onset of the previously neutral stimulus (CS) precedes the onset of the unconditioned one, which then leads to corresponding behaviour. Thus, the neutral stimulus can be considered as a kind of cue or warning that the US is following.

If the two stimuli are overlapping in time, it is called **delay conditioning**, in contrast to **trace conditioning**, when the CS and US are separated by a stimulus-free trace interval.

Contrary to forward conditioning, **backward conditioning** is the exact opposite, namely when the US precedes the CS. Alternatively, **simultaneous conditioning** describes the exposure of both stimuli at equal start- and endpoint.

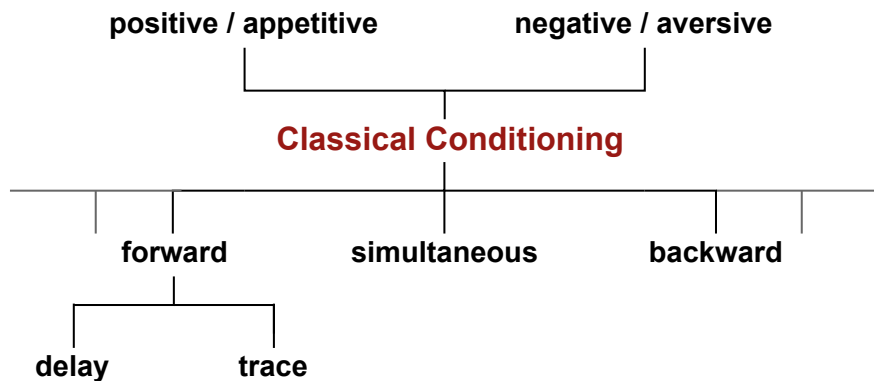


**Figure 2.3: Classification of classical conditioning.** An overview of the most important types of classical conditioning. Figure based on [69].

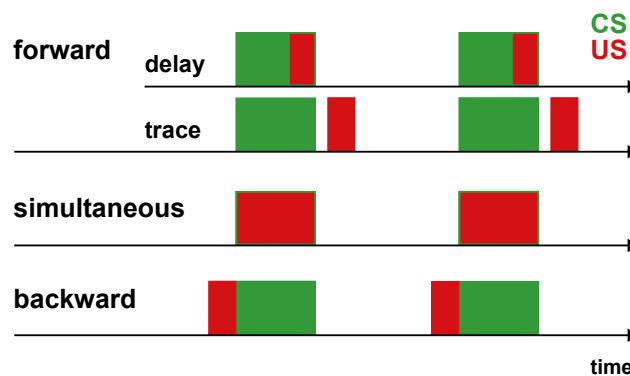


**Figure 2.4: Timing aspect of classical conditioning.** Forward: CS precedes US. Delay: CS and US are overlapping. Trace: CS and US are separated by an interval. Simultaneous: CS and US are presented at same time. Backward: US precedes CS.

## Operant Conditioning

The expression of operant conditioning has first been described by Skinner [63] and uses the consequences of an animal's response to a stimulus to alter the occurrence and form of behaviour. In other words, a certain response to a stimulus can influence the presence or absence of the stimulus and therefore change the stimulus induced behaviour prospectively.

Depending on its consequences, behaviour is either strengthened or weakened. **Reward** or **reinforcement** increases the probability of desired behaviour, in contrast to **punishment**, which decreases the recurrence of that behaviour.

Here, I will focus on reinforcement, which is the type of operant conditioning used in this

work (see Figure 2.5).

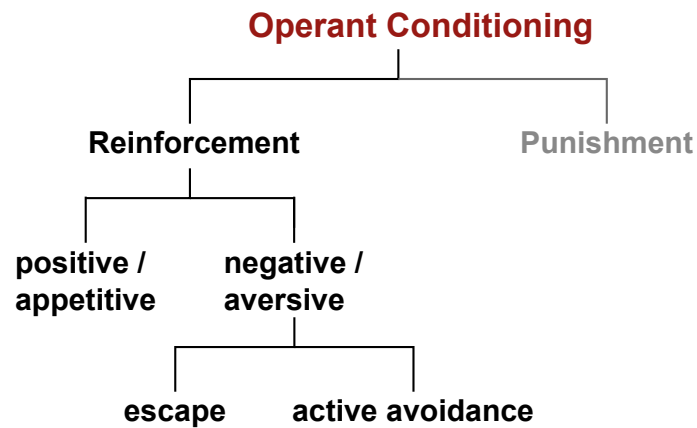


**Figure 2.5: Classification of operant conditioning.** An overview of types of operant conditioning. Completeness cannot be guaranteed. Adapted from [73].

Being a more complex form of associative learning, two forms may be distinguished, depending on the perception/valence of the stimulus. **Positive reinforcement** means that an animal must produce a response in order to receive an appetitive stimulus, while **negative reinforcement** includes choices in order to avoid an aversive stimulus. In context of negative conditioning, the aversive stimulus can either be removed altogether by turning it off following correct behaviour (**escape**), or a certain behaviour actively avoids the stimulus (**active avoidance**). The ability of operant learning, and especially its neurological ontogeny, is much less explored than classical conditioning [68].

### 2.2.2 Existing Associative Learning Paradigms in Zebrafish

Not many learning experiments have been used for zebrafish, only a few of them concern non-associative learning. Most of the non-associative learning techniques are related to habituation, e.g. ref. [22] demonstrated that locomotion is modulated during light adaptation in larval zebrafish. A good summary of publications about non-associative learning in zebrafish is given in ref. [17].

This section will give an overview of existing paradigms for associative learning in zebrafish: **classical** and **operant** conditioning paradigms.

Some conditioning paradigms found in literature cannot be clearly assigned to the classification terms of learning defined in the previous section. They are named in a different way or present a combination of more tasks, which makes it difficult to draw an exact line between classical and operant conditioning. Similar learning protocols are often defined differently in several papers or simply named with a broader term like *associative reinforcement learning* or just *associative*

*learning.*

The learning protocols described in ref. [8] and [74] for example, are strictly speaking a combination of a classical and an operant procedure. The learning process itself is based on the classical approach by association of a neutral stimulus (CS) with an US. During training, animals have the chance to avoid the US if they apply appropriate behaviour when the warning CS arrives, which relates to an operant approach.

My subsequent categorization of existing learning paradigms refers to the rule to classify as operant conditioning once the presence of stimuli depends on animal's response. If the animals have the chance to avoid the stimulus through behavioural response, it is an operant paradigm, regardless whether the learning process itself is based on classical conditioning or not.

### **Learning paradigms in adult zebrafish**

Most of these learning paradigms exist mainly for free-swimming adult zebrafish due to advanced ontogeny of the brain and therefore better learning performance of adult animals.

It has been shown by Valente et al. [68] that for two visual *avoidance* conditioning paradigms, a classical and an operant one, learning improves throughout development and starts significantly at week 4 for classical and around week 3 for operant conditioning. In both assays zebrafish reach maximum performance levels at week 6. In the classical avoidance conditioning assay, fish were trained to associate a visual pattern, presented on a screen beneath the tank, with a light whole-tank electroshock. With respect to this the only difference during operant conditioning is that the presence of the stimuli is dependent on the animal's position in the visually separated halves of the tank.

Other **classical** fear conditioning procedures use visual or olfactory cues paired with electric shocks or alarm pheromones [2, 34].

Classical conditioning of adult zebrafish with food as an *appetitive* unconditioned stimulus have been used successfully in several studies (e.g. [19, 62]). They showed either a training of paired food reward with visual cues or a fixed location, or paired with a behaviourally neutral odorant. However, the most prominent classical conditioning procedure in zebrafish is the *conditioned place preference (CPP)* paradigm due to the popularity of zebrafish in behavioural pharmacology. This CPP test is used mainly for studying the behavioural effect of various drugs, for instance addiction. During the training of this paradigm, a drug is paired with a specific context such as a coloured or visually distinct tank compartment to measure the preference for that context subsequently (e.g. in ref. [24]).

More common than classical conditioning approaches for adult zebrafish are **operant** conditioning techniques.

One operant conditioning paradigm that has been used successfully in zebrafish is *avoidance reinforcement* conditioning. There are various reports of successfully trained zebrafish, which had to learn to respond to a specific cue by moving to/avoiding a certain location in the tank in order to avoid an aversive stimulus, e.g. a mild electric shock [8, 15, 56, 68, 74]. In most cases this indication of the shock is a visual signal, like a red LED lamp [8, 56] or another visual context, like a lighted and a dark side of the tank [15, 74]. To avoid the aversive stimulus, fish

can either be trained to swim to another or to stay in one compartment of the tank, whichever behavioural response has been rewarded.

For this avoidance paradigm, zebrafish show a relatively rapid and high learning ability. Therefore, it is the most prominent operant conditioning approach found in literature.

Some *appetitive* conditioning procedures are reported for zebrafish as well. In most of them food is applied as appetitive reinforcer. Zebrafish are conditioned to swim into chambers marked with a light signal in order to receive food reinforcement, e.g. in ref. [14].

In general, aversive procedures produce results with less variability and are therefore the ones to favour, since aversive stimuli like electroshocks offer more experimental control than manually presented ones, such as food. Additionally, avoidance behaviour can be reported in a more robust way or even be recorded automatically.

The reader is advised to consult some reviews for a good overview and a more extensive summary of existing paradigms for adult zebrafish, e.g. in ref. [17, 49].

### **Learning paradigms in larval zebrafish**

To date only a few successful conditioning procedures exist for larval zebrafish and it is still not entirely clear at which stage of development zebrafish are capable of learning.

Most of these reported conditioning approaches refer to free-swimming and late larval or early juvenile zebrafish, meaning older than 3 weeks [43, 68].

An **operant** paradigm, where 3 to 5 week old zebrafish are trained to avoid a light when pairing it with a mild shock, was established by Lee et al. [43].

When trying to modify the **classical** conditioning task established for 3 to 4 week old zebrafish [68], Valente et al. could not display a learning effect for larval zebrafish of 7 day old embedded in agarose gel [59].

The only published report that shows successful learning at the early larval stage of 6 to 8 day old zebrafish, describes a classical fear conditioning paradigm. During training zebrafish larvae develop an enhanced behavioural response to flashes of light when pairing it with an aversive touch stimulation [5].

Additionally, an unpublished study has also demonstrated that 6 to 8 day old larvae are able to learn an operant conditioning paradigm. Restrained animals are trained to terminate an aversive heat stimulus with a directional tail movement (Florian Engert, private communication [28]). That study provides a promising well-established conditioning paradigm, and has been the motivation and basis for this thesis.

This summary shows that to date there are only very few learning paradigms for larval zebrafish, which are highly favoured for imaging purposes and other reasons as discussed previously (see Section 2.1). For that reason it is worthwhile to investigate the capability of learning in the early stage of development and to establish appropriate conditioning assays.



## 2.3 Imaging of Neuronal Activity

### 2.3.1 Basics of Neuroanatomy & Neuronal Activity

This section gives basic informations about the neuroanatomy of the zebrafish and a short description of fundamental procedures of neuronal activity and signal transmission.

#### Neuroanatomy of zebrafish

One crucial advantage of the larval zebrafish in respect to imaging neuronal activity is the small size of its brain. The larval brain occupies a volume of only about  $800 \times 400 \times 300 \mu\text{m}$  and consists of about 100 000 neurons [58].

The larval brain can be segmented in 3 major regions, the forebrain, midbrain and hindbrain (see Figure 2.6). The most anterior parts are mainly responsible for olfactory sensation, the olfactory epithelium (OE) and the olfactory bulb (OB). Beside other regions like the telencephalon (Tel), diencephalon and habenula (Hb), these parts belong to the forebrain, whereas optic tectum (Teo) takes up a great part of the midbrain. The Cerebellum (Cb) can be rated as a part of the hindbrain and lies inbetween the midbrain and the medulla (Md), which converges into the spinal cord (see Figure 2.6).

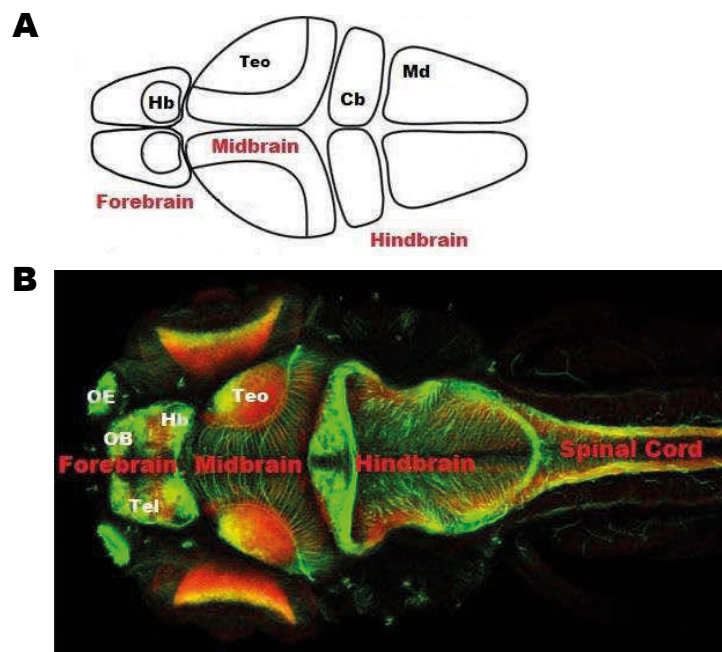


**Figure 2.6: The larval zebrafish brain.** Dorsal view of the larval zebrafish brain. (A) Schematic outlining relevant brain regions in the zebrafish larvae. Adapted from [55]. (B) 4 day old zebrafish embryo labelled with Synaptic Vesicle Protein 2 and acetylated tubulin antibodies. Taken and adapted from [46]. OE, olfactory epithelium; OB, olfactory bulb; Hb, habenula; Tel, telencephalon; Teo, optic tectum; Cb, cerebellum; Md, medulla.

## Neuronal signalling

In order to understand the following basics of imaging neuronal activity, it is important to illustrate fundamental processes in neuronal signalling and characteristics of nerve cells (see Figure 2.7).

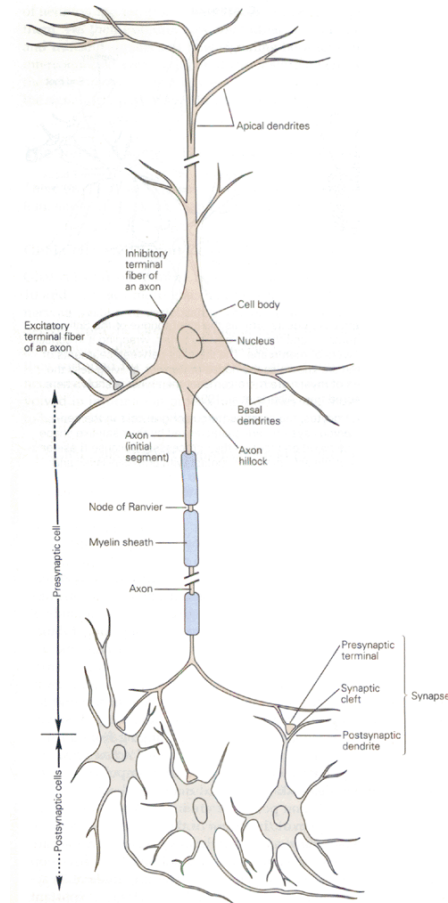


**Figure 2.7: The basic structure of a neuron.** Main features of a vertebrate neuron: the cell body (soma) with the nucleus, dendrites as input elements receive signals from other neurons, the axon as transmitting element propagates signals to postsynaptic cells. The action potential originates at the axon hillock. Figure from [41].

Neurons are the basic units of the brain and elementary building blocks of the nervous system. They are responsible for signal transmission in the nerve system and are the essential elements for sensory processing and cognition.

Signal transmission in neurons and the contraction of muscles are premised on the diversity of ions and their unequal concentrations in the intra- and extracellular space. At rest, neurons exhibit a constant membrane potential of around  $-70$  mV, called the resting potential. This negative voltage difference between inside and outside the cell arises from the large gradient of mainly  $Na^+$  and  $K^+$  ions, where intracellularly the concentration of  $K^+$  is much higher than the one of  $Na^+$ , but extracellularly it is much lower.

This equilibrium potential can be achieved due to the membrane's ability to be selectively permeable for different ions and to actively maintain this concentration gradient by ion pumps.

By contrast, an action potential is a temporary deflection from the resting potential, a travelling wave of membrane potential. It can rise in electrically excitable cells, such as neurons, and is the basis for communication within the nerve system.

The synaptic input of preceding neurons results in local changes of the membrane potential. An action potential is initiated when these potentials reach a certain threshold at the axon hillock. This is the region with the highest density of voltage-gated  $Na^+$  channels, which are activated by a potential of around  $-50$  mV. Below-threshold excitations do not trigger any action potential, while above-threshold potential always induce action potentials of the same form and intensity (the all-or-none law).

These action potentials arise by the opening of voltage-gated  $Na^+$  channels which leads to a gradient induced massive influx of  $Na^+$  ions into the cell and therefore to an increase of the membrane potential up to  $35$  mV, called depolarization. This locally short state of positive voltage induces the propagation of this highly stereotyped potential along the axon. The electrical signal is conducted towards the axon terminal, the output region, where the electrical signal is transformed into a chemical one.

The propagated action potential to the nerve terminal causes the opening of voltage-gated  $Ca^{2+}$  channels at chemical synapses, which follows an influx of  $Ca^{2+}$  ions since the concentration of  $Ca^{2+}$  inside the cell is much lower than outside. This resulting high concentration of intracellular  $Ca^{2+}$  leads to the fusion of vesicles containing neurotransmitters with the presynaptic membrane and their release into the synaptic cleft. The binding of these neurotransmitters to specific receptors changes the conductance of  $Na^+$  channels in the postsynaptic membrane and can consequently cause the generation of an action potential in the postsynaptic cell [41] [66] (see Figure 2.8).

### Optical reporters of neuronal activity

One of the most promising methods to investigate neural activity of awake, behaving animals are non-invasive optical recording techniques. These methods allow activity to be recorded not only in independent single cells, but also across large populations of neurons. This provides spatial information and allows circuit dynamics of whole brain networks to be characterized. Other available techniques such as electrophysiology, are mostly invasive and also limited in recording from single or, at best, a subset of neurons. By contrast, optical methods open up the possibility of simultaneous recording from a great many neurons or from only specifically targeted ones. An important step in advancement of these methods was the development of indicator dyes. Besides voltage-sensitive dyes, which translate the membrane potential directly into an optical signal, ion-sensitive dyes, such as  $Ca^{2+}$  dyes have been engineered and are constantly improved [64]. Voltage indicators suffer from a lower signal-to-background signal compared to  $Ca^{2+}$ , which produce larger signals and make it possible to measure the responses from single neurons. Therefore, most functional imaging studies do not record voltage directly, but take advantage of the  $Ca^{2+}$  to be involved in different aspects of neuronal signal transduction. As described,  $Ca^{2+}$  plays an essential role in neuronal signaling, the  $Ca^{2+}$  concentration changes due to spiking behaviour of neurons. Although the intracellular change of  $Ca^{2+}$  concentration has slower dynamics, neuronal activity can be assessed indirectly by measuring recent spiking

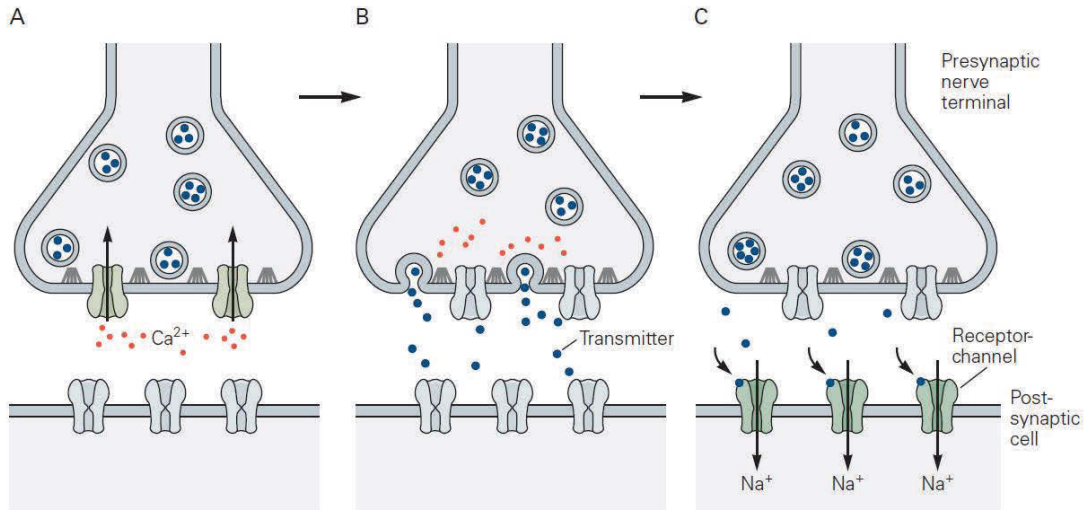


**Figure 2.8: Synaptic transmission at chemical synapses.** (A) The action potential at the terminal causes the opening of voltage-gated  $Ca^{2+}$  channels, which causes an influx of  $Ca^{2+}$  ions into the cell. (B) The high concentration of intracellular  $Ca^{2+}$  leads to the fusion of vesicles containing neurotransmitter with the presynaptic membrane and their release into the synaptic cleft. (C) The conductance of  $Na^{+}$  channels in the postsynaptic membrane is changed by the binding of neurotransmitters and can cause the generation of an action potential in the postsynaptic cell. Figure from [41].

activity by these  $Ca^{2+}$ -sensitive dyes. The intracellular calcium rises and drops within 1 ms and 10 to 100 ms respectively, which therefore limits the speed of imaging when using  $Ca^{2+}$ -sensitive dyes [37].

Constant improvements of these dyes bring along higher signal-to-noise ratio and higher sensitivity in detection of neural activity [6, 64, 67].

Labeling of neurons by injection of small molecule  $Ca^{2+}$ -sensitive dyes is a challenging procedure [64]. A more promising method to report the rise in  $Ca^{2+}$  concentrations is the use of genetically encoded calcium indicators (GECIs). GECIs based on fluorescent proteins are powerful tools for optical recording. Using transgenic techniques, they can be targeted to specific neuronal subtypes and therefore used to relate the activity of particular cell types to stimuli or behaviours. Recently, more and more scientists take the advantage of GECIs to measure intracellular changes of  $Ca^{2+}$  in neurons of zebrafish, one of the first demonstrations can be found in ref. [36].

Among the category of GECIs, a protein called GCaMP is widely used as such a  $Ca^{2+}$  reporter. The GCaMP family is most extensively developed and widely adopted [6, 67] and contains the green fluorescent protein (GFP), which changes conformation and alters the fluorescent levels once  $Ca^{2+}$  is binding. These single wavelength, intensity based sensors are created by coupling the  $Ca^{2+}$ -binding protein calmodulin (CaM) and the M13 peptide from myosin light chain kinase to the backbone of GFP. Recent efforts in optimization of this GCaMP sequence resulted

in GCaMP5 variants, which are widely in use at present [6].

GECIs can be targeted to specific tissue or cell types in zebrafish by coupling to a particular promotor or using driver/reporter systems such as GAL4/UAS [9, 60, 61]. A promotor called *elav13* (previously known as HuC) [36] is commonly used to drive the expression of the  $Ca^{2+}$  indicator GCaMP5 in most neurons throughout the brain, thus being responsible for neuronal specificity. With the help of these genetic tools it is possible to generate stable transgenic fish lines expressing the specific proteins in a controlled and reproducible way.

Several optical tools, based on  $Ca^{2+}$ -sensitive dyes and GECIs, have provided access to neurons in larval zebrafish and enable recording of neuronal activity *in vivo* (e.g. [4, 5, 31, 33, 50, 55, 58]).

### 2.3.2 Whole-Brain Imaging Techniques

To record neuronal activity indirectly by measuring changes of fluorescence signals using genetically encoded calcium indicators, appropriate optical instruments are required. When monitoring a large population of neurons of biological samples like larval zebrafish brains, sufficient spatial and temporal resolution, imaging speed and recording volume are desirable. Convenient advancements of fluorescence microscopy techniques can manage to meet this kind of requirements.

To date two-photon point scanning microscopy [25, 35], and to some extent confocal microscopy are the standard fluorescence imaging techniques in order to image thick scattering tissue of several model organisms. Within this method the excitation light is focused to a small spot and scanned in the lateral plane throughout the volume. This technique may allow functional  $Ca^{+2}$  imaging of living tissue, but leads to low temporal resolution due to the point scanning mechanism what makes it hard to monitor multiple neurons at high-speed.

One possibility to speed up this scanning mechanism is to excite the tissue with a line or a plane of light instead of a point [3, 4]. This imaging method, called light-sheet microscopy, relies on the scanning of a thin "sheet" of light through the sample by one or more excitation objectives. These are positioned orthogonally to the detection camera, which images the illuminated plane, resulting in a high spatial and improved temporal resolution. The disadvantage of this imaging method is the orthogonal excitation-detection scheme which implicates restrictions in applicability on various model organisms, such as mice.

In order to make up a 3D volume, it is required to scan in axial direction, which is a time-consuming mechanism.

Another imaging technique, which enables to capture a whole volumetric sample at once is called light field microscopy. This technique shows lower spatial resolution, but due to its high temporal one it is applicable to capture neuronal dynamics throughout the brain of larval zebrafish [20, 44, 57].

In this work I used light field microscopy, hence its general principle needs to be explained in more detail.

### 2.3.3 Light Field Microscopy Technique

Light field microscopy (LFM) was first demonstrated by Levoy et al. [44] and refined under the name of light field deconvolution microscopy by Broxton et al. [20]. LFM is an advanced epifluorescence microscope technique, which has to date been applied mainly in imaging of nonbiological samples [44].

#### Epifluorescence microscopy

Before describing the basic functionality of LFM in more detail, it is important to understand the fundamental principle of the more general epifluorescence microscopy technique (see Figure 2.9).

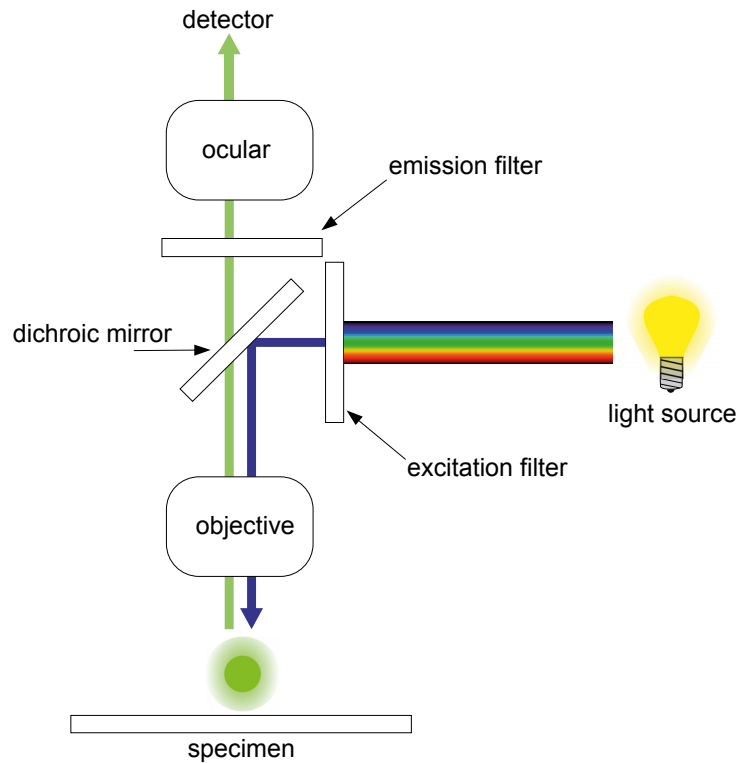


**Figure 2.9: Principle of an epifluorescence microscope.** Light of a specific wavelength coming from a light source is selected by an excitation filter (blue). The specimen is illuminated and absorbs the excitation light. The emitted light (green) goes through an emission filter, which separates the fluorescence from the illumination light and is focused to a detector. The dichroic mirror selectively reflects light of the illumination wavelength, while passes the emitted light. Figure from [26].

In an epifluorescence microscope, the sample is illuminated with light of the excitation wavelength, which is very often visible blue light, and absorbed by the fluorescent compound in the specimen. For excitation an intense, near monochromatic illumination is required. Hence, lasers or high-power LEDs can be used as a light source. To select the specific wavelength of the

excitation light an excitation filter is placed between the light source and the objective. The absorption of light causes the specimen to emit light of another wavelength and thus of a different color. The emitted light is focused onto a detector, in general a camera, through an emission filter, which separates the fluorescence from the illumination light. In contrast to more advanced light microscope designs, such as a confocal microscope, the light emitted by the specimen is focused by the same objective lens that is used for excitation in epifluorescence microscopes. The dichroic mirror is the essential part for selectively reflecting light of a small range of the illumination wavelength while passing the emitted light from the sample [65, 70].

In order to image whole volumes from biological samples, such as larval zebrafish brains, a microscope producing clear images of focal planes even deep within a sample is desired. With traditional wide-field fluorescence microscopes, specimens in focus can be recorded with a high resolution image, but details are lost when capturing volumetric samples and specimens whose thickness exceeds the dimensions of the focal plane.

Confocal microscopy benefits from the aspect that objects out of focus interfere with the image only if they are illuminated. It avoids the problem of bad resolution in depth by illuminating the sample with a scanning laser, but at the cost of being time-consuming. The quality of optical sectioning and resolution in depth can be improved by making illumination specific to only the focal plane and eliminating out-of-focus light, such as being done in light-sheet microscopy.

In light field microscopy, the entire specimen is illuminated and imaged simultaneously and thus prevents the time-consuming issue of confocal microscopy, but is apart from that applicable to capture dynamic events in volumetric specimens.

### **The general principle of LFM**

The emitted fluorescence from the whole 3D volume is detected at once in light field microscopy. The microscope captures a set of "rays" emitted through the volume, called the light field. These "rays" of light are multiplexed into a single two-dimensional image at the sensor of a camera, instead of recording single points in sequence. Depending on the depth of a point source, quite distinct light patterns are formed at the sensor, which provide a coding of the position into the image (see Figure 2.10). With the measured emission of the light field, the imaged volume can be reconstructed by solving a computed tomography problem with the help of implemented deconvolution algorithms [57]. Hence, the temporal resolution is limited only by the speed of the camera, but at the cost of reduced spatial resolution.

### **Application and experimental realization**

The application of LFM to functional  $Ca^{2+}$  imaging of biological samples was demonstrated in our lab for the first time and it could be shown that LFM is a powerful technique for brain-wide recording of neuronal activity in larval zebrafish [38, 57].

With this non-invasive functional imaging technique it is possible to capture whole volumes simultaneously in awake, behaving zebrafish without scanning. During 3D imaging of neuronal activity, almost single-neuron resolution can be achieved and the temporal resolution is limited only by the speed of the sensor system and the properties of the calcium indicator.

This is achieved by placing a microlens array into the image plane, which allows the sensor

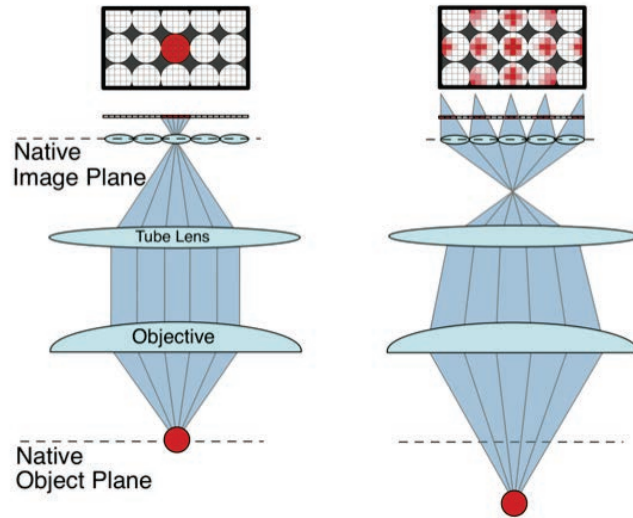


**Figure 2.10: Principle of light field microscopy.** Image formation in the light field microscope is depending on the position of a point source. Ray diagrams show how images of a point source at different depths get formed in the LFM.

system to capture both the 2D location and the 2D angle of the incident light, called the 4D light field (see Figure 2.11) [44].

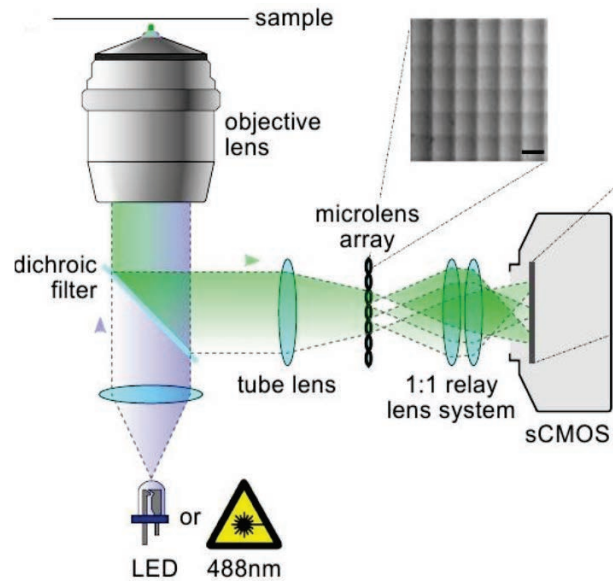


**Figure 2.11: Realization of light field microscopy.** A microlens array was placed into the image plane of a wide-field fluorescence microscope. A scientific complementary metal-oxid semiconductor (sCMOS) camera system was used for capturing images. Figure adapted from [57].



Each of these captured single images possess the information of the entire 3D volume and the focal stack can be post-synthesized computationally. The combination of this imaging technique with computational reconstruction methods based on 3D deconvolution [1, 20] provide for application to functional biological samples.

For more informations on theoretical foundations and the most beneficial implementation of LFM, as well as for illustration of achieved performance results during imaging of neuronal activity in zebrafish larvae, see ref. [38, 57].

The main goal of this study was the establishment and implementation of an operant conditioning paradigm for larval zebrafish. This was motivated and mainly based on the unpublished work realized in the lab of Florian Engert at Harvard University (private communication [28]), but adapted and expanded for internal purposes. In this work I wanted to investigate the ability of learning of zebrafish in the early larval stage and get insights into activity changes of neurons in their brain during conditioning by combination with LFM imaging. Successful learning could be observed in the operant conditioning assay, procedures and results are shown and the combination with light field microscopy is demonstrated.



## Materials & Methods

### 3.1 Animals and Procedures

For all experiments, unless specified otherwise, larval zebrafish between 6 to 10 days post fertilization (dpf) of the *nacre*<sup>-/-</sup>/*mitfa*<sup>-/-</sup> mutant strain, which lacks pigmentation of the skin, were used. Zebrafish expressing the pan-neuronal GCaMP5 protein by using the stable lines HuC:GCaMP5G or HuC:Gal4/UAS:GCaMP5G were bred and raised in our lab and used for all conditioning experiments, as well as imaging experiments with LFM.

A larval zebrafish at the age of one week is about 1 mm wide and between 3 and 4 mm long. For experimentation, zebrafish were embedded in 2 % low-melting-point agarose (Promega) in a custom designed fish chamber (see Figure 3.1 A), which is affixed on an microscope slide. Agarose covering the tail was removed with a scalpel to allow the tail to move freely and refilled with E3 medium. The medium consists of 5 mM NaCl, 0.17 mM KCl, 0.33 mM CaCl<sub>2</sub>, 0.33 mM MgSO<sub>4</sub> and 0.1 % methylene blue (Sigma). For experiments with odor stimulation, the nose was cleared of agarose additionally. The fixation of the head enables the recording and analysis of the tail position, as well as the measurement of neuronal activity simultaneously (see Figure 3.1 B).

To adapt the new condition of being partially restrained, fish were incubated for at least a few hours before experimentation or even overnight for later experiments. All experiments were performed at day-time, between 10 am and 8 pm.

### 3.2 Experimental Setup

An experimental setup for head-fixed zebrafish larvae, which allows the conditioning as well as brain-wide imaging simultaneously, was needed. Therefore, a portable setup was developed, which meets conditions for the conditioning experiments and enables the placement of the setup below the light-field microscope for ensuing imaging experiments as well.

The setup was mounted on an optical breadboard (Thorlabs) to allow transportation and consists of a stage, wherein the removable chamber carrying the immobilized fish can be placed

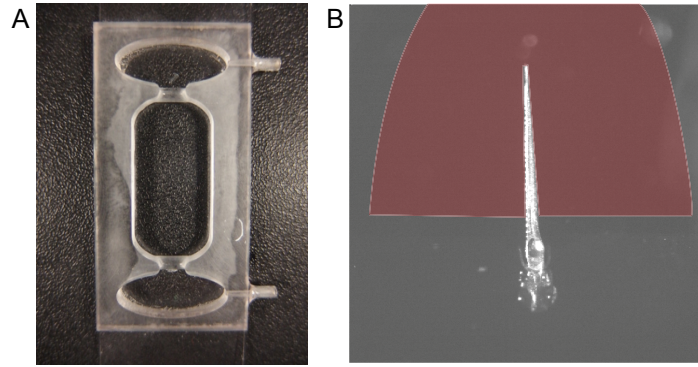


**Figure 3.1: Chamber for embedding and immobilized zebrafish larva.** (A) A custom designed fish chamber for embedding, affixed on a microscope slide. (B) A larval zebrafish is embedded in 2% low-melting-point agarose with the tail cleared. Red area is indicating the removed part of agarose.

(see Figure 3.2 A). To monitor tail movements, the fish was illuminated from the side with an infrared LED of the wavelength of 950 nm, which is affixed at the stage.

A USB3 camera for behavioural tracking (Point Grey, Grasshopper 3 with CMOS sensor, GS3-U3-41C6M-C) captured images from below at about 180 frames per second (fps). Between camera and fish a pair of achromatic lenses (Thorlabs, NIR achromatic pairs, MAP10100100-B) and a right-angle kinematic mount (Thorlabs, KCB1E) with an elliptical mirror (Thorlabs, PFE10-P01) were mounted via lens tubes. A near-infrared (NIR) bandpass filter (Thorlabs, FB950-10) was placed in front of the camera to block ambient visible light, as well as the blue excitation light of LFM when performing imaging experiments.

The aversive heat stimulus for conditioning was delivered by an infrared laser of 980 nm wavelength with an attached multi-mode fiber (both from Roithner Lasertechnik, core diameter of fiber: 400  $\mu\text{m}$ ). A collimator (Thorlabs, FC/PC Fiber Collimator  $f = 11.17$  mm, F220FC-1064) was coupled to the fiber, which enables the collimation of the laser beam before focusing it to a smaller beam diameter by a lens (Thorlabs,  $f = 60$  mm, AR Coated: 650 – 1050 nm, AC254-060-B-ML). These optical components were mounted in a cage system (Thorlabs, Kinematic cage mount, KC1-T) via a fiber collimator adaptor and a lens holder, which can be tilted and therefore allows manual positioning of the laser beam. Hence, the light could be precisely aligned with the head of the larva before each experiment. During the development of the setup, various combinations of collimators, lenses and laser powers were used to achieve desired stimulus-evoked tail movements of the animals (details on components and photographs are provided in Appendix A).

The presence of the heat stimulus was controlled by a data acquisition board (DAQ-board, National Instruments, NI USB-6008). Images of tail positions captured by the camera were analyzed by a custom-written Matlab software (code provided in Appendix C), which controls the delivery of aversive heat in a closed loop (see Figure 3.2 B).

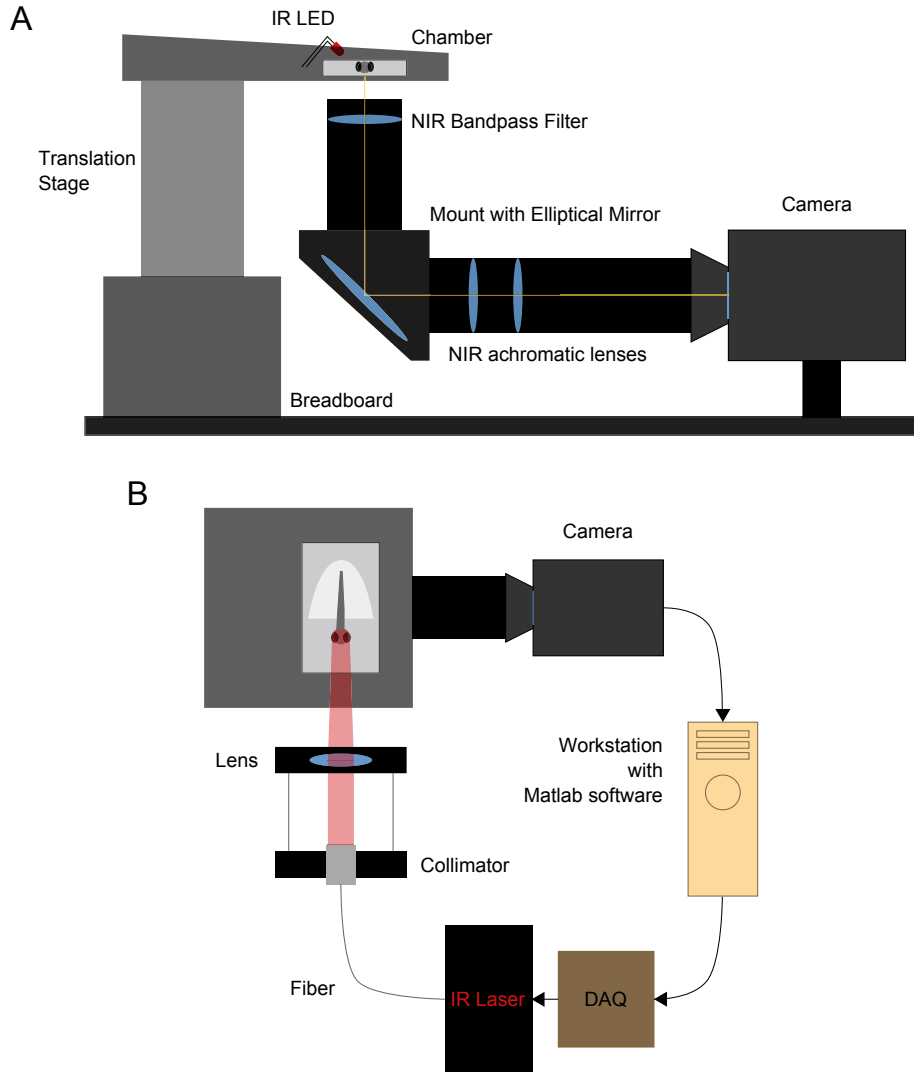


**Figure 3.2: Experimental setup.** (A) Lateral view. Chamber with the immobilized zebrafish larva is placed in a translation stage. Fish is side-illuminated with an infrared LED of the wavelength of 950 nm affixed at the stage. A camera for behavioural tracking captures images from below. A pair of achromatic lenses and a right-angle mount with an elliptical mirror are placed between camera and fish. A near-infrared (NIR) bandpass filter is placed in front of the camera to block ambient light. (B) Top view. The heat stimulus is delivered by an infrared laser of 980 nm wavelength with an attached multi-mode fiber. The laser beam is collimated before focused by a lens to the head of the larva. Images are acquired and analyzed by a custom-written Matlab software, which triggers a DAQ-Board for heat delivery. Detailed information on distances and dimensions are provided in Appendix A.

### 3.3 Automated Tail Tracking

The fish's movements were recorded in order to analyze the behaviour in response to a certain stimuli, as well as to correlate behaviour and neuronal activity. In the first instance, an automated tail tracking algorithm was implemented for the operant conditioning protocol, since the presentation of the heat stimulus is dependent on tail movements of the larva.

I implemented such a tracking algorithm in Matlab (code provided in Appendix C); the functional principle is described in this section.

#### Functional Principle of the Tracking Algorithm

Each frame taken by the behavioural camera was processed in Matlab to detect the tail movements automatically. The tracking algorithm implemented in Matlab finds points along the tail to get its skeletal representation, by sequentially searching for the brightest pixels along lines of a fixed length and distance (see Figure 3.3).

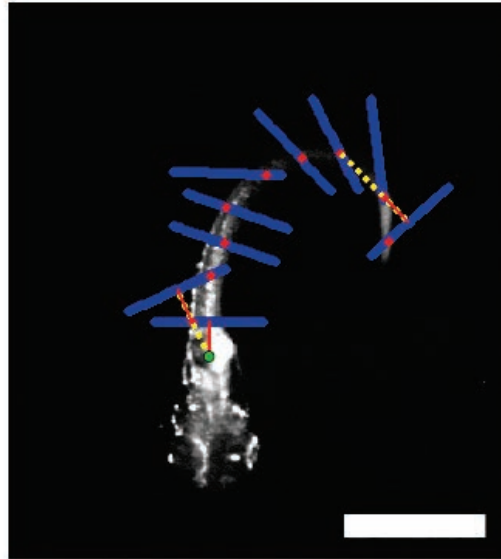


**Figure 3.3: Functional principle of the tracking algorithm.** The skeletal representation of the tail detected by the automated tracking algorithm is indicated by red points. The anchor point (green) is defined manually on the trunk of the body, the algorithm searches upwards in the image. The first point found by the algorithm (red) is the brightest point along the horizontal line (blue line) in a fixed distance  $r$  (orange line). For any other points the connecting line of the previous two points (indicated by a dashed yellow line) is extended of the fixed length  $r$  (orange line). The algorithm searches for the brightest point along the perpendicular line in each case (blue lines). Scale bar: 1 mm.

Starting from a manually defined anchor point on the trunk of the body by clicking into a

reference image, the algorithm searches for the pixel of maximal intensity (brightest pixel) along the horizontal line of a fixed length  $l$  at a fixed distance  $r$ . When connecting this point with the anchor point and lengthening the line by  $r$ , the next point is found on the perpendicular line by the algorithm. Every other point is found similarly on the line perpendicular to the connecting line of the last two points after extending it of the length  $r$ . An detailed mathematical description of this principle follows below. The algorithm stops if the intensity value of the brightest pixel comes below a defined threshold. Typically the tail is represented by 9 points from the trunk to the tip of the tail, but the number of points found by the algorithm is dependent on the length of the tail.

The exact position of the tail with reference to the camera can slightly vary between experiments, therefore the alignment of the fish must be determined before calculating the deflection angle of the tail. The position is determined by manually setting a reference line in the image of the tail before each experiment. The deflection angle  $\alpha$  is calculated and extracted for each frame, defined as the angle made by the tip of the tail (represented by the last point found by the algorithm) with respect to the reference line (see Figure 3.4). Deflections to the left from the observer's view are defined to be positive angles, whereas negative angles represent deflections to the right and an angle of  $0^\circ$  means the absence of any movements of the tail. The length of the reference line represents the length of the tail and therefore determines the number of points for the skeletal representation.

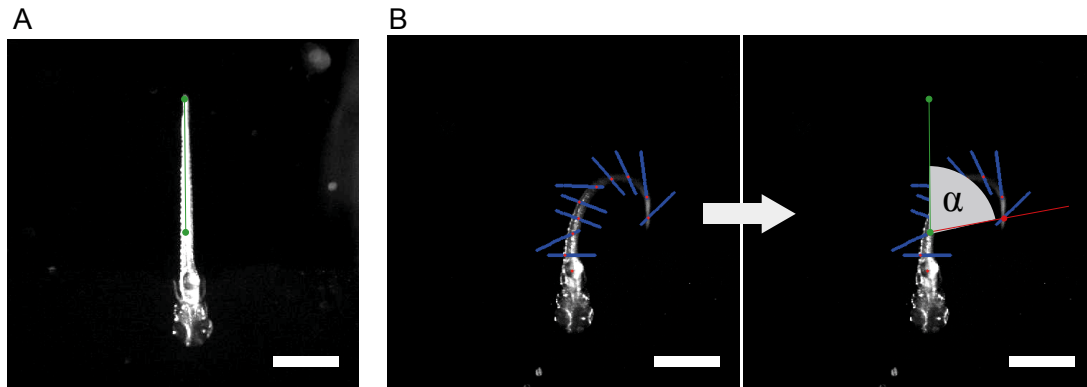


**Figure 3.4: Deflection angle of the tail.** (A) The alignment of the larva is determined by setting a reference line manually (green line). (B) For each frame taken by the camera, the algorithm finds points along the tail to get its skeletal representation. The deflection angle  $\alpha$  is defined as the angle between the reference line and the last point found by the algorithm (representing the tip of the tail) in respect to the anchor point (red line). Scale bars: 1 mm.

Since the presentation of the heat stimulus is dependent on tail movements of the larva in the operant conditioning assay, it is crucial to track the movements of the tail in real-time. With common settings for the camera ( $2 \times 2$  binning of the image and a region of interest of  $480 \times 380$

pixels) each frame is captured and processed by the software automatically in about 7 ms in average. A typical turn is captured by about 5 to 10 frames from start of the movement to the maximal point of deflection, which corresponds to a duration of about 35 to 70 ms. A time series of a typical tail deflection and the appropriate real-time extraction of the deflection angle can be seen in Figure 3.5.

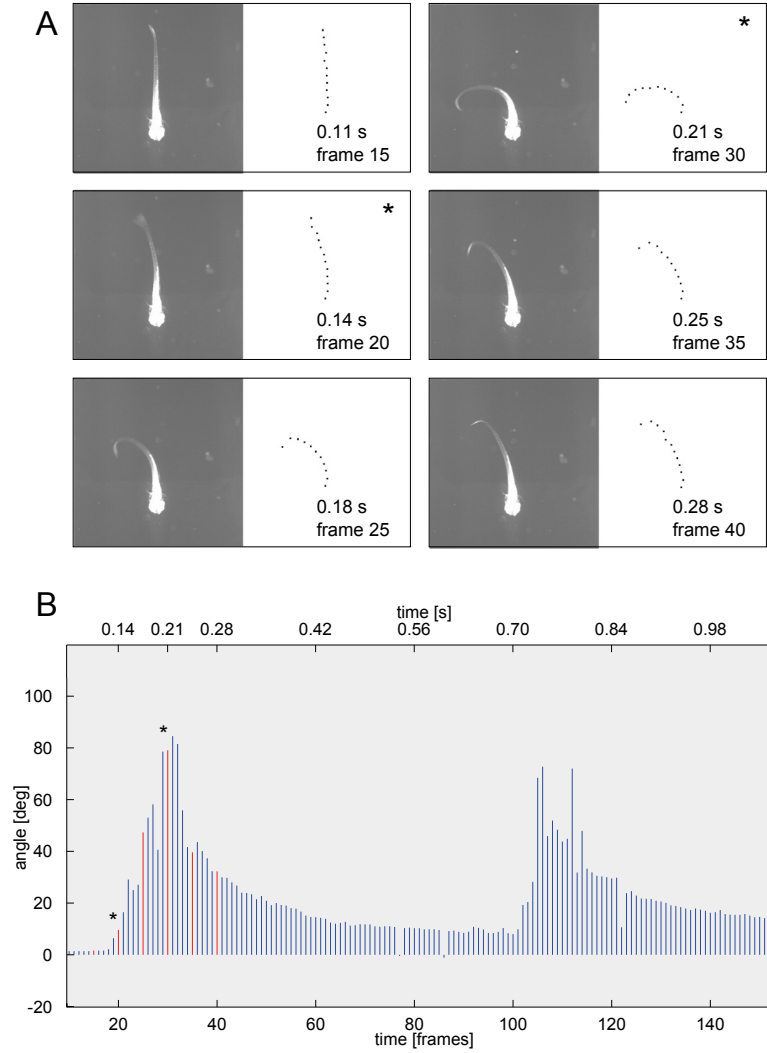


**Figure 3.5: Tail deflection and angle extraction.** (A) A typical tail deflection to the left, demonstrated by a time series. Every fifth frame is plotted with the appropriate skeletal representation. The frames showing the start of the turn and maximal deflection are indicated by asterisks. (B) The extracted deflection angle is plotted, the corresponding angles of the frames shown in the time series are marked as red lines. The time axis given in seconds (top) is estimated based on the average processing time of 7 ms per frame.



### Mathematical description

The manually defined anchor point with the image coordinates  $P_0 = \begin{pmatrix} p_{0,1} \\ p_{0,2} \end{pmatrix}$ , as well as the first directional (vertical) vector  $\vec{r}_{P_0} = \begin{pmatrix} r_{P_0,1} \\ r_{P_0,2} \end{pmatrix} = \begin{pmatrix} 0 \\ -1 \end{pmatrix}$ , the distance  $r \in \mathbb{N}$  and the length  $l \in (2k)_{k \in \mathbb{N}}$  of the lines  $B_i, i = 1, 2, \dots$ , which contain the points for the skeletal representation of the tail, are fixed values and serve as inputs for the algorithm (see Figure 3.6).

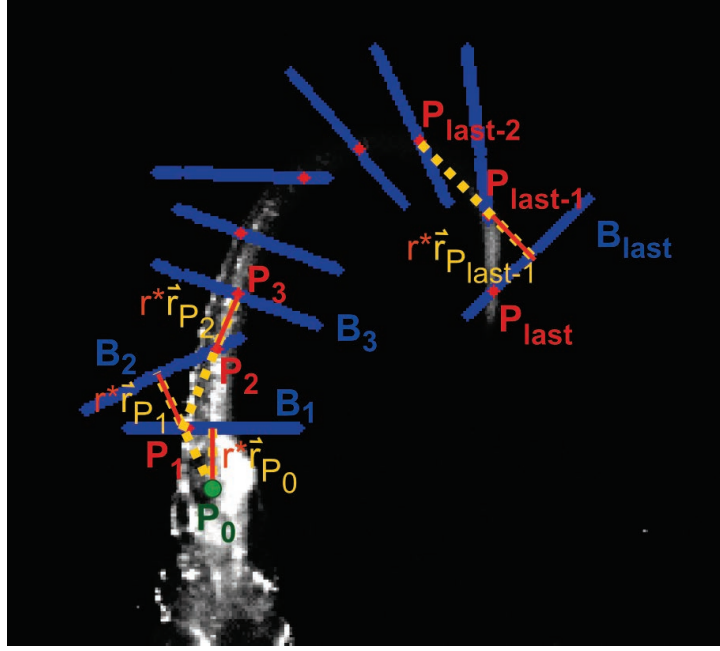


**Figure 3.6: Mathematical descriptions for the tracking algorithm.** The anchor point  $P_0$  (green point) is manually defined. The vertical vector  $\vec{r}_{P_0}$  (yellow dashed line), as well as the distance  $r$  (orange line) and the length  $l$  of the lines  $B_i, i = 1, 2, \dots$  (blue lines) are fixed values. The points  $P_i, i = 1, 2, \dots$  (red points), representing the tail, are calculated iteratively by the directional vectors  $\vec{r}_{P_{i-1}}$  (yellow dashed lines), obtained by the last two points  $P_{i-1}$  and  $P_{i-2}$ . Each point  $P_i$  represents the pixel with the maximal intensity value of the pixels along the line  $B_i$ .

Each of these lines  $B_i, i = 1, 2, \dots$  consists of a set of pixels in the image  $X_{i,t}, t = \frac{-l}{2}, \dots, \frac{l}{2}$ , which can be calculated iteratively by the general formula

$$B_i := \{X_{i,t} \mid X_{i,t} = P_{i-1} + r \cdot \vec{r}_{P_{i-1}} - t \cdot \vec{n}_{P_{i-1}}, t = \frac{-l}{2}, \dots, \frac{l}{2}\},$$

where  $\vec{n}_{P_{i-1}}$  is the normal vector of  $\vec{r}_{P_{i-1}}$  ( $\vec{n}_{P_{i-1}} \perp \vec{r}_{P_{i-1}}$ ), which gives the direction of the connecting line of the last two points  $P_{i-1}$  and  $P_{i-2}$ . The directional vectors can be calculated

by

$$\vec{r}_{P_i} = \begin{pmatrix} r_{P_i,1} \\ r_{P_i,2} \end{pmatrix} = \frac{P_i - P_{i-1}}{|P_i - P_{i-1}|}, i = 1, 2, \dots$$

and the normal vector is given by

$$\vec{n}_{P_i} = \begin{pmatrix} -r_{P_i,2} \\ r_{P_i,1} \end{pmatrix}.$$

Hence, the lines  $B_i, i = 0, 1, 2, \dots$ , which are orthogonal to the connecting lines, can be written as

$$B_i := \{X_{i,t} \mid X_{i,t} = \begin{pmatrix} p_{i-1,1} + r \cdot r_{P_{i-1},1} - t \cdot (-r_{P_{i-1},2}) \\ p_{i-1,2} + r \cdot r_{P_{i-1},2} - t \cdot r_{P_{i-1},1} \end{pmatrix}, t = \frac{-l}{2}, \dots, \frac{l}{2}\}.$$

The skeletal representation of the tail is given by the points

$$P_i = \begin{pmatrix} p_{i,1} \\ p_{i,2} \end{pmatrix} = \max\{intens(X_{i,t})\}, i = 1, 2, \dots,$$

where  $\{intens(X_{i,t})\}$  represents the set of intensity values of the pixels along the lines.

The reference line is manually defined by two points in the image, represented by  $R_1$  and  $R_2$  (see Figure 3.7).

The length of the reference line, given by  $L = |R_2 - R_1|$  determines the maximal number of points  $n \approx \frac{L}{r}$  found by the algorithm.

The last found point  $P_{last}$  defines the angle of deflection by regarding the connecting line  $\vec{a} = P_{last} - R_1$ .

The positive, acute angle  $\alpha$  between this line  $\vec{a}$  and the reference line  $\vec{c} = R_2 - R_1$  can be calculated by the formula

$$\alpha = \arccos \frac{\vec{a} \cdot \vec{c}}{|\vec{a}| \cdot |\vec{c}|}.$$

The sign of the cross product  $\vec{a} \times \vec{c}$  decides if the vector  $\vec{a}$ , and with it the point  $P_{last}$ , is to the right or to the left of the reference line  $\vec{c}$  in the image. Vectors  $\vec{a}$  to the right of the line  $\vec{c}$ , which results in a negative sign of the cross product, implicate the change of the sign of the angle to a negative one. Therefore, deflections to the right are represented by negative deflection angles  $\alpha_{right} < 0$ , whereas deflections to the left result in positive ones  $\alpha_{left} > 0$ .

The tracking code written in Matlab is provided in the Appendix C.

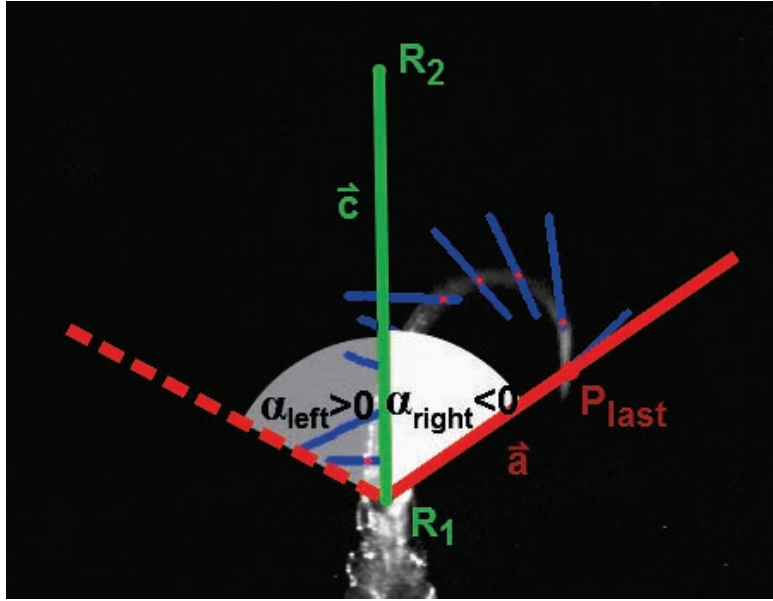


**Figure 3.7: Mathematical descriptions for calculating deflection angles.** The reference line  $\vec{c}$  (green line) is manually defined by two points  $R_1$  and  $R_2$  (green points). The last found point  $P_{last}$  (red point) defines the angle of deflection by regarding the connecting line  $\vec{a}$  (red line). Vectors  $\vec{a}$  to the right of the line  $\vec{c}$  result in deflection angles with negative sign  $\alpha_{right} < 0$ , whereas deflections to the left are represented by positive ones  $\alpha_{left} > 0$  (indicated by a dashed red line).

## Graphical User Interface

To make the software applicable for the experimentation and accessible for other users, a graphical user interface (GUI) was implemented. The GUI provides point-and-click control of the software and eliminates the need to type commands in order to run the application. Before starting the experiment, a reference image of the animal was taken to define the anchor point and to determine the position of the tail by setting the reference line manually by clicking into the image (see Figure 3.8). The conditioning protocol can be selected and specific parameters set by the user before starting the fully automated conditioning experiment based on the tracking algorithm (more details are provided in Appendix B).

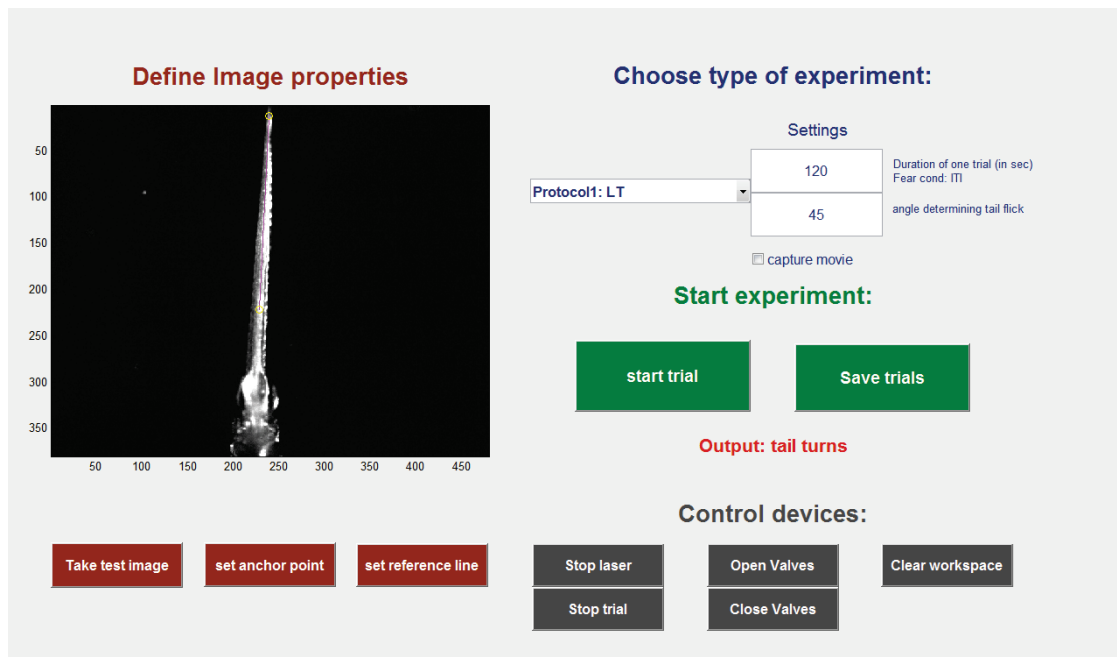


**Figure 3.8: Graphical User Interface (GUI).** Before starting an experiment, a test image can be taken for defining the anchor point and the reference line by clicking buttons. The type of experiment can be selected and parameters, like the duration of one trial, as well as the threshold of the deflection angle, which defines a turn can be set by the user. Each trial is started manually by clicking a button, during the experiment different devices can be controlled by the user.

### 3.4 Operant Conditioning Paradigm

The main goal for this thesis was to establish an operant conditioning assay for head-fixed zebrafish larvae in which the fish can be trained to escape an aversive heat stimulus provided by the infrared laser with correct behaviour. Guidance provided by Florian Engert on basis of the unpublished work [28] served as a fundamental basis for the development of this negative reinforcement assay. By the immediate removal of the aversive stimulus after a correct turn, zebrafish larvae can be conditioned to perform a tail flick in the rewarded direction whenever applying the laser heat.

#### 3.4.1 Conditioning Protocol

In this conditioning paradigm, embedded but tail-free larvae have the chance to turn off the infrared laser with a directional tail flick (see Figure 3.9). Each conditioning experiment was performed in maximal two blocks, each block consists of 25 up to 30 trials, unless specified otherwise. One trial had a fixed length of two minutes and started with the exposure of the heat stimulus provided by the invisible infrared laser. The head of the zebrafish was heated until the animal flicks its tail in the rewarded direction. Using a real-time tracking algorithm of the larval tail movements (see Section 3.3), the heat was terminated immediately when a correct turn was completed by the fish and detected by the closed-loop software. If the larva fails to escape the heat stimulus by turning it off within two minutes, a stimulus-free pause of about 20 seconds was given before the next trial started with renewed heat exposure. For the first block of 25 to 30 trials, the rewarded direction was held constant.

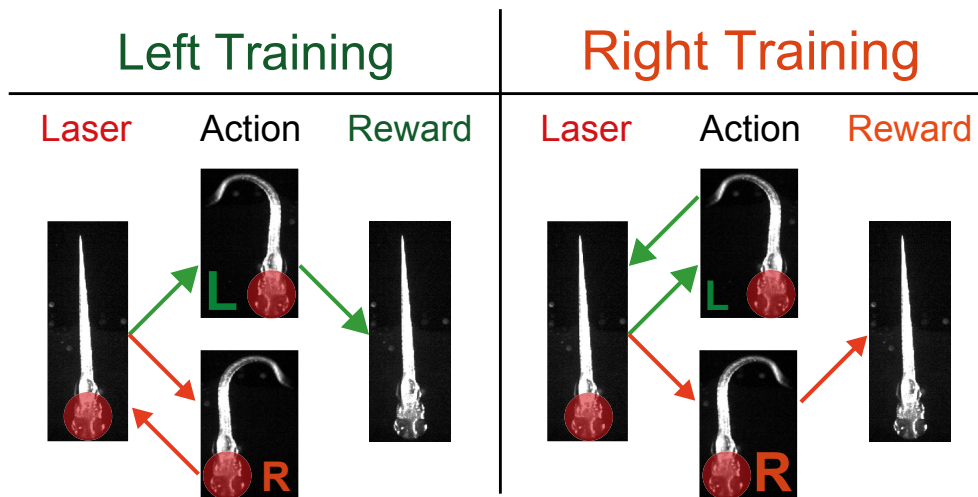


**Figure 3.9: Operant conditioning protocol.** The fish larva is exposed to the heat stimulus provided by an infrared laser. The head of the fish is heated until the animal generates a turn in the rewarded direction. If left is the rewarded direction (left training), the laser is terminated if the fish flicks its tail to the left, otherwise the heating continues. In right training, the fish is rewarded by laser termination, if a turn to the right is generated.

Turns usually have a start bias, meaning that a preference in stimulus-evoked turn direction exists. At the beginning of each experiment, prior to the first block, a single trial was performed, where a heat step was delivered to determine any turn direction preference. The direction of the first stimulus-evoked turn was defined as the bias. In the first training block the opposite of this initial preference was picked as the rewarded training direction. After completion of the trials which were part of the first block, the rewarded direction was reversed at the beginning of the second block. The second block consisted of 25 to 30 trials as well. For time reasons the second block was performed only if the animal showed a good learning performance during the first block (precise definition later in this section). Hence, all behavioural experiments were divided into bias determination and two training blocks maximally, the entire protocol took roughly two hours.

A turn, detected by the tracking algorithm, was defined as a tail flick with a deflection angle exceeding a fixed threshold. The reward of struggling and closely consecutive turns was not wanted (rapid turn-counterturn movements), because it would interfere the association of the laser termination with a specific directional tail flick. For this conditioning assay, routine turns instead of rapid movements were desirable, which typically occurred at slower succession (cf. Figures 3.12 and 3.19 below). Therefore, a correct turn was only rewarded if the previous incorrect turn had been performed at least 200 ms ago.

In order to quantify the success of training and measure the learning performance subsequently, each trial was defined either as a correct or incorrect trial (see Figure 3.10). If the direction of the first stimulus-evoked turn was consistent with the rewarded direction, the trial was counted as a correct trial, while an incorrect trial started with a turn which was not rewarded.

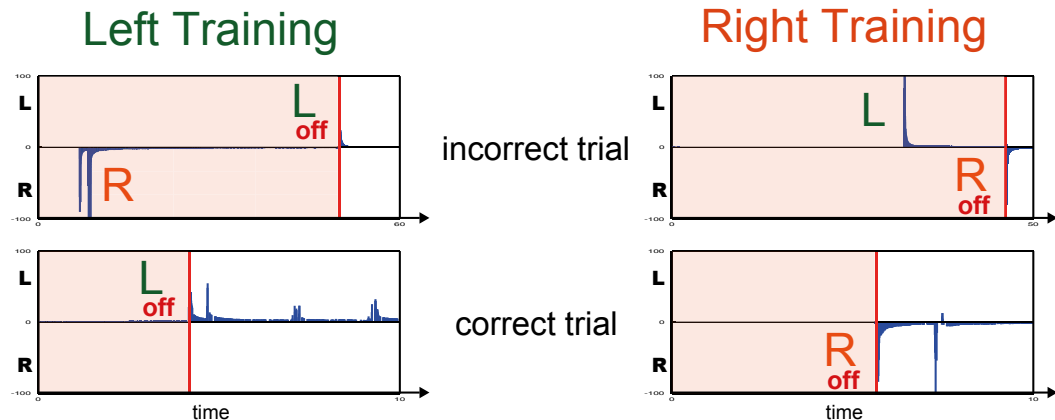


**Figure 3.10: Correct and incorrect trials.** Each trial can be defined either as a correct or incorrect trial. For left training (left is the rewarding direction), a trial is named as a correct trial, if the first stimulus-evoked turn is to the left. Whereas, an incorrect trial starts with a turn to the right. For right training (right is the rewarding direction), it is exactly the other way around.

## Quantification of learning performance

In order to quantify the progression of learning and perform statistical analyses, a measure for the learning performance needed to be defined. The learning progress can be measured by the fraction of correct trials in the previous six trials and can be defined as **recent performance** [28].

This metric can be calculated for each point  $\text{idx} = i - 5$  after every trial  $i$  from the sixth trial onwards:

$$\text{recent performance}(\text{idx}) = \frac{\# \text{ correct trials from trial } i - 5 \text{ to } i}{6}, i \geq 6.$$

In order to illustrate the learning progress from the first to the last trial when averaging more experiments (cf. Figures 4.2 - 4.7), recent performance is calculated for trial indices below six as well, by defining the recent performance of trial  $i$ ,  $i < 6$  as

$$\frac{\# \text{ correct trials from trial 1 to } i}{i}, i < 6.$$

A learning progress could be observed, when the recent performance increased across the trials within one block.

With this definition of learning performance, it was possible to review the success of training after performing the training blocks.

## Classification of learners and non-learners

If a learning effect appeared during the training blocks, the learning performance increased across the trials of a block. When measuring the progression of learning by the recent performance, a classification of learners and non-learners could be made.

If the recent performance increased across the trials and reached a final performance greater than 0.5 at the end of each block (asymptotic performance), the fish was defined as a **learner** (see Figure 3.11 A). Usually animals performed poorly at the beginning of each block, because the opposite of their intrinsic bias was chosen for the rewarded direction. Learners showed a learning progress across the training trials, so that at the end of each block the asymptotic performance exceeded a value of 0.5.

Animals which showed an asymptotic performance less than 0.5 in at least one block and less than a two-fold improvement in the other block, when comparing the initial recent performance and the final one, were defined as **non-learners**.

Among this class, a **non-learner type 1** described an animal, which showed an asymptotic performance less than 0.5 in the first block (see Figure 3.11 B). This means that the animal did not show a learning progress during the first block and performed poorly even at the end of the block. For time reasons a second training block was not realized in this case.

A larva showing less than a two-fold improvement in the first block and an asymptotic performance less than 0.5 in the second block, was referred to as a **non-learner type 2** (see Figure 3.11 C). Animals which showed a final recent performance greater than 0.5 in the first block,

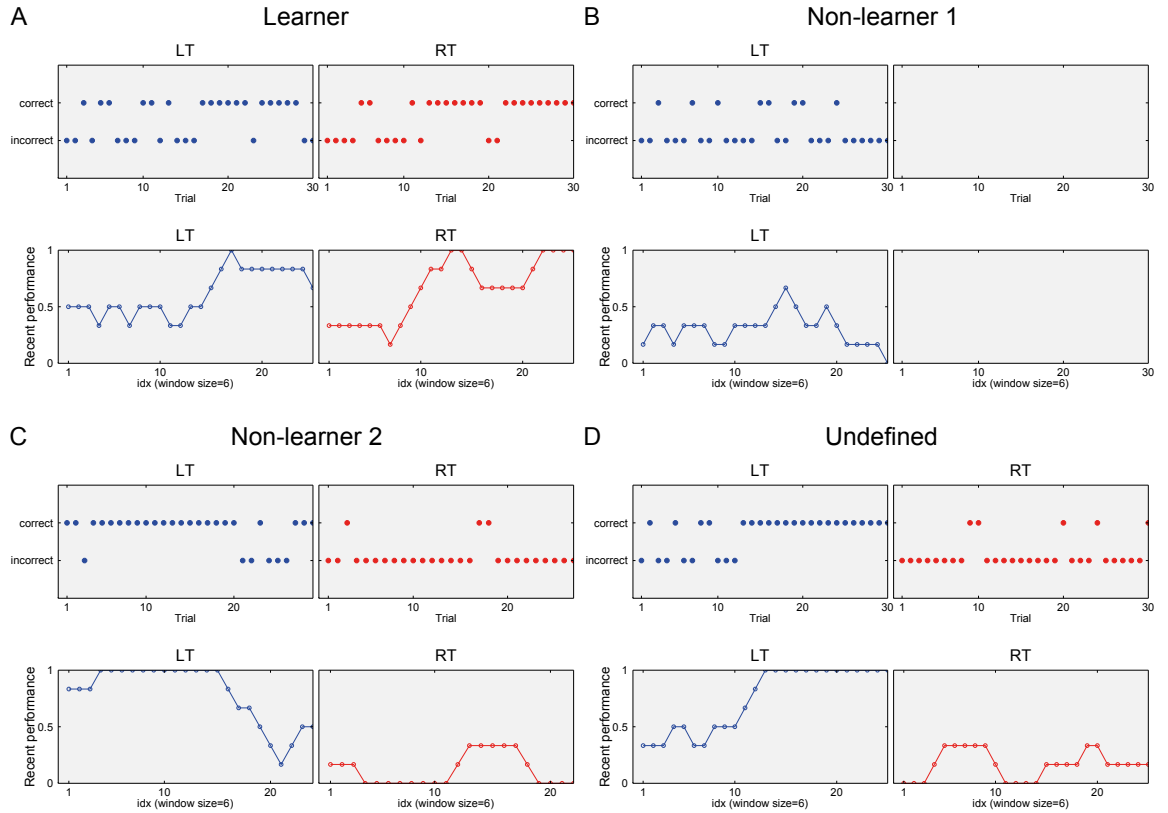


**Figure 3.11: Classification of learners and non-learners.** The process of learning can be measured by the fraction of correct trials in the last six trials, defined as recent performance. The figure shows sample results for each class. The incorrect and correct trials for both blocks of each experiment are plotted, as well as the resulting recent performance. In all samples (A)- (D), left training (LT) was performed in the first block (indicated in blue) and right training (RT) in the second block (red). (A) A learner showed an asymptotic performance greater than 0.5 in both blocks. (B) A non-learner type 1 showed an asymptotic performance less than 0.5 in the first block. The second block was not performed for this class. (C) A non-learner type 2 showed less than a two-fold improvement in the first block and an asymptotic performance less than 0.5 in the second block. (D) The animal, denoted as undefined, showed more than a two-fold improvement in the first block, but an asymptotic performance less than 0.5 in the second block. Animals, which fell into this class were excluded from the analysis.

but the learning progress was small compared to the initial performance, fall into this class. This was particularly the case when the fish did not show a strong intrinsic bias and the initial performance was relatively high even at the beginning of the training.

Animals which showed an, at least, two-fold improvement in only one block, but a low asymptotic performance in the other, were excluded and not observed in the statistical analysis, this class was denoted as **undefined** (see Figure 3.11 D). For a summary of the classification, see Table 3.1.



Class	Definition
Learner	Asymptotic performance $\geq 0.5$ in both blocks
Non-learner type 1	Asymptotic performance $< 0.5$ in first block ( $< 2$ -fold improvement in second block)
Non-learner type 2	$< 2$ -fold improvement in first block Asymptotic performance $< 0.5$ in second block
Undefined	$\geq 2$ -fold improvement in one block Asymptotic performance $< 0.5$ in other block

**Table 3.1:** Classification of learners and non-learners

### 3.4.2 Experimental Realization

The experimental settings for the heat stimulation had an influence on the turning behaviour of the fish.

The heat intensity and therefore the turning behaviour of the fish was dependent on laser power and beam diameter, which in turn are dependent on certain components used for the setup. Various combinations of lenses, laser fibers and collimators resulted in different beam diameters and, therefore, in heat intensity. More details on investigations on laser settings are given in Appendix A.

The usage of a measured laser power of around 150 to 200 mW at the location of the fish and a beam diameter of about 2 mm provoked no struggling or escape behaviour, indicated by fast and repetitive side to side movements, but caused the animal to respond with single turns (see Figure 3.12 and cf. Figure 3.19 below). The resulting surface power density (power per unit area) amounted to approximately 55 mW/mm<sup>2</sup>. These conditions elicited a turning behaviour after a few seconds of heat stimulation and caused no detectable damage to most of the animals during experimentation. Therefore, these values provided the final conditions for the operant conditioning experiments.

In most experiments the agarose and water in the chamber, in which the fish larva was embedded, was warmed to about 26 °C by using a chamber with integrated infrared LEDs to ensure proper contrast. Some experiments were performed with a water flow pumped through the chamber and provided by an odor-delivery setup, necessary for upcoming experiments with odor stimulation (see Section 3.4.3, all details on the setup are provided in Section 3.5.2 and Appendix A).

Depending on these factors, different values for the laser power needed to be used to obtain similar turning behaviour of the fish (in Appendix A).

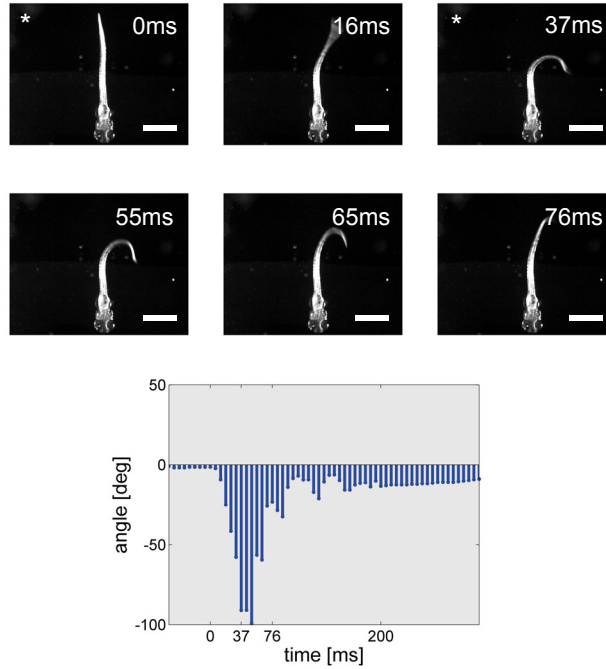


**Figure 3.12: Sample routine turn.** Laser power of around 150 to 200 mW and a beam diameter of about 2 mm caused the animal to respond with single turns during operant conditioning. A typical routine turn is illustrated and takes about 40 ms from start to maximal deflection (indicated by asterisks). Struggling and escape behaviour is undesired (cf. Section 3.5). Scale bars: 1 mm.

During the training protocol, the heat was terminated immediately when a correct turn was generated by the fish, whereas every tail flick with a deflection angle exceeding the fixed threshold of  $45^\circ$  was defined as a turn. This value was chosen in order to exclude swimming movements, but was dependent on the placement of the reference line and could therefore be changed by the user. Usually the first point of the reference line and the anchor point were placed on the trunk of the body, at the level of the border between agarose and the removed part. The computational implementation of the conditioning protocol is described in Appendix C.

### 3.4.3 Conditioning with Additional Odor Stimulation

A modified protocol of the operant conditioning paradigm can be used to investigate olfactory learning and memory. By presenting an additional odor stimulus during only one of the two training blocks, it could be investigated if larvae were able to associate a neutral odor with a specific direction of tail movement (see Figure 3.13).

For odor stimulation, different single amino acids were dissolved in E3 medium freshly before each experiment. Various AAs were used (Lysine (Lys), Alanine (Ala), Cysteine (Cys)) in final concentrations between  $100\text{ }\mu\text{M}$  up to  $500\text{ }\mu\text{M}$ . In order to pump forward the odor pulse, the same odor-delivery setup as for classical fear conditioning was used (see Section 3.5.2).

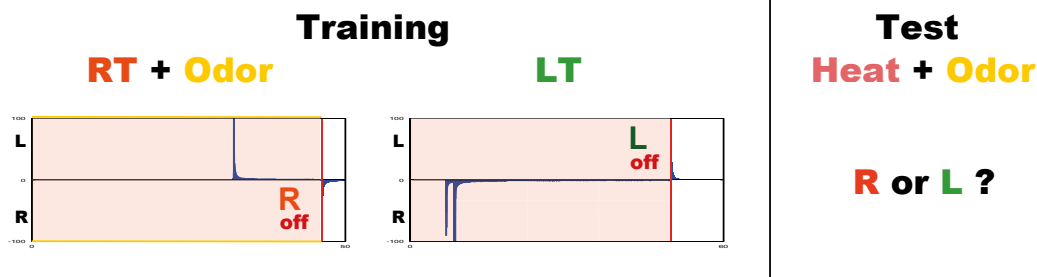


**Figure 3.13: Protocol of operant conditioning with odor stimulation.** In the first block of training (RT in this case), the fish larva was exposed to the heat stimulus simultaneously with odor stimulation. Both stimuli were terminated once the animal generated a turn in the rewarded direction (right). In the second training block, the rewarded direction was reversed (LT) and only the heat stimulus was presented until the animal generated a tail flick to the left. In the subsequent test block consisting of 10 trials, heat and odor stimuli were again presented simultaneously to the fish and the direction of the first-stimulus evoked turn of each trial was recorded.

Similar to operant conditioning but due to the modified conditions, the aversive heat stimulus provided by the infrared laser was adjusted to a higher laser power of about 550 to 600 mW, resulting in a surface power density of about 180 mW/mm<sup>2</sup>.

The protocol resembled that of operant conditioning (see Section 3.4.1), but consisted of an extra test block after training. In the first of the two training blocks an additional odor stimulus simultaneous to the aversive heat stimulus was presented to the fish. At the beginning of each trial, the valve of the odor-delivery setup opened, which induced the transport of an odor pulse to the fish chamber. In order to ensure that the odor arrived at the fish's nose preferably at the same time as the heat stimulus was presented, the valve was opened two seconds before laser exposure. The valve closed at the same time as the laser was terminated, once the animal performed a tail flick in the rewarded direction. One trial lasted two minutes, the length of the stimuli-free period was again dependent on the moment of stimuli termination. If the animal met conditions to be classified as a learner after performing the second block, a test block consisting of ten trials was realized after the training. Similar to the first training block, each test trial started with simultaneous heat and odor stimulation. Both stimuli were terminated once the animal performed the first stimulus-evoked turn. The majority of either left or right turns in these ten test trials gave indication if the larva associated the odor with a specific direction.

### 3.5 Classical Fear Conditioning Paradigm

Beside the operant conditioning paradigm, I also tried to establish a classical fear conditioning paradigm, in which the zebrafish larvae should learn to associate an odor stimulus (CS) with a short aversive heat pulse (US) provided by the infrared laser, which by itself leads to an increased tail movement (UR). After successful associative learning the previously neutral odor stimulus itself should cause an increased turning response (CR) (see Figure 3.14 A).

In contrast to the operant conditioning paradigm, the presence of the stimuli is not dependent on behavioural responses of the fish.

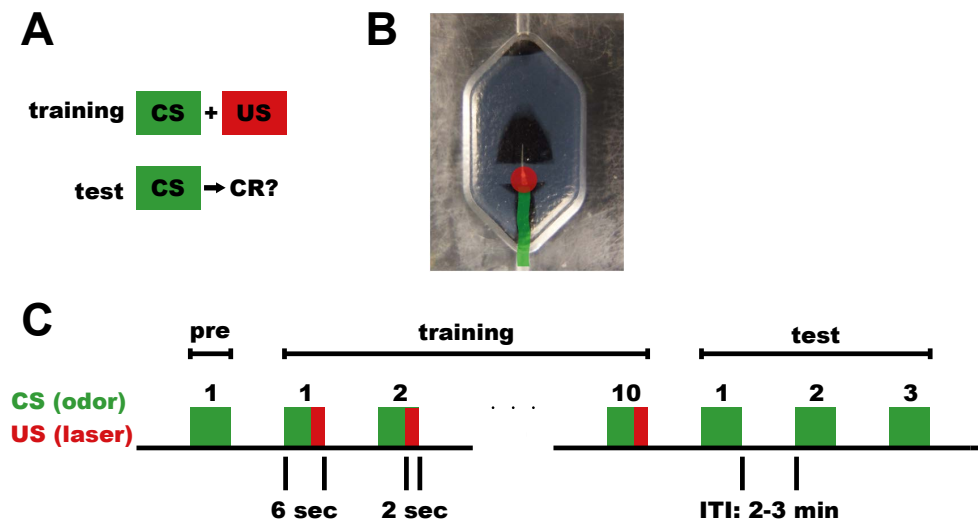


**Figure 3.14: Classical conditioning protocol.** (A) During training, the CS and US were repeatedly paired. The US itself leads to an increased tail movement (UR). After successful learning, a test block is performed in which the CS alone is presented and should cause an increased response (CR). (B) As CS, a neutral odor pulse consisting of a single amino acid (AA) was presented to the fish. The IR laser provided the aversive heat stimulus (US). (C) All classical conditioning experiments were divided into pre-trials, training and test-trials. During pre- and test-trials only the CS (odor) was presented to the fish and no heat stimulus was delivered. Before training, the fish was exposed to at least a single CS (pre-trial) in most experiments. During the training block consisting mostly of 10 trials, the CS and US (short laser pulse) were repeatedly paired. The length of the interval between the trials (ITI) was at least two minutes. The odor pulse lasted about four seconds (IS) and was followed by the aversive heat stimulation with a duration of about two seconds.

#### 3.5.1 Conditioning Protocol

As conditioned stimulus, a neutral odor pulse consisting of a single amino acid (AA) was presented to the fish (see Figure 3.14 B). The IR laser provided the aversive unconditioned stimulus, which elicited an increased tail movement, interpreted as a fear response. Therefore, this assay can be classified as an aversive or fear conditioning paradigm.

All classical conditioning experiments were divided into pre-trials, training and test-trials (see

Figure 3.14 C). During pre- and test-trials only the CS (odor stimuli) was presented to the fish and no heat stimulus was delivered.

Before training, the fish was exposed to at least a single CS to examine the animal's response to the CS alone (pre-trial) in most experiments. During training, the CS (odor) and US (short laser pulse) were repeatedly paired. In the first performed experiments ten paired trials were presented with an inter-trial interval (ITI) of at least two minutes, these values changed throughout development (see below). At the start of each trial, a stimulus-free period of about 20 seconds preceded the presentation of the odor stimulus. Then, the odor pulse lasted about four seconds (inter-stimulus interval, IS) and was followed by the aversive heat stimulation with a duration of about two seconds. The protocol was designed such that the two stimuli overlapped but ended simultaneously. Due to the preceding onset of the CS and overlap of CS and US, the assay refers to as forward delay conditioning. This form of conditioning was chosen because it shows the highest learning rate, as mentioned in Section 2.2.1.

After training, only the odor stimulus without heat was presented to the fish in three test trials to determine if the CS itself provoked a behavioural response.

### Quantification of learning progress

In order to quantify the enhanced movement during odor stimulation, an appropriate measure needed to be defined, which compared the motor responses in the period of the CS with movements during a stimulus-free interval.

For training trials, the period of CS for measure calculation was defined from the time point of opening the valve, inducing the transport of the odor pulse to the chamber, until the heat stimulus was activated. This interval, denoted as  $I_{CS}$  in Figure 3.15 on top, represented the period of odor stimulation before the US was presented. For test trials, where the odor pulse alone was presented,  $I_{CS}$  was prolonged (see Figure 3.15 at bottom). In order to determine the baseline activity when no stimuli were presented, an interval from the start of the trial until the opening of the valve was defined, denoted as  $I_{base}$ .

The activity of an animal during these periods of time were obtained by tracking the tail deflections. After filtering the data for outliers and subsequent interpolation, resulting in a smoothed deflection curve, only deflection angles with absolute values greater than five were observed in order to ignore slight tail deflections due to pump pulsation or swimming movements. When observing only these activity events, the Riemann integral of absolute deflection angles for corresponding frames was calculated during  $I_{base}$ , as well as during  $I_{CS}$ , denoted as  $A_{base}$  and  $A_{CS}$ , respectively. These metrics based on area comprised the information of both intensity and duration of activity. In order to investigate the increase of the activity during CS over baseline, the measure  $A_{increase}$  was defined as the ratio of  $A_{CS}$  and  $A_{base}$  after scaling them to the same length of period,  $A_{increase} = \frac{A_{CS}}{A_{base}}$ .

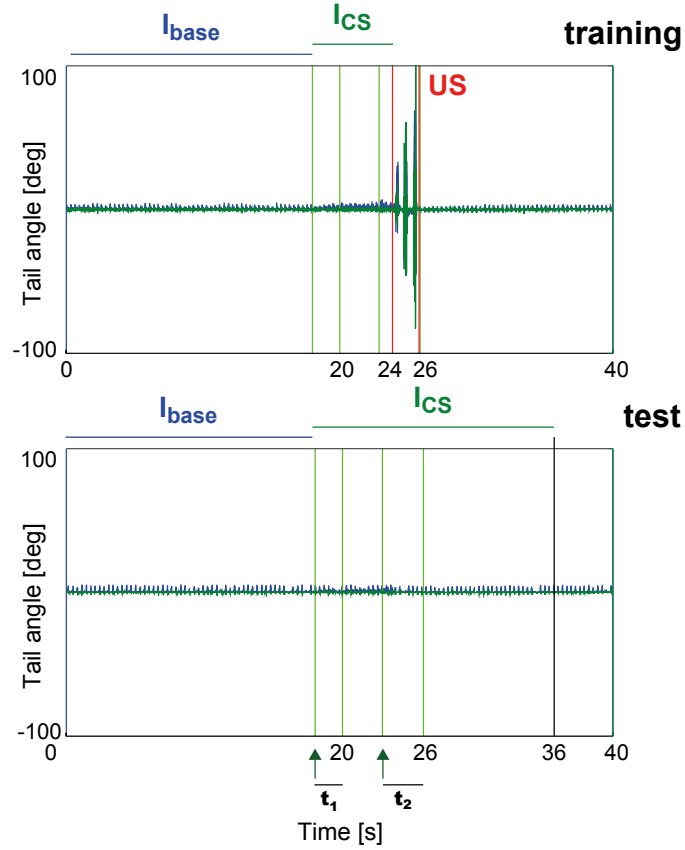


**Figure 3.15: Quantification for classical conditioning experiments.** The first 40 seconds of a sample training and a test trial are outlined. The baseline and the CS interval ( $I_{base}$  and  $I_{CS}$ ) in order to calculate the measure  $A_{increase}$  are illustrated for both trials. Dashed green lines indicate the instant of opening and closing the valves of the odor-delivery system, the solid green lines show the time period when the odor stimulus (CS) was present at the fish's nose according to the estimation of  $t_1$  and  $t_2$  (cf. Section 3.5.1). During a training trial (top),  $I_{CS}$  was defined from the time point of opening the valve until the US was presented (indicated by red lines). The US lasted two seconds. For test trials (bottom),  $I_{CS}$  was prolonged by adding ten seconds to the supposed end of the odor stimulus. The baseline activity was determined from the start of the trial until the opening of the valve.

### 3.5.2 Experimental Realization

Before experimentation, the fish larva was embedded in a custom-designed small chamber with access paths, which enabled the odor stimulation. The inflow path was directly in front of the fish's nose and the small volume allowed a low dilution, as well as a fast washout of the odor (see Figure 3.16, detailed information on dimensions is provided in Appendix A).

The olfactory CS was provided by a custom-designed tube-pump system, which delivered an odor pulse of arbitrary duration and time. This odor-delivery setup consisted of valves with

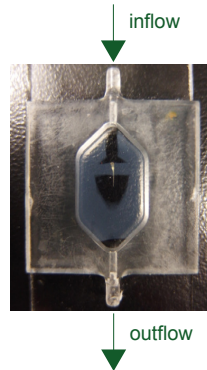


**Figure 3.16: Chamber for odor stimulation.** For odor stimulation, the fish larva is embedded in a small chamber with access paths for inflow and outflow.

three ports (The Lee company, LFY 3-Way 156 MINSTAC Solenoid Valves), its switching was controlled by the DAQ-board implemented in the software, and tubing pumps (Masterflex C/L Tubing Pump, HV-77122-24 and Masterflex C/L Dual-Channel Tubing Pump, HV-77120-42) for forwarding the liquids through tubes (Carl Roth, Tygon ID 1.6 mm).

The setup consisted of two separate parts, in which two liquids were circulating and forwarded by the dual-channel pump (see Figure 3.17). The liquid in the chamber was pumped out with the second pump. In order to prevent overflow, the flow rates of both pumps were adjusted to similar values of about  $60 \mu\text{l/s}$  according to the minimal possible flow rate of the pump for the outflow. In one of these circles fish water was pumped forward, whereas in the second one the odor was circulating. Both liquids were heated in a warming bath before arriving at the fish chamber with about  $26^\circ\text{C}$ . For most of the experiment, fish water was passed through the fish chamber, the odor was circulating in the meantime. A software command induced the switching of the valves, followed by the transportation of the odor to the fish (detailed informations and photographs of the setup are provided in Appendix A).

With this system odor pulses of specific length could be presented to the animal in the classical conditioning paradigm.

For the unconditioned stimulus, an odor was desirable, which causes strong neuronal activity but no behavioural response. It is known from literature, that some single amino acids induce neuronal responses in the olfactory bulb (e.g. in [45], see Figure 3.18).

For my conditioning experiments, different pure amino acids were dissolved in E3 medium freshly before each experiment. Unless specified otherwise, the amino acids Methionine (Met) and Lysine (Lys) were used in final concentrations of  $100 \mu\text{M}$  up to  $1 \text{ mM}$ .

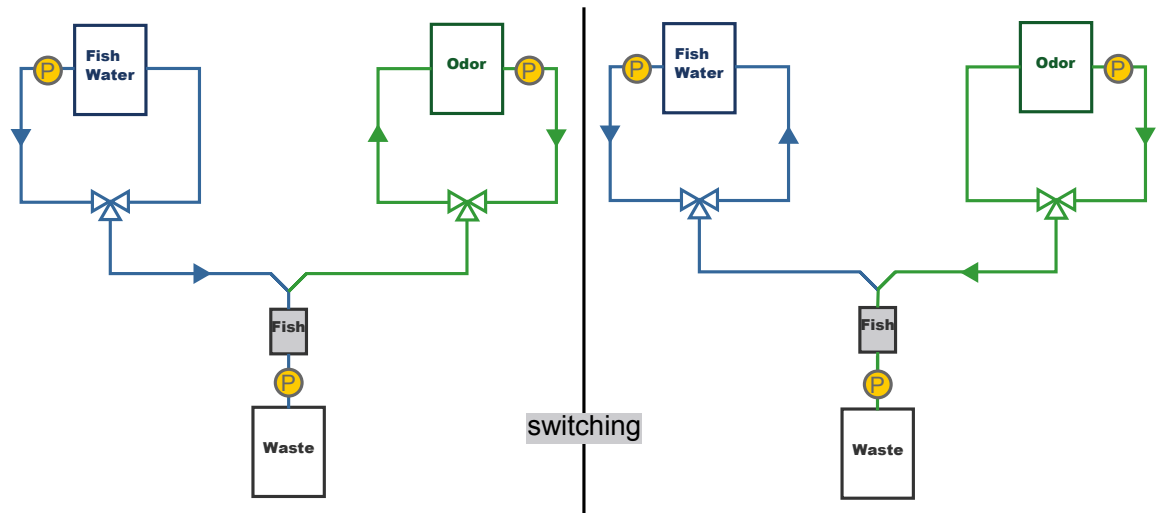


**Figure 3.17: Odor-delivery setup.** A sketch of the setup for odor-delivery. Left: Water (indicated in blue) is transported to the fish chamber. Right: After switching of the valves, odor (indicated in green) is passed through the chamber. The setup consists of valves with three ports each (indicated by triangles) and tubing pumps (indicated by yellow circles). In the left circle (blue) water stored in a tank is forwarded, in the right one (green) odor is circulating.

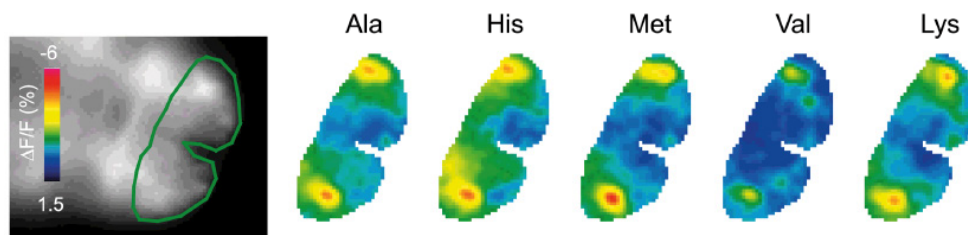


**Figure 3.18: Neuronal activity evoked by odor stimulation.** Activity response in the olfactory bulb of larva at 5 days post fertilization (dpf) when presenting different amino acids with a concentration of 1 mM. Figure taken from [45].

For classical fear conditioning it is crucial to present a short, intense stimulus as the US, which evokes a fear response. Therefore, a short heat pulse was provided by the infrared laser, adjusted to a higher power level than in operant conditioning. The laser intensity could be increased by diminishing the beam diameter to 1.4 mm and by increasing the measured power to about 550 mW, resulting in a surface power density of about 360 mW/mm<sup>2</sup>. These adjustments of the laser intensity resulted in fast and intense tail movements (see Figure 3.19).

Before starting an experiment, fish were introduced to the water flow for a few minutes. The timing of both stimuli and its computational implementation were crucial for the classical con-



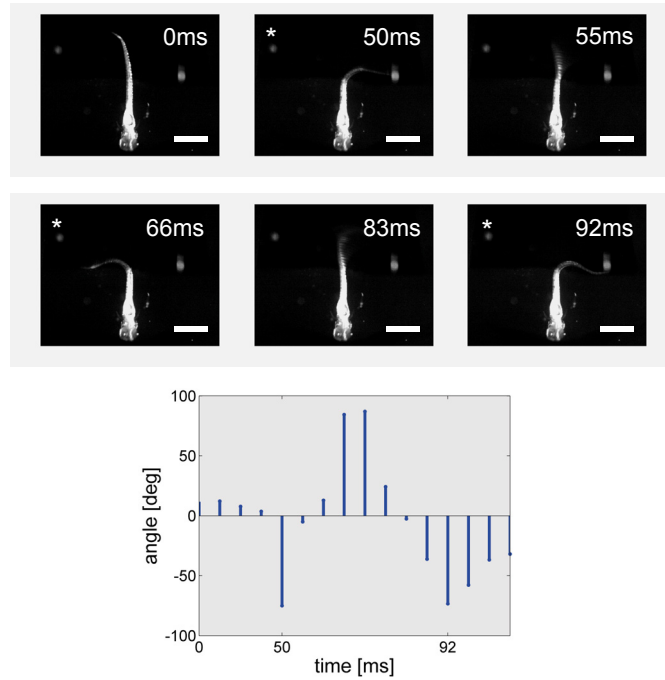


**Figure 3.19: Sample escape behaviour.** Struggling or escape behaviour is demonstrated in the time series, as typically provoked with a laser power of around 550 mW and a beam diameter of about 1.4 mm during classical conditioning. This behaviour can be characterized by fast and repetitive side to side movements. A typical side to side movement (indicated by asterisks) takes only about 20 ms on average. Such kind of movements are undesired during operant conditioning (cf. Section 3.4). Scale bars: 1 mm.

ditioning experiments (see Figure 3.20).

The odor pulse needed about two seconds to reach the fish's nose after switching the valves, therefore this duration needed to be taken into account when implementing the protocol ( $t_1$  in Figure 3.20). This duration could be estimated by measuring the length of tubing to the fish and considering a flow rate of  $60 \mu\text{l/s}$ . A length of  $l \approx 60 \text{ mm}$  gives a volume of  $V \approx 120 \mu\text{l}$ , therefore the period of time can be estimated by  $t = \frac{V}{\text{flowrate}} = 2 \text{ s}$ . The odor stimulus should be present for four seconds before the heat pulse was exposed, which lasted for two seconds. The interval between the onset of the CS and the onset of the US is called the inter-stimulus interval (IS). The design of the protocol intended, that both stimuli ended at the same time. The delay when closing the valves until the odor was rinsed out, must also be considered when implementing the protocol ( $t_2$  in Figure 3.20). These duration as well as  $t_1$  were additionally estimated by using water coloured with methylene blue.

During experimental realization, the number of pre-, as well as training trials varied. In order to obtain more data for comparing behavioural responses between stimulus and stimulus-

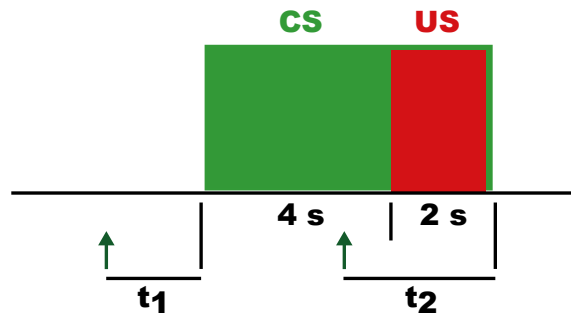


**Figure 3.20: Timing aspects for the classical conditioning protocol.** The time between the onset of the odor stimulation (CS) and the heat pulse (US) is planned to be four seconds (IS). The heat pulse lasts for two seconds and both stimuli should end at the same time. Arrows indicate the time for opening and closing the valves, the durations  $t_1$ ,  $t_2$  can be estimated.

free baseline periods, some experiments included up to three pre-trials. Since the pre-exposure of odor could influence the success of learning, pre-trials were skipped in some experiments to start directly with the training block. The total number of training trials also changed to fewer and more than ten during the course of development (seven to 20 training trials). The inter-trial interval (ITI), meaning the time from the end of US to the start of the subsequent trial, varied from two to maximal five-and-a-half minutes within all experiments. Some experiments were performed with a longer inter-stimulus interval (IS) than four seconds, defined from the onset of the CS to the onset of the US. Likewise, the duration of the US varied from two up to ten seconds.

### 3.6 Imaging Experiments

In order to get insights into neuronal computations in the larval zebrafish brain during conditioning, experiments of operant conditioning were combined with light field microscopy.

The preparation procedures before experimentation and the execution of the experiments took place under similar conditions as for operant conditioning without imaging (described in Section 3.4). The whole setup was then positioned below the objective of the microscope to allow imaging and simultaneous tail-tracking necessary for conditioning. Imaging of intracellular  $Ca^{2+}$  fluctuations was accomplished using an upright LFM with a  $20\times/0.5NA$  water-immersion objective (cf. Section 2.3.3).

During execution of a conditioning experiment, images were typically taken at 5 Hz for the first 30 or 60 seconds of single training trials, resulting in 150 or 300 frames for each trial respectively. Images of three trials in the beginning of the training block as well as at the end were stitched together to create time series consisting of 450 or 900 frames each. Frames taken by the behavioural camera were recorded with time stamps to allow for subsequent synchronization of neuronal activity with behavioural events.

Images captured by the camera system of LFM were then light field deconvolved by a reconstruction algorithm described in [38] (cf. Section 4.3).

Since axial resolution is limited, neurons cannot be identified by commonly used segmentation methods. Therefore, recordings obtained from zebrafish brain with LFM were fed into a signal extraction routine based on spatial independent component analysis (ICA) [48]. ICA is a possibility to extract the fluorescence signal indicating neuronal activity out of data. This signal extraction procedure tries to exploit the time domain to find statistically independent single volumes, resulting in identification of characteristic components. A post-selection procedure selected filters with specific size and spatial dispersion. A detailed description of this method and its implementation for extraction of activity traces, as well as more informations concerning reconstruction algorithms can be found in [38].

Due to computational reasons, the whole volume was divided into a group of up to 16 sub-volumes, each processed by the ICA separately. Data was reduced by keeping only 20 % of the voxels with highest variance. As a post-processing step, detrending of the data was performed by using a global detrend curve calculated during ICA in order to avoid bleaching effects of the fluorescent dye over time. Filters that did not show any response during recording were rejected, whereas a response was defined as a signal change of at least two standard deviations. The brain area was selected manually, so that filters identified outside the brain, such as within eyes, were rejected and only filters within the selected area were kept. After performing these post-processing steps, the fluorescence traces of all remaining spatial filters could be extracted through all time frames.



---

## Results

### 4.1 Operant Conditioning Experiments

I implemented an operant conditioning assay for 6 to 10 day old zebrafish, in which the larvae learned to escape an aversive heat stimulus provided by an infrared laser. By performing a tail flick in the rewarded direction, the animals were relieved from the aversive stimulus by turning it off.

#### **Example: a successful training experiment**

An example performance of a 7 day old larva is shown in Figure 4.1. The animal was trained to perform a tail flick to the left side in the first block (left training) and to turn right in the second block (right training). During an incorrect trial, turns to the non-rewarding direction were preceding the flick which initiated the relief of the aversive stimulus, whereas during a correct trial, the first turn pointed in the rewarded direction. The number of correct trials grew across the trials of one block during a successful training experiment (see Figure 4.1 A and B). The moment of laser termination exceeded the latency to the first stimulus-evoked action when the first turn was an incorrect one. In case of a correct trial, the time when the heat stimulus was terminated equated to the latency (see Figure 4.1 C). The recent performance could be calculated based on the number of correct and incorrect trials and outlined across each trial of one block (see Figure 4.1 D).

#### **Results of all performed experiments**

In total, 37 learners could be identified out of 95 performed experiments, meaning a fraction of 39 %.

Considering all learners ( $n = 37$ ), the mean recent performance increased across the trials of each block and reached an asymptotic value of 74 % in the first block and 70 % in the second block (see Figure 4.2). Both values were calculated for the last trial of each block and were significantly greater than 0.5 ( $p < 0.0001$ , one-sample t-test). Mean performance became significantly above chance within 11 trials in the first block ( $p = 0.018$ , one-sample t-test) and within 18 trials in the second one ( $p = 0.019$ , one-sample t-test).

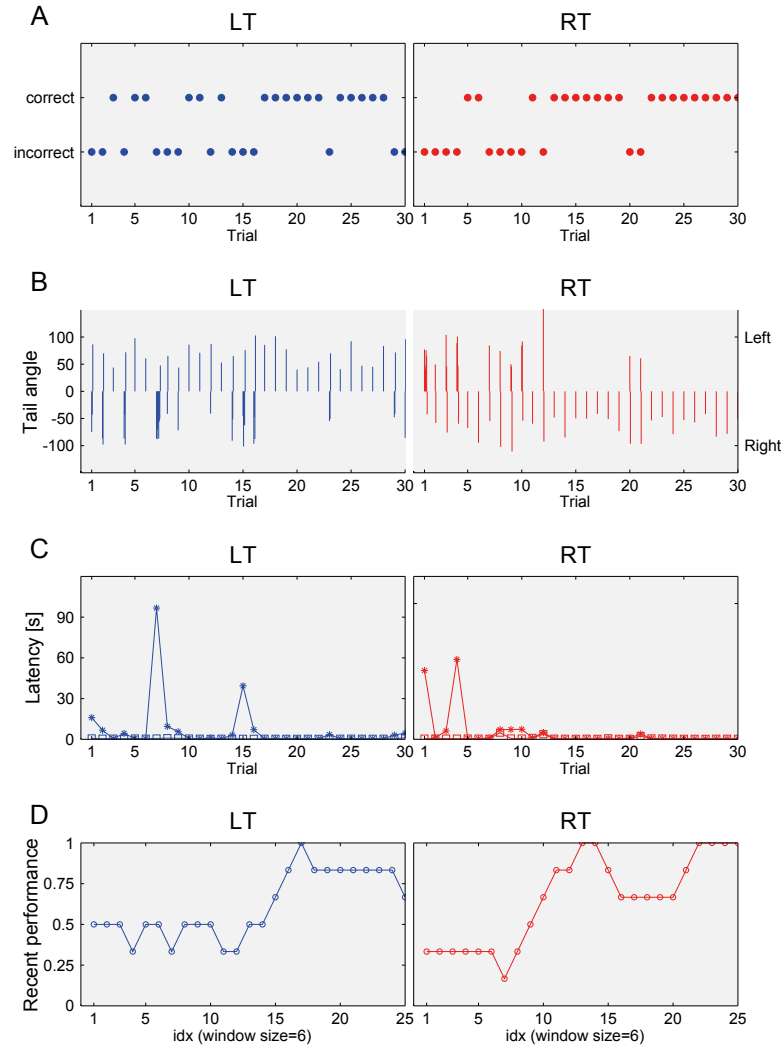


**Figure 4.1: A successful training experiment.** Example performance of a 7 day old larva, classified as a learner. The animal was trained to the left in the first block (LT) and to the right in the second block (RT), each block consisted of 30 trials. (A) In the first block, a trial was denoted as correct, if the first stimulus-evoked turn pointed to the left, and as incorrect if it pointed to the right. In the second block it was exactly the other way around. Correct trials appeared more often the higher the index of the trial within one block. (B) The direction of tail flicks until the correct turn are displayed. At the beginning of the left training, first stimulus-evoked turns to the right happened more often than at the end. For right training, the opposite effect can be observed. (C) The latency to the first stimulus-evoked action is plotted for both blocks (indicated by squares and a solid line). The time when terminating the heat stimulus is displayed as well (indicated by asterisks and dotted line). For correct trials, both points in time coincided, whereas the moment of laser termination exceeded the latency for incorrect trials. (D) The recent performance was calculated from the sixth trial on, based on the number of correct trials (cf. Section 3.4.1).

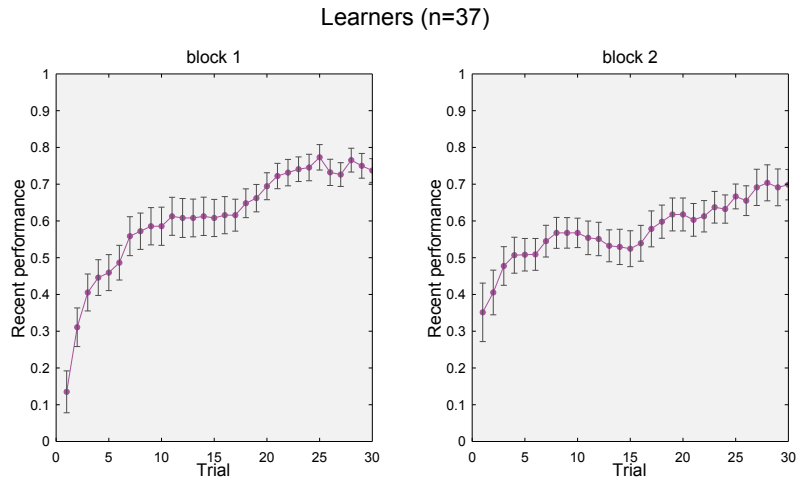


**Figure 4.2: Recent performance of learners.** Recent performance for learners ( $n = 37$ ) is plotted for both blocks. It reached an asymptotic value of 74 % in the first block and 70 % in the second block. Each point represents the mean recent performance of all learners in a given trial  $\pm$  SEM.

47 animals fell into the category of non-learners 1, which did not show a positive learning progress in the first block (see Figure 4.3). The mean performance of all animals of this class stayed below 0.5 at the end of the block, reaching a value of 19 %. It differed significantly from the asymptotic performance of learners in the first block ( $p < 0.0001$ , two-sample t-test after one-sample Kolmogorov-Smirnov test for normal distribution).

11 animals showed a final performance less than 0.5 in the second block and no improvement in learning in the first block. Thus, they were counted among the class of non-learners 2 (see Figure 4.4). The performance at the end of the second block reached a mean value of 19 %, which was significantly different from the asymptotic performance of learners in the second block ( $p < 0.0001$ , two-sample t-test after one-sample Kolmogorov-Smirnov test for normal distribution). From beginning to the end of the first block no significant improvement in learning could be obtained (two-sample t-test).

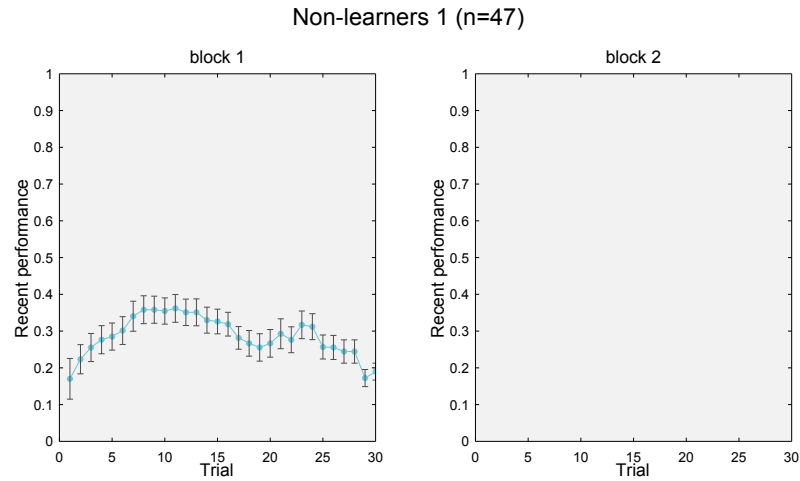


**Figure 4.3: Recent performance of non-learners 1.** Recent performance for non-learners 1 ( $n = 47$ ) is plotted for the first block, the second block was not performed in this case. The recent performance at the end of the first block amounted to 19 %. Each point represents the mean recent performance of all non-learners 1 in a given trial  $\pm$  SEM.

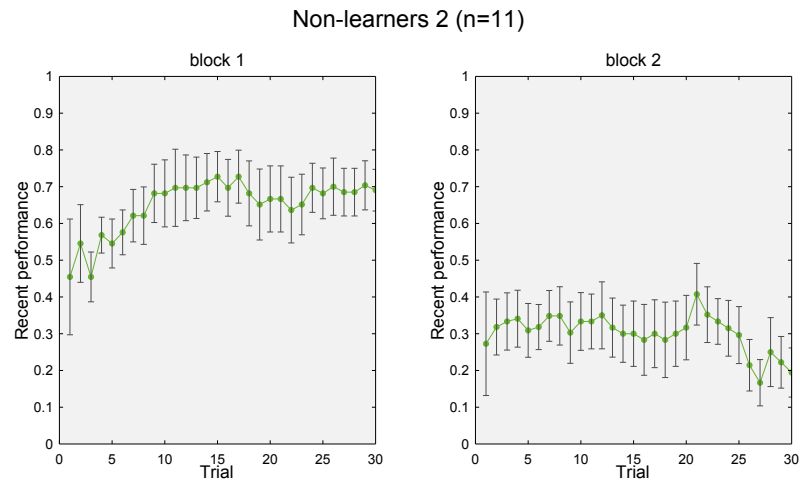


**Figure 4.4: Recent performance of non-learners 2.** Recent performance for non-learners 2 ( $n = 11$ ) is plotted for both blocks. The performance at the end of the second block was 19 %, no improvement in the first block could be obtained. Each point represents the mean recent performance of all non-learners 2 in a given trial  $\pm$  SEM.

#### Performances based on differing experimental conditions

Some parameters were crucial for the success of training and thus influenced the quantity of learners. As mentioned before, in one part of the experiments the agarose and water within the chamber, where the fish larva was embedded, was warmed to about 26 °C by using a cham-



ber with integrated infrared LEDs. Apart from that, some experiments were performed with a water flow provided by an odor-delivery setup for odor stimulation (see Section 4.1.1). The ratio of learners and non-learners varied, depending on experimental conditions (see Figure 4.5).

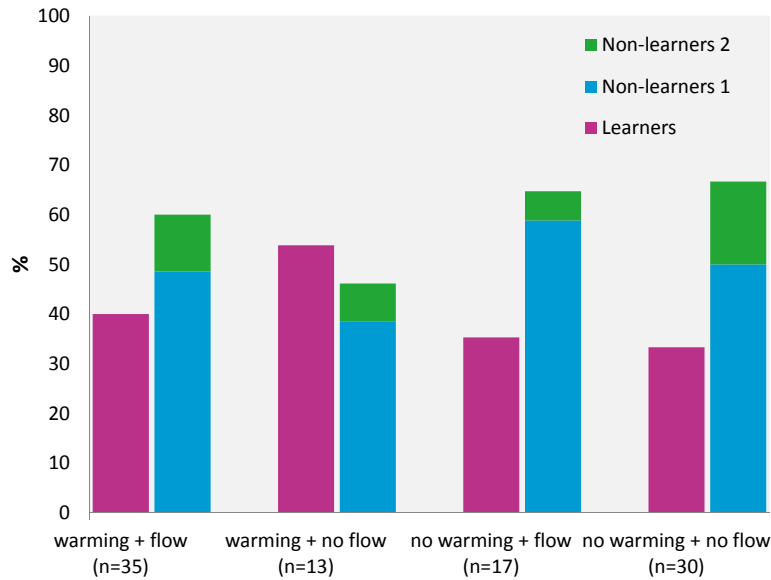


**Figure 4.5: Ratio of learners and non-learners dependent on differing experimental conditions.** 35 of the experiments were performed with warming and water flow, resulting in a fraction of 40 % learners, 49 % non-learners 1 and 11 % non-learners 2. 13 experiments were performed with warming of the chamber, but without a water flow. These conditions resulted in a fraction of 54 % learners, 38 % non-learners 1 and 8 % non-learners 2. 17 experiments with no warming but water flow resulted in a fraction of 35 % learners, 59 % non-learners 1 and 6 % non-learners 2. 30 experiments were performed with neither warming nor water flow, resulting in a fraction of 33 % learners, 50 % non-learners 1 and 17 % non-learners 2.

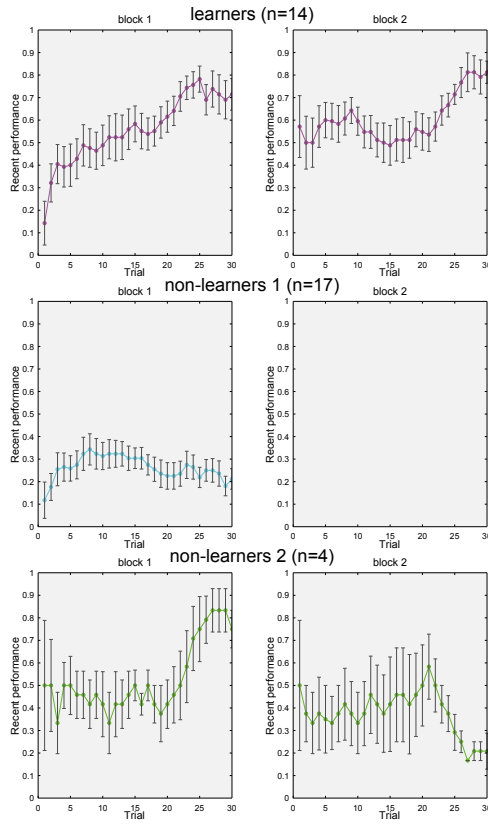
35 out of a total of 95 experiments were performed with water flow, whereby the water was warmed beforehand. These experiments resulted in 14 learners, 17 non-learners 1, and 4 non-learners 2, which gives a fraction of 40 % of successful training experiments (40 % learners, 49 % non-learners 1 and 11 % non-learners 2).

If the inward of the chamber was warmed with integrated LEDs without a water flow, 7 learners out of 13 experiments could be obtained, meaning a relative value of 54 %. 5 of the non-learners were of type 1, and only 1 of type 2 (54 % learners, 38 % non-learners 1 and 8 % non-learners 2).

Otherwise, if there was no warming during the experiment, but water passed through the chamber, 35 % of the 17 experiments showed successful training, meaning 6 learners, 10 non-learners

1, and 1 non-learner 2 (35 % learners, 59 % non-learners 1 and 6 % non-learners 2). 30 experiments were performed with neither warming nor water flow, resulting in 10 learners, 15 non-learners 1 and 5 non-learners 2. Therefore, only 33 % of these experiments were successful (33 % learners, 50 % non-learners 1, and 17 % non-learners 2). These results indicated, that an important condition for a successful training experiment was to warm up the inward of the chamber to about 26 °C. Flow did not have such an influence as warming, but better success of training was achieved for experiments without flow. The corresponding recent performances of learners and non-learners separated by differing conditions are represented in Figures 4.6 A, B and 4.7 C, D.

**A warming + flow (n=35)**



**B warming + no flow (n=13)**

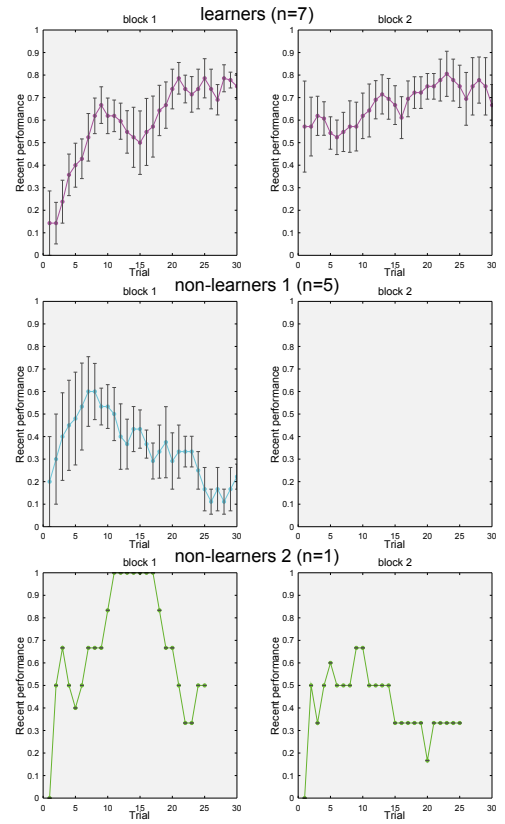
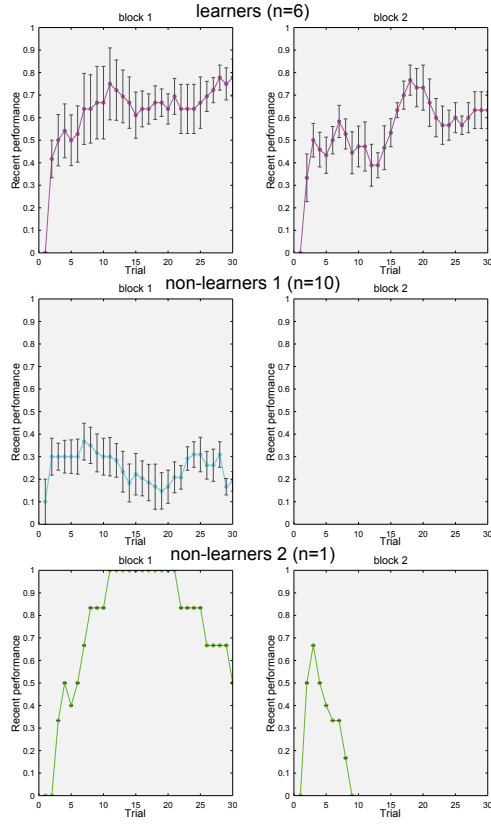


**Figure 4.6: Performances based on differing experimental conditions: with warming.** The recent performances of learners and non-learners separated by differing conditions for 95 experiments altogether. (A) 35 of the experiments were performed with warming and water flow, resulting in a fraction of 40 % successful training experiments. (B) 13 experiments were performed with warming of the chamber with integrated LEDs, but without a water flow, 54 % of experiments were successful.

C no warming + flow (n=17)



D no warming + no flow (n=30)

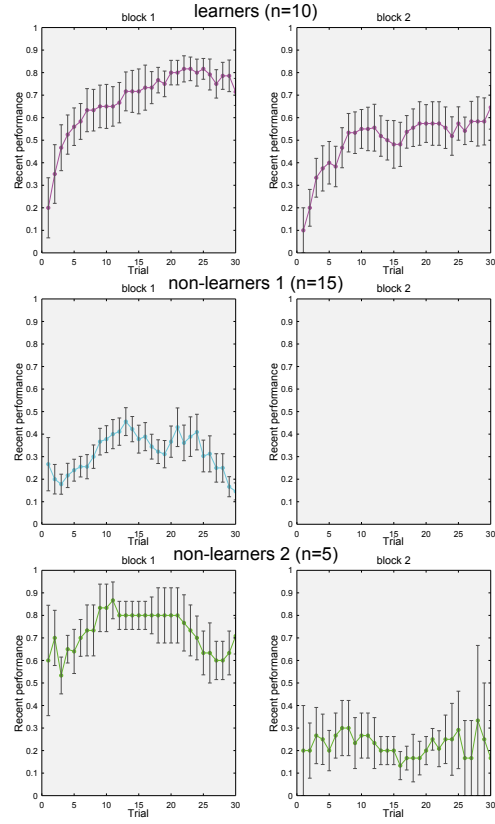


**Figure 4.7: Performances based on differing experimental conditions: without warming (continued Figure 4.6).** (C) No warming but water flow resulted in a fraction of 35 % successful trainings. (D) 30 experiments were performed with neither warming nor water flow, resulting in 33 % successful experiments. (A)-(D) Each point represents the mean recent performance of respective fish in a given trial  $\pm$  SEM.

### Latency modulated by recent performance

Figure 4.8 shows the latency to the first stimulus-evoked turn as a function of recent performance. There was a slight trend, that the latency to the first action, either a correct or an incorrect turn, was modulated by recent performance.

It is known that learning can shorten latency to respond to a rewarded stimulus in primates [42], a similar relationship could be shown in [28] for an aversive stimulus with relief presented to larval zebrafish. Similar to the unpublished work of Florian Engert it could be obtained, that the latency to the first stimulus-evoked turn decreased as performance improved when observing data of every trial from all learners ( $n = 37$ ). This difference is statistically significant when comparing latency values for low recent performance ( $= 0$ ) and for high recent performance ( $= 1$ ) ( $p = 0.009$ , Welch-t-test).

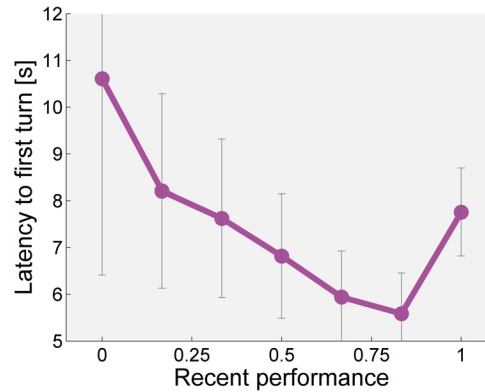


**Figure 4.8: Latency modulated by recent performance.** Latency to the first stimulus-evoked turn decreased as performance improved. Each point represents the median of latency of all trials performed by learners ( $n = 37$ ) as a function of recent performance  $\pm$  SEM.

#### 4.1.1 Experiments with Additional Odor Stimulation

In order to investigate if larvae are able to associate a neutral odor with a specific direction of tail movement, an additional odor stimulus during the first training block within an operant conditioning experiment was presented to the fish (see Section 3.4.3).

The test block gave indication for the association of odor with a specific direction by counting the amount of turns in the respective direction. The block including ten test trials was performed only for learners (4 out of 10 experiments). The data of these four successful conditioning experiments are shown in Figures 4.9 - 4.12.

The bias determination for these four experiments resulted in left training during the first training block. In experiments 1 and 2, Lysine in the final concentration of  $100 \mu\text{M}$  was used as odor stimulation during the first training block and the test block, whereas in experiment 3 the amino acid Alanine was presented in the same concentration. In experiment 4 the fish was stimulated with  $500 \text{ mM}$  Cysteine. The second block (right training) was performed without any odor stimulation in each case.

In experiments 1 to 3 no increased turning to the first training direction (left) could be observed during the test block (experiment 1: 1 out of 10 to the left, experiment 2 and 3: 2 out of 10). In experiment 4, the animal's tail pointed to the left in 7 out of 10 test trials. Thus, one out of four fish showed a turning behaviour predominately into the odor trained direction, indicating that in this case an association between Cysteine and the directional tail flick to the left took place. In the other three experiments, the majority of first stimulus-evoked turns within the test trials pointed to the right, which corresponded to the training direction immediately before the test block.

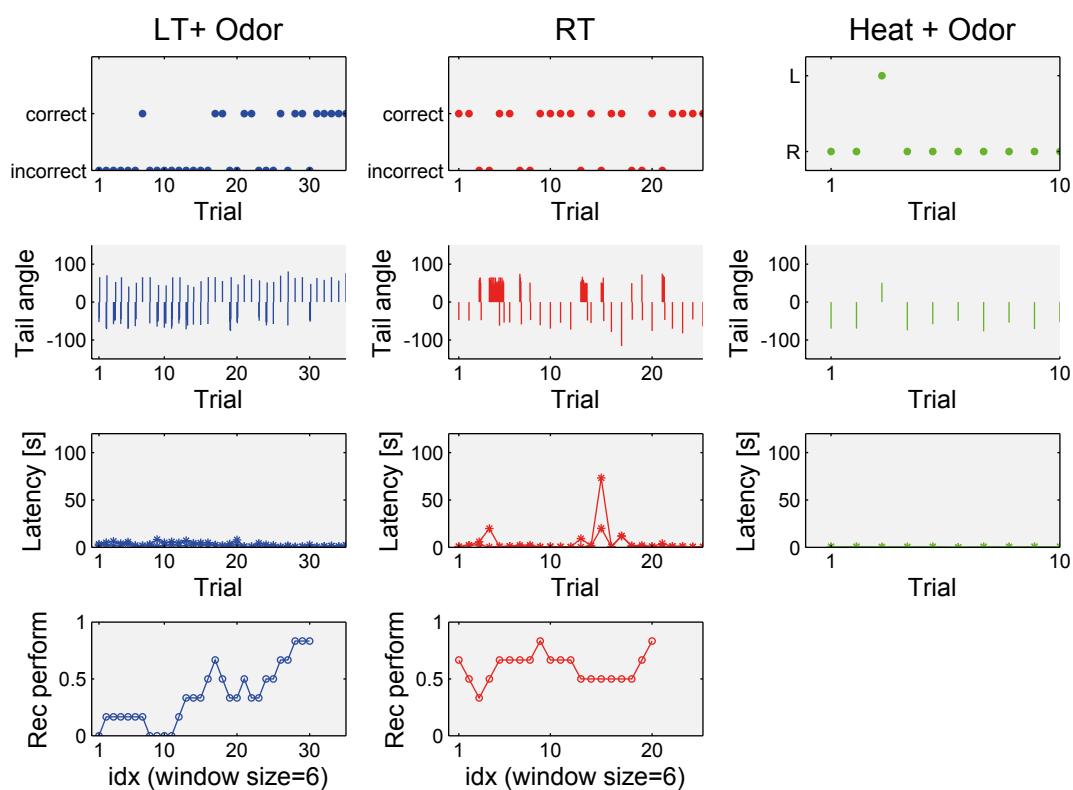


**Figure 4.9: Operant conditioning with odor stimulation: Experiment 1.** During the first block (left training) an additional odor pulse was presented simultaneously to the heat stimulus (100  $\mu$ M Lysine). In the test block, where again heat and odor was presented, only one first stimulus-evoked turn pointed to the left.

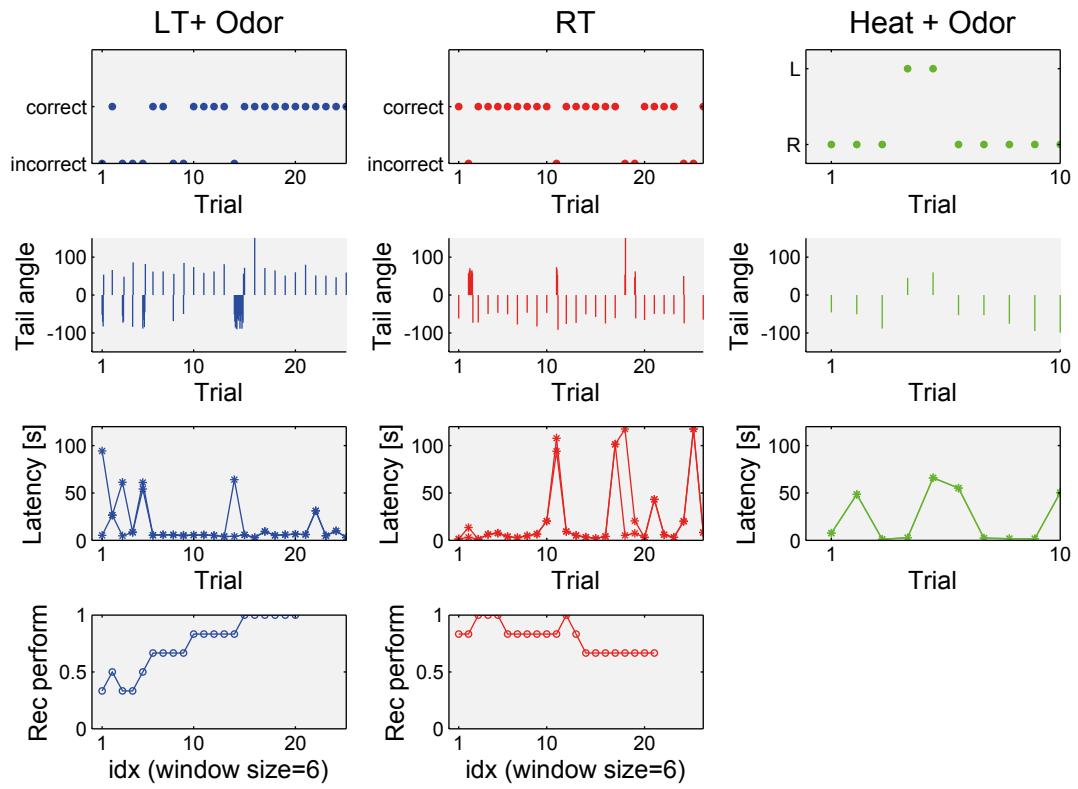


**Figure 4.10: Operant conditioning with odor stimulation: Experiment 2.** 100  $\mu$ M Lysine was presented to the fish simultaneously with heat during the first block (left training). Only two of 10 test trials showed a stimulus-evoked turn to the left.

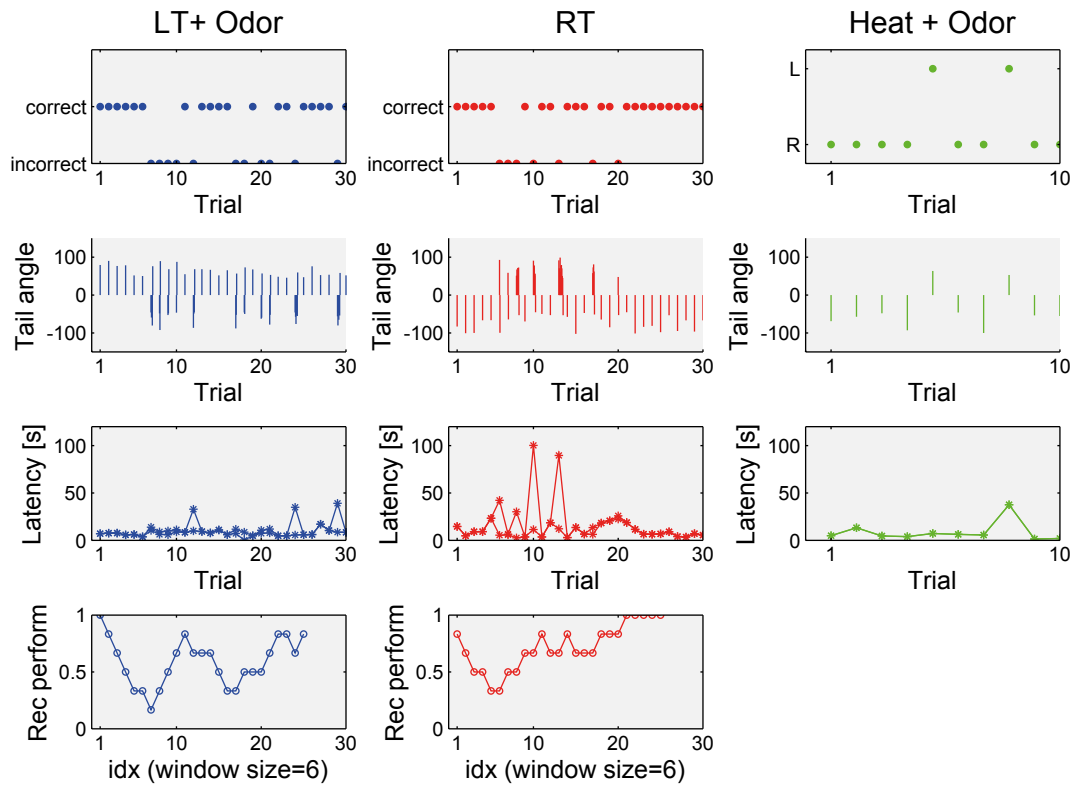


**Figure 4.11: Operant conditioning with odor stimulation: Experiment 3.** 100  $\mu$ M Alanine was used for odor stimulation in the first (left training) and the test block. Only in two test trials the animal performed a turn to the left.

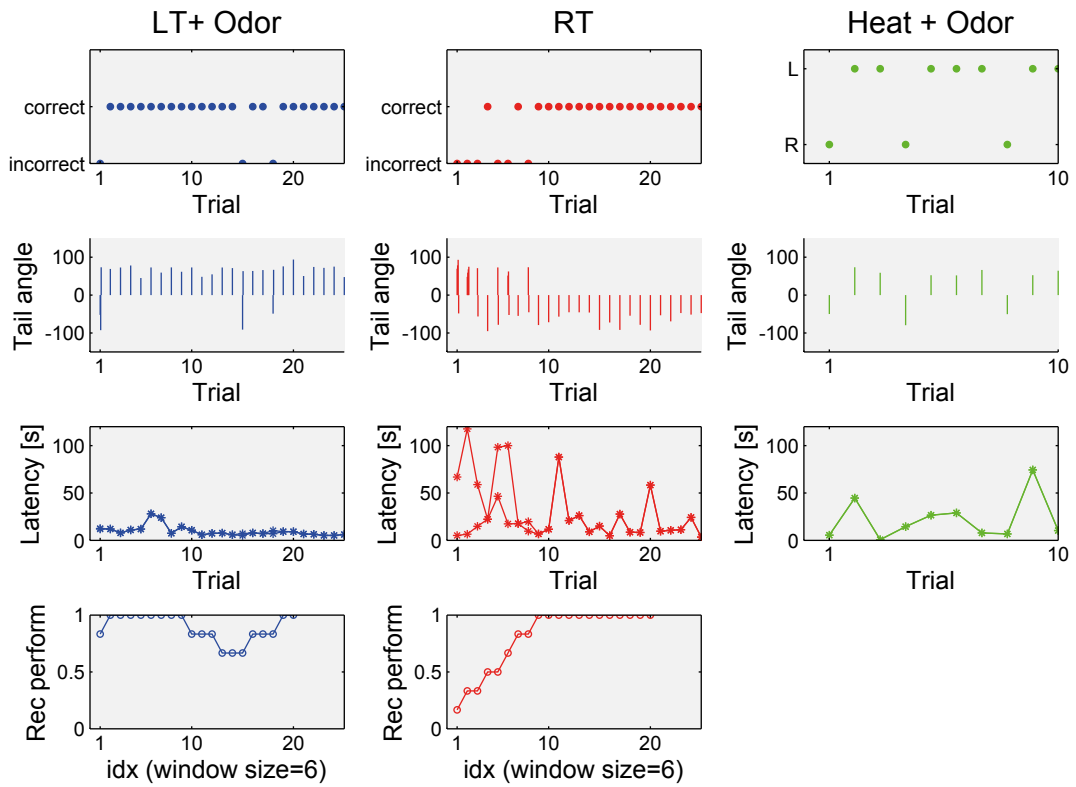


**Figure 4.12: Operant conditioning with odor stimulation: Experiment 4.** During left training in the first block, Cysteine in the concentration of  $500 \mu\text{M}$  was presented to the fish. After successful training, odor and heat were exposed to the fish resulting in a first stimulus-evoked turn to the left in 7 out of 10 test trials.

Since only one of four experiment showed tail flicks more often to the odor-related direction than into the other, a clear learning effect could not be displayed for this assay. In order to ensure the ability of larvae to associate a single amino acid with a tail flick in a specific direction, the experiment with similar conditions needs to be repeated more often.



## 4.2 Classical Fear Conditioning Experiments

I established a classical fear conditioning protocol for embedded zebrafish larvae, in which the fish were trained to associate an olfactory CS paired with a short aversive heat stimulus (US) resulting in enhanced tail movements (UR). After training, the odor pulse alone should lead to an increased response (CR).

In order to quantify potential tail movements during the odor stimulation, the measure  $A_{increase} = \frac{A_{CS}}{A_{base}}$  was defined (see Section 3.5.1). It compared the motor responses in the period of the CS (described by  $A_{CS}$ ) with spontaneous tail movements during a stimulus-free interval ( $A_{base}$ ).

By calculating this measure for each trial of the training and test block, the CR during the CS could be identified for every single trial and compared to each other. The effect after successful learning would be an enhanced tail movement during the CS but before US presentation in training trials in the ideal case, resulting in an increasing  $A_{increase}$  across the trials, but at least enhanced values of  $A_{increase}$  in the test trials.

The effect of paired stimuli during the training block could be investigated by plotting the measure  $A_{increase}$  for each trial of training, as well as for test trials. Figure 4.13 shows the progress of  $A_{increase}$  across ten training trials and three test trials for two experiments. Similar activity during the CS and the baseline interval within one trial resulted in  $A_{increase} \approx 1$ , whereas  $A_{increase} > 1$  indicated an enhanced movement during the CS. High values of  $A_{increase}$  in the test trials and a slight increase of the measure when coming to the end of the training block could be observed for the experiment shown in Figure 4.13 A, suggesting a success of training. Another example of a typical experiment is shown in Figure 4.13 B, where no higher values of  $A_{increase}$  at the end of training compared to the beginning could be obtained.

### Results of all performed experiments and classification

Altogether, 41 experiments following the classical conditioning protocol were performed, whereas for a few of them an increased activity during the CS interval, resulting in high values of  $A_{increase}$ , could be obtained. Experiments, in which animals showed behavioural responses just as the valves were opened or closed, were excluded from further analysis.

When observing the performances of an animal during the test trials and the progress of  $A_{increase}$  across the training trials, different cases could be observed. In most experiments, neither a trend in increasing values across the training must be obtained, nor enhanced tail movements during the CS in the test trials. In some experiments, fish showed an enhanced tail movement when the odor was presented shortly before the heat stimulus arrived during training or at least in the CS interval of the test trials.

According to that observation, all experiments were manually classified into three groups. If fish showed a higher  $A_{increase}$  during the test trials or additionally at the end of training than in the beginning, the experiment was suggested to be "positive". The class "in between" contained experiments, where no definite trend of an increasing  $A_{increase}$  across the training trials could be observed, but where at least one test trial showed a high value of  $A_{increase}$ . In order to be

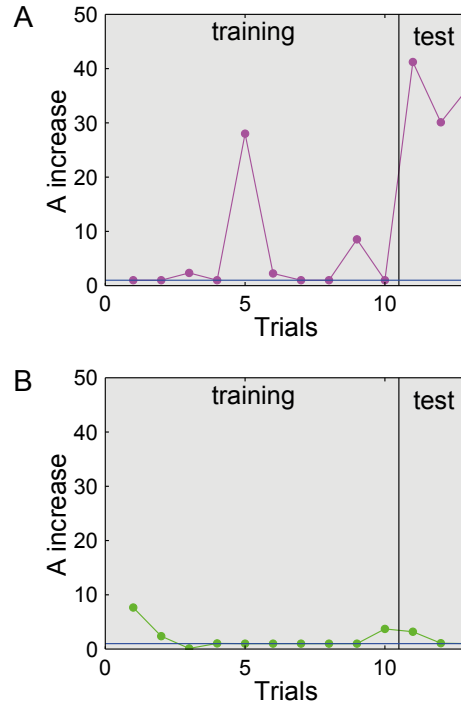


**Figure 4.13: Learning progress for two sample experiments.** The progress of the measure  $A_{increase}$  across ten training trails and three test trials for two sample experiments. (A) High values of  $A_{increase}$  in the test trials and isolated increased values during the training could be observed, suggesting a success of training. (B) Figure shows sample data of another experiment, no learning progress across the trials could be obtained.

classified as "negative", neither increasing values across the training must be observed, nor in the test trials.

By means of this manual classification, 8 experiments fell into the class "positive", 17 into "in between" and 16 were defined to be "negative". By averaging over  $A_{increase}$  values of single fishes amongst a category, the training performance for each class is shown in Figure 4.14.

When including all performed experiments ( $n = 41$ ) and comparing the mean values of  $A_{increase}$  at the beginning of training (training 1-4) and the test block (test 1-3), a significant increase of  $A_{increase}$  could be observed ( $p = 0.002$ , Welch-t-test). The mean value at the beginning of training was  $2.1 \pm 0.3$  and of the test block  $4.9 \pm 0.8$ .

When observing only "positive" experiments ( $n = 8$ ), the mean of  $A_{increase}$  from beginning of training significantly differed from that of the test block ( $p < 0.001$ , Welch-t-test), with mean values  $2.1 \pm 0.8$  and  $12.6 \pm 2.5$ , respectively.

Likewise, for the class defined as "in between" ( $n = 17$ ),  $A_{increase}$  at the beginning of training significantly differed from testing ( $p = 0.04$ , Welch-t-test). The mean values were  $1.8 \pm 0.6$  and  $4.7 \pm 1.3$  for beginning and testing, respectively. For "negative" experiments ( $n = 14$ ), no significant increase of the measure  $A_{increase}$  from beginning of training to the test block could

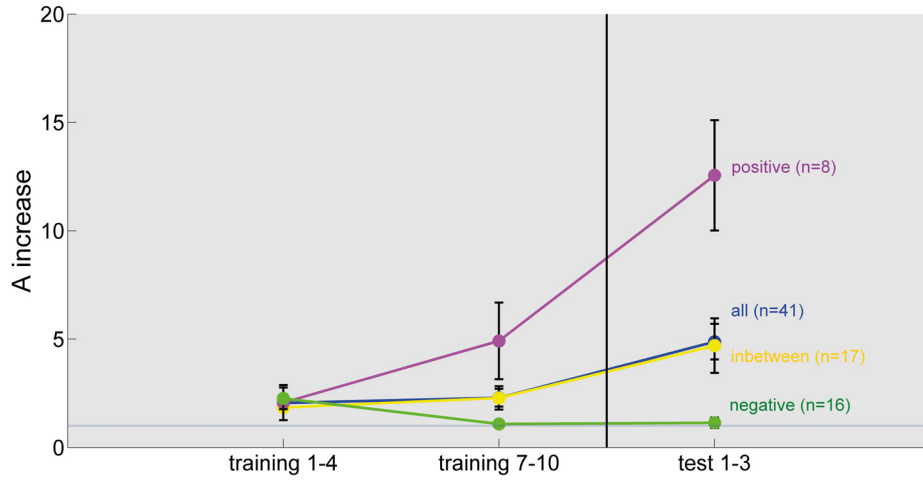


**Figure 4.14: Training progress of animals classified into three groups.** Altogether 41 experiments were performed (indicated in blue). By means of the manual classification, 8 experiments were defined as "positive" (magenta), 17 as "in between" (yellow) and 14 as "negative" (green). When comparing the mean values of  $A_{increase}$  at the beginning of training (training 1-4) and the test block (test 1-3), a significant increase could be obtained for the classes "positive" and "in between", as well as for all experiments. Each point represents the mean  $A_{increase}$  value for all fish amongst each class in a given training status  $\pm$  SEM.

be obtained, mean values were  $2.3 \pm 0.5$  and  $1.1 \pm 0.2$ .

In order to investigate a potential learning progress throughout the experiments, the probability distribution for each training status was calculated. Figure 4.15 shows data in logarithmic scale of all experiments ( $n = 41$ ) averaged for the distinct training statuses.

A measure for the asymmetry of a probability distribution of a defined variable is the skewness. When plotting the data points for each training status in logarithmic scale, a symmetric distribution around the value  $10^0 = 1$  would result in a skewness of zero, meaning that the number of data points above and below 1 are equal. This would be the case if all animals showed the same activity during the CS compared to the baseline activity on average, meaning a mean  $A_{increase}$  value of 1.

The distribution of the data points amongst the first training status, meaning the beginning of training (tr 1-4), had a skewness of 0.2, indicating an almost symmetric distribution (with a 90 %- confidence interval of  $[-1.2, +2.0]$  from the bootstrap distribution of skewness).

A general trend for enhanced  $A_{increase}$  values across the training would result in a shift of the skewness to more positive values when observing the distributions of subsequent training statuses.

The distribution of data points at the end of training (tr 7-10) was positive skewed, the value of

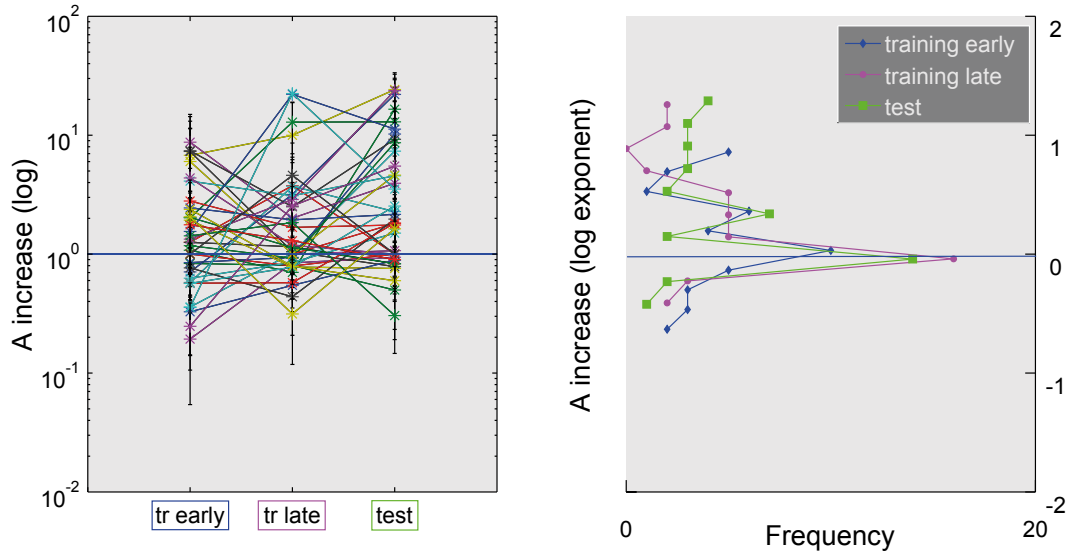


**Figure 4.15: Distribution of  $A_{increase}$  for all experiments.** *Left:* The mean values of  $A_{increase}$  for the three training statuses (training early means trials 1-4, training late means trials 7-10, test) were plotted in logarithmic scale for single experiments. When considering all experiments in a given training status, a symmetric distribution of the data points around  $10^0 = 1$  would indicate no increase in activity during the CS compared to the baseline activity on average. **Right:** The distributions of all data points for a given training status are plotted in logarithmic scale (training early in blue, training late in magenta, test in green). When calculating the skewness of the distributions, a slight shift of the distributions could be observed. The corresponding skewness values were 0.2 for training early, 1.2 for training late and 0.5 for test.

skewness is 1.2 (with a 90 %- confidence interval of  $[-0.7, +2.8]$  from the bootstrap distribution). For the test trials, the distribution was slightly positive skewed as well with a skewness of 0.5 (with a 90 %- confidence interval of  $[-0.6, +3.1]$  from the bootstrap distribution). This outcome indicated a slight training effect in the classical conditioning assay when considering data of all performed experiments.

### 4.3 Preliminary Results of Imaging Experiments

In order to get insights into neuronal computations in the larval zebrafish brain during conditioning, experiments of operant conditioning were combined with light field microscopy. Whole brain imaging was performed with LFM before and after learning, which allowed neurons to be identified and analyzed.

During execution of an operant conditioning experiment, images of the brain were taken during single training trials at the beginning and at the end of one block (cf. Section 3.6). Images captured by the camera system of LFM were then light field deconvolved by a reconstruction algorithm described in [38], which yielded a reconstructed volume for each frame displaying the zebrafish brain. The volume is represented by 51 equidistant planes spaced  $4\text{ }\mu\text{m}$  apart ranging from  $-100\text{ }\mu\text{m}$  to  $100\text{ }\mu\text{m}$ . Several z-slices of a reconstructed zebrafish brain taken from different z-depth are shown in Figure 4.16 to illustrate the  $Ca^{2+}$  signal across the brain.

By employing the signal extraction procedure based on ICA on a reconstructed dataset consisting of 900 frames in time, more than 2000 spatial filters across the brain of a zebrafish larva could be identified (see Figure 4.17).

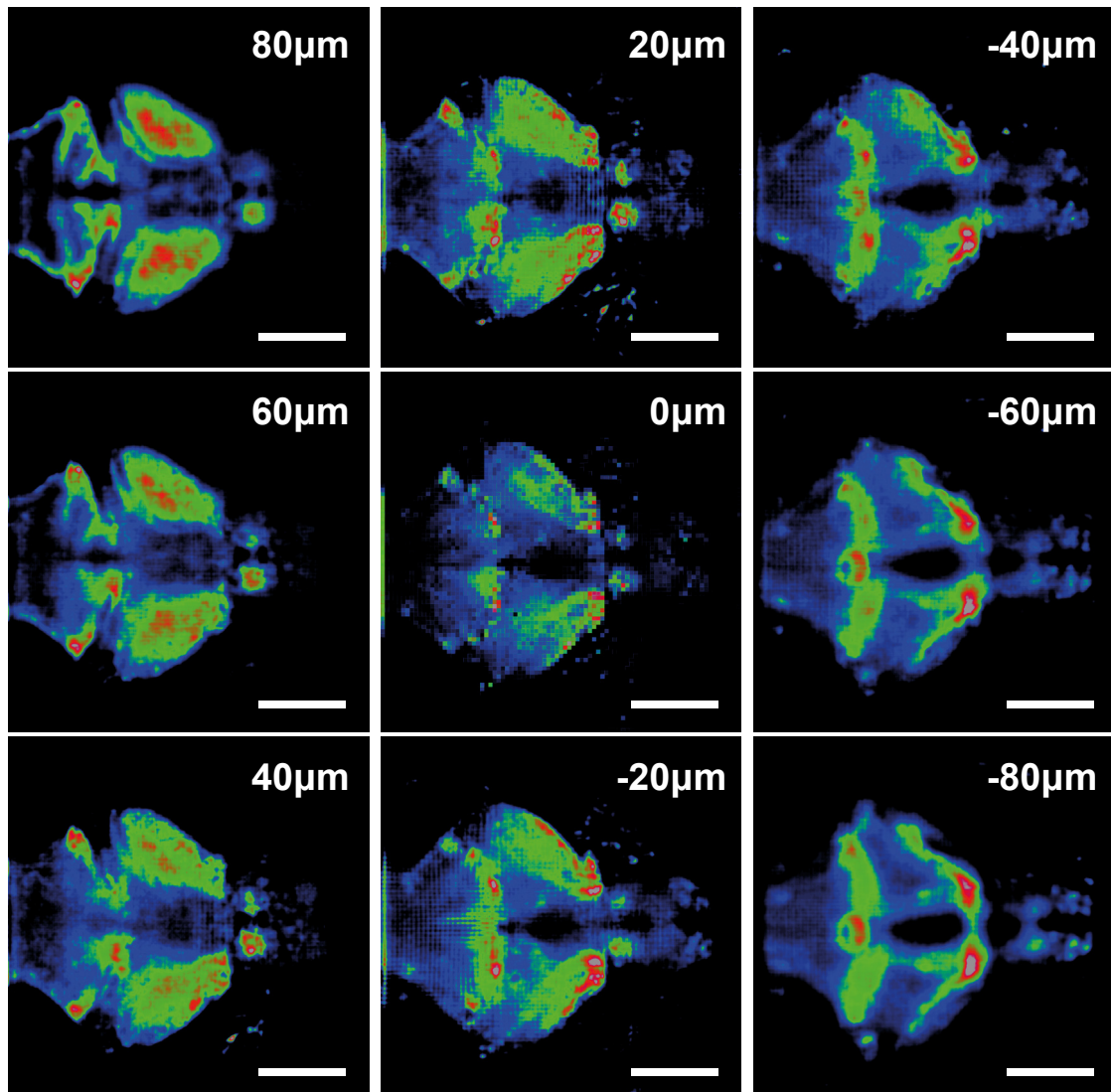


**Figure 4.16: Reconstructed brain of zebrafish larvae.** Several z-slices after reconstruction of a zebrafish brain. Reconstruction space extended from  $-100\ \mu\text{m}$  to  $100\ \mu\text{m}$  in  $4\ \mu\text{m}$  steps. Structures of the forebrain, such as olfactory bulb and habenula, are observable, as well as the midbrain and parts of the hindbrain. Scale bar:  $150\ \mu\text{m}$ .

#### **Recordings of neuronal activity during conditioning**

One operant conditioning experiment combined with imaging was performed, where the fish could be classified as a learner. The fish was trained to perform a turn to the right direction in the first block (right training). The performance of the animal during successful training is shown in Figure 4.18.

During the experiment, 30 s long recordings at 5 Hz of neuronal activity were done for several

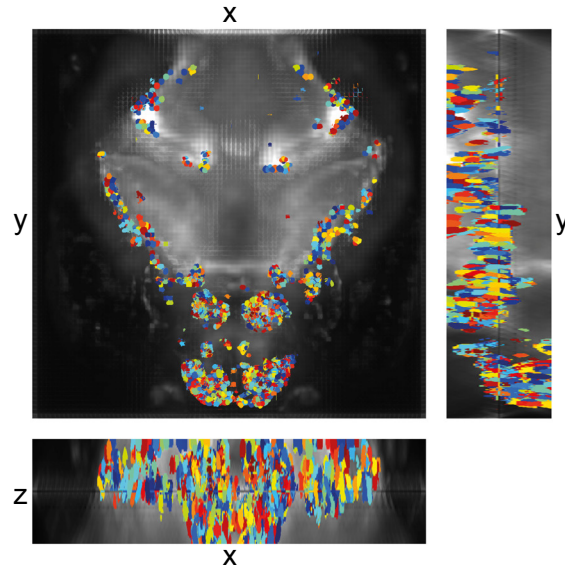


**Figure 4.17: Identified spatial filters by ICA.** By employing ICA procedure on a reconstructed dataset more than 2000 spatial filters across a larval zebrafish brain were identified. They are shown overlayed with maximum intensity projections of the volume.

trials before learning, meaning at the start of the first training block (indicated as "RT start"), as well as after learning, meaning at the end of the first block ("RT end"). In order to ensure the observation of activity traces of equal neurons, images of three trials were stitched together in each case, resulting in time series consisting of 450 frames each.

Processing of the data resulted in a set of about 600 spatial filters for "RT start" and almost 1900 for "RT end" (see Figure 4.19 A and 4.20 A).

Corresponding activity traces of spatial filters are given as the change in fluorescence  $\Delta F$  over baseline fluorescence  $F_0$  along time in Figures 4.19 B and 4.20 B. Neuronal activity was synchronized subsequently with events of the conditioning protocol and behaviour. Thus, the time of heat exposure and termination as well as tail movements could be mapped within activity traces.

In order to obtain subsets of neurons with similar responses, a partitioning method based on k-means clustering was performed on data. Clusters containing neurons which showed sufficient activity changes were selected manually and the corresponding fluorescence responses plotted over time (Figures 4.19 C and 4.20 C).

Especially when observing single clusters, a coincidence of activity changes with events was partly identifiable. Even though some neurons showed activity without stimulation, meaning before heat exposure, they also responded to the heat stimulation with increased or decreased activity. Neurons particularly responding when performing a turn to the left or right, as well as general patterns in activity changes consistent throughout the experiment could not be identified. Further investigations and analysis tools would be necessary to correlate specific neurons with

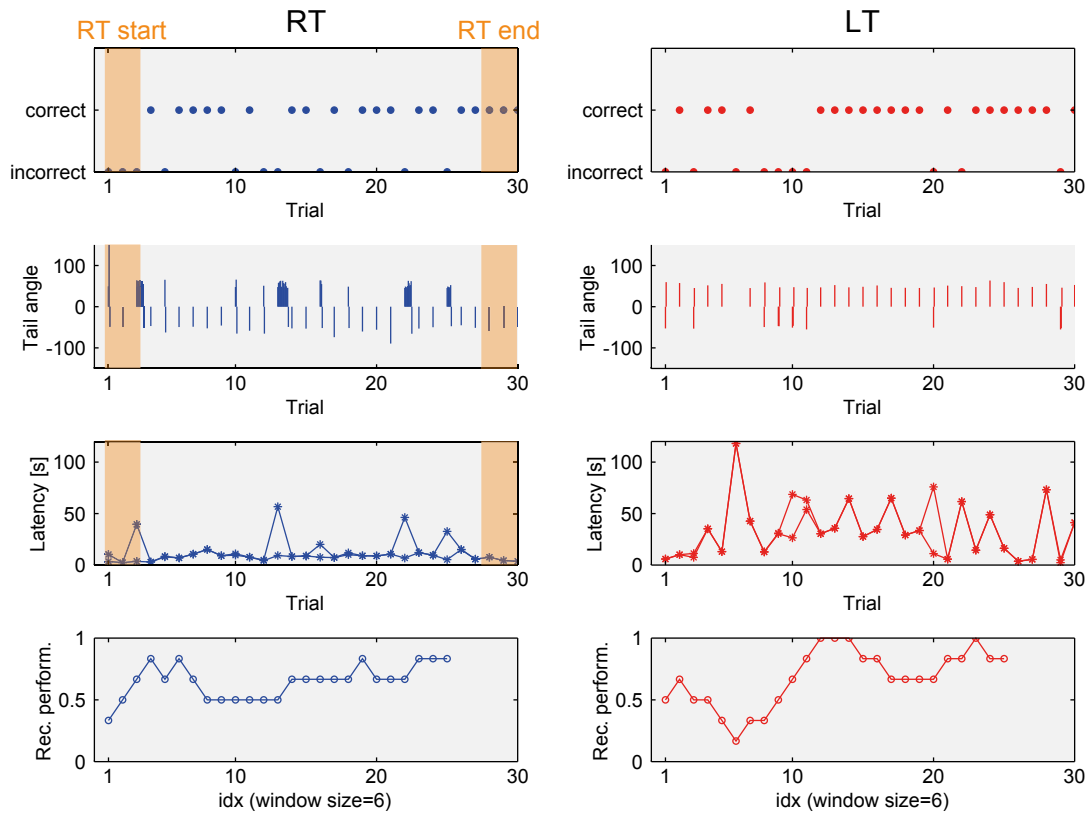


**Figure 4.18: Performance of learner combined with imaging.** The conditioning experiment combined with imaging consisted of two training blocks (RT and LT) of 30 trials each and yielded a learner. Imaging was performed for the first 30 or 60 seconds of single trials at the beginning and at the end of the first training block, images of three trials were combined in each case for reconstruction and further analysis (signed in orange color and indicated as "RT start" and "RT end").

behavioural responses. The habenula located in the forebrain would probably be one of the most interesting part to look at in further investigations of neuronal processes that underlie learning and memory [2, 43, 28].



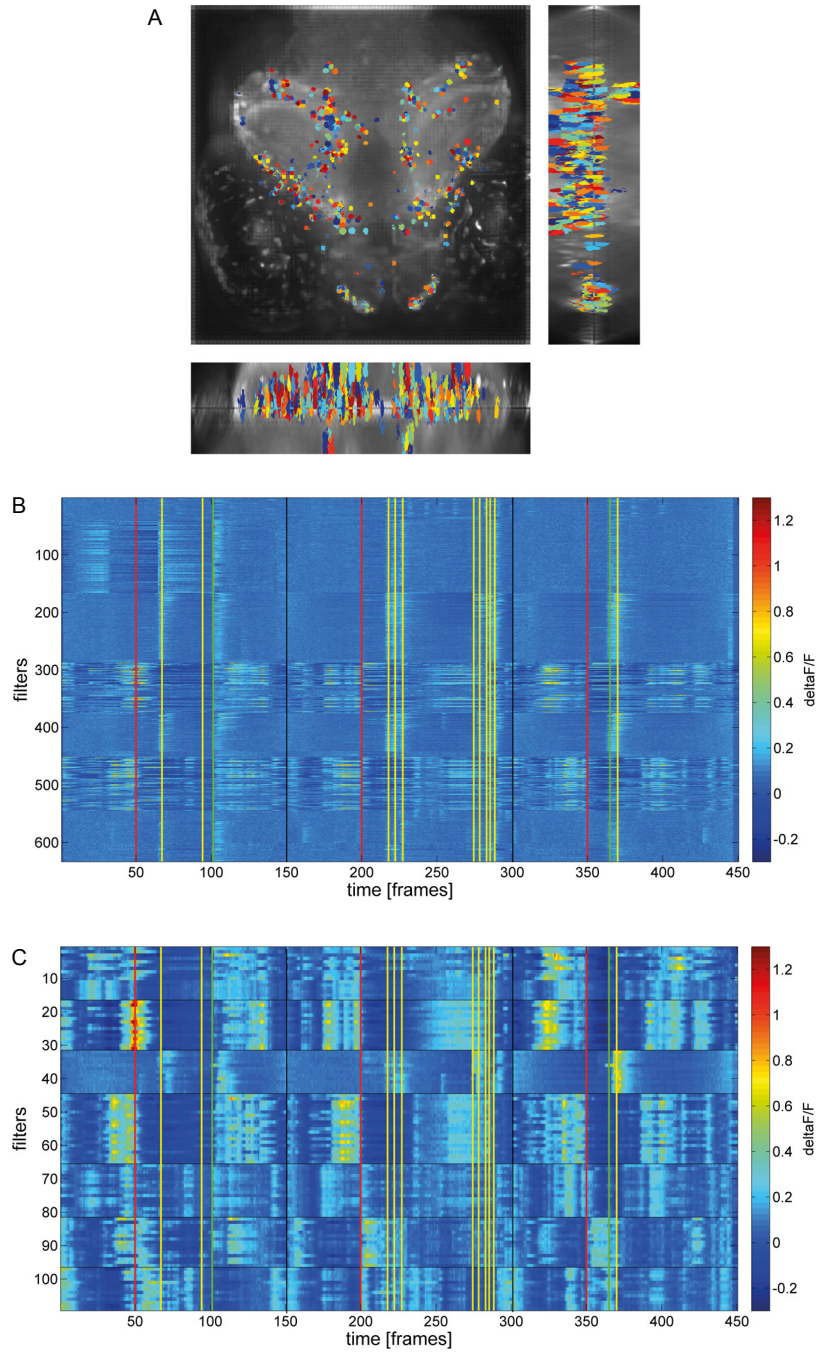


**Figure 4.19: Recording of neuronal activity before learning.** (A) Extracted spatial filters by ICA are shown overlaid with a maximum intensity projection of the volume. (B) The corresponding activity traces of the spatial filters shown in (A) are plotted for the sequence of three trials. (C) K-means clustering was performed on data in order to obtain subsets of neurons with similar responses. Fluorescence responses of manually selected clusters are plotted over time. (B)-(C) The joint regions between two trials are indicated by dashed black lines. Time of heat exposure is indicated by a red line, turns in the non-rewarded direction (left) are indicated by yellow lines. Tail flicks in the rewarded direction (right) implicating instant laser termination are indicated by green lines.

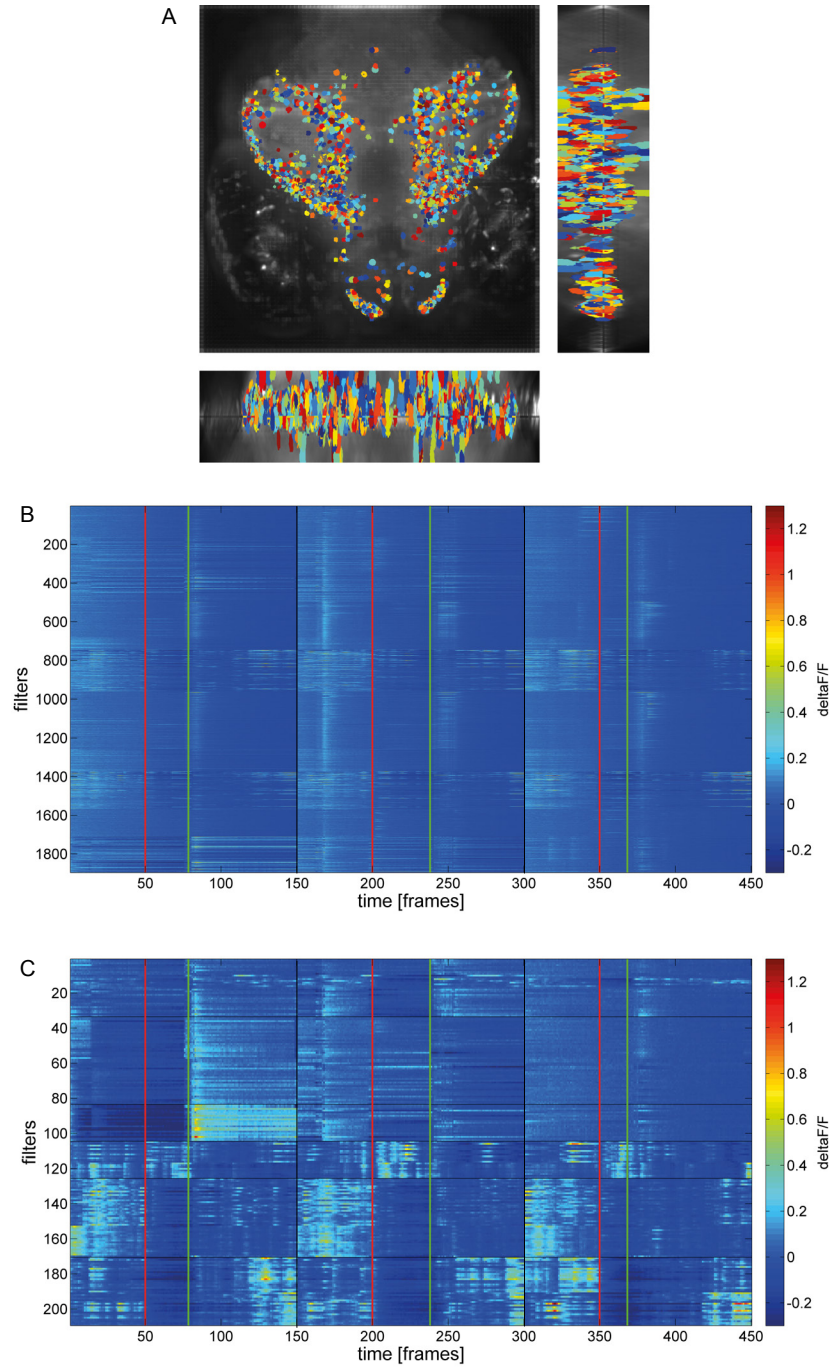


**Figure 4.20: Recording of neuronal activity after learning.** (A) Extracted spatial filters by ICA are shown overlaid with a maximum intensity projection of the volume. (B) The corresponding activity traces of the spatial filters shown in (A) are plotted for the sequence of three trials. (C) K-means clustering was performed on data in order to obtain subsets of neurons with similar responses. Fluorescence responses of manually selected clusters are plotted over time. (B)-(C) The joint regions between two trials are indicated by dashed black lines. Time of heat exposure is indicated by a red line. During illustrated trials after learning, first stimulus-evoked turns are performed only in the 68rewarded direction (right) implicating instant laser termination (indicated by green lines).

---

## Discussion & Outlook

The work presented in this thesis involved the development of experimental learning assays and systematic characterization of learning with the aim of investigating the extend of learning ability of zebrafish in the larval stage. In order to digitize movements of the animals, establishing a robust algorithm for tail tracking provided the basis of presented and potentially future conditioning assays. The compatibility of the constructed setup with technical requirements of the light-field microscope enables recording of neuronal activity simultaneously to conditioning. The study shows that fish larvae at the age of 6 to 10 days are able to learn an operant conditioning paradigm, which can be performed in combination with light-field microscopy. The execution of possible modifications of the conditioning assay as well as other conditioning forms, such as classical conditioning are introduced, which provide the foundation to investigate the functional basis of neuronal circuits during various behaviours.

### Discussion of issues concerning operant conditioning

During the execution of 95 **operant conditioning** experiments, the number of learners amount to 37, meaning a fraction of 39 % in this study. The best achievable success rate when only observing experiments performed under optimal conditions was 54 % (cf. Section 4.1). These results can be compared with the unpublished work of Florian Engert [28], which provided the basis of the establishment of the assay. In this unpublished study, a number of 92 learners within 144 performed experiments, resulting in a fraction of 64 % is specified. This reputedly better result could arise due to several reasons.

Engert and colleagues used a slightly distinct setup during conditioning experiments. For example, the collimated beam was positioned directly, meaning only a few millimetres in front of the fish's head. They did not provide all detailed informations on their setup, therefore other differences are possible. Further, they experimented with larvae of younger ages, namely between 5 and 8 days. In my experience, using animals a few days older should not be a drawback concerning learning ability, but rather the opposite. Moreover, experiments presented in their work were performed under equal conditions, not during a developmental process for finding out the optimal training conditions as in this study. The classification of learners and non-learners was

slightly different as well due to distinct experimental execution. Throughout all experiments, they performed two whole training blocks independent on the outcome concerning performance in the first block. In this work, the experiment was terminated after the first block for time reasons for animals classified as non-learners 1. In these individual cases it could happen in theory that animals would show an improvement in the second training block. If this was the case, the animal would change over to the class of undefined and not be included in the statistics. These differences result in a possible distortion of the fraction of learners and have an influence on the final success rate of all experiments.

In this work, the trend of a shorter latency with increasing recent performance during operant conditioning could only be obtained when averaging over all conducted experiments of learners (cf. Figure 4.8). Data shown in this figure contained experiments with different conditions concerning beam diameter and laser powers, resulting in diverse latency periods.

In order to compare the success rates of performed experiments and to confirm the observation of decrease in latency, a further study with conduction of experiments under equal and optimal conditions is necessary.

For **operant conditioning experiments with additional odor stimulation**, complete clarification concerning the reason of bad outcome of experiments was not provided (cf. Section 4.1.1). One possible reason is the imperceptibility of the odors used during experimentation. The perception depends on the age of fish, kind of odor and their concentrations. The assumption of perceiving amino acids in final concentrations used in this study based on diverse literature [18, 32, 45, 75] as well as ongoing experiments on odor perception in our lab. Further, animals may fail to make an association between odor and a directional tail flick in general, since learning the protocol of this assay is a more complicated task than straight operant conditioning. Clarification of odor perception in larval zebrafish would require the execution of further experiments and represents an important matter for classical conditioning experiments as well.

### **Discussion of issues concerning classical conditioning**

In **classical conditioning**, further issues could contribute to the indefinite learning success presented in Section 4.2, for instance factors attributable to the setup. Possibly, involuntary mechanical stimuli like pressure differences induced by the valves of the odor-delivery setup, as well as the permanent pulsation induced by the pumps may influence the learning progress. Additionally, it might be the case that residuals of odors are left in the setup for example in the tubing.

Furthermore, animals may miss to make an association between the two stimuli, perhaps due to improper timing of the two stimuli. This is because the exact period of odor presence is not known and can only be estimated (cf. Section 3.5.2). Therefore, the conditions for forward delay conditioning, namely that the onset of the odor precedes the onset of the heat as well as simultaneous ending, may not be fulfilled. In general, it cannot be ruled out that the association between the two specific stimuli used in this study do not succeed.

In order to obtain clearer indications of learning ability in the classical conditioning assay, different improvements could be realized in the future. In order to prevent issues concerning invol-

untary pulsations during conditioning, an odor-delivery setup without pumps based on gravity instead would be beneficial. Excluding a potential habituation to the odor stimulus over time could be achieved by using a second odor instead of water to enhance the distinct perception. Else, one or the other stimuli could be replaced in order to ensure a potentially better association. Instead of the odor stimulus, it would be beneficial to use a stimulus which can be timed very precisely, so that the exact knowledge of onset and offset is ensured as a visual cue for instance. Important at the selection of the CS is that it is not interacting with imaging, therefore a neutral auditory stimulus would be a possible option.

In order to confirm the results of classical conditioning experiments presented in this study, one could perform the following control experiments. Replacing the odorant solution with pure water during experimentation would investigate possible involvements of mechanical stimuli in the learning effect. Furthermore, it needs to be tested whether an unpaired presentation of both stimuli or the complete omission of the aversive US brings similar results as in paired exposure. In general, it cannot be totally ruled out that classical conditioning paradigms are not working as properly as operant conditioning for zebrafish in the very early stage. Only one published work about classical conditioning of larval zebrafish does exist so far [5].

### **Discussion of issues concerning conditioning combined with imaging**

During the realization of **conditioning experiments combined with imaging**, some issues emerged and give reason for improvements for further experiments.

When the brain of a zebrafish was recorded during a whole experiment with a duration of about two hours, motion artefacts appeared and caused the displacement of neuron's location in captured images. One possibility in order to maintain the imaging plane and reduce motion artefacts would be a three-dimensional image registration.

Longer imaging times or higher imaging rates result in more frames in the time-domain. The signal extraction procedure based on ICA exploits the time domain to identify characteristic components. Therefore, applying the procedure on more frames produce better results, meaning more identified spatial filters. Since the visible excitation light for imaging caused partly strong behavioural responses of the animal, the level of light intensity of the blue LEDs necessary to ensure sufficient quality of images was kept as low as possible by adapting exposure times and imaging frequency respectively. This was an issue in finding the right trade-off between enough fluorescence response for adequate images and low behavioural responses to illumination.

Behavioural responses arose due to the intense illumination by wide-field excitation of the entire head of the larvae, including eyes. The illumination can be thought of as an additional aversive stimulus and therefore could have an impact on the learning behaviour. Recording of each single trial of an entire conditioning experiment even caused death in a number of cases, presumably because of stress and intense responses to the permanent light excitation. Furthermore, it must be kept in mind that resulting neuronal activity traces include light initiated activity and must therefore be considered in analysis and interpretation of the data. One possible solution for future experiments in order to avoid these problems is to affix a custom-designed mask into the illumination pathway of the microscope. This action would allow light excitation of only the brain and prevent illumination of the eyes.

Various other improvements should be realized in future experiments, when conditioning is combined with imaging. In order to ensure easier identification of neurons by methods like ICA, fish lines expressing nuclear GCaMP could be used. The nuclear version implicates an improved spatial resolution, but at the cost of a slower rise time, meaning temporal resolution. Furthermore, the conditioning protocol needs to be synchronized automatically with LFM image acquisition to ensure better correlation of neural activity and stimuli, as well as behaviour.

Beside obtaining single neuron traces over time and find correlations between activity and behaviour, a possibility to analyze and interpret imaging data would be to observe "brain states". This means considering the state of all neurons for a certain time point and investigate the dynamics of these states.

In summary, I could show with this work that fish larva in the very early stage with under-developed brain connectivities are already able to learn. To come upon convenient and efficient conditioning techniques for larval zebrafish is not straightforward, but needs endurance and proceeding in a systematic way.

By developing various conditioning assays and reliable methods for the analysis of learning, the foundation is laid for further investigations on neuronal activity correlated to behavioural responses.

---

## List of Figures

2.1	Zebrafish ( <i>Danio rerio</i> ) . . . . .	3
2.2	Types of learning . . . . .	5
2.3	Classification of classical conditioning . . . . .	7
2.4	Timing aspect of classical conditioning . . . . .	7
2.5	Classification of operant conditioning . . . . .	8
2.6	The larval zebrafish brain . . . . .	11
2.7	The basic structure of a neuron . . . . .	12
2.8	Synaptic transmission at chemical synapses . . . . .	14
2.9	Principle of an epifluorescence microscope . . . . .	16
2.10	Principle of light field microscopy . . . . .	18
2.11	Realization of light field microscopy . . . . .	18
3.1	Chamber for embedding and immobilized zebrafish larva . . . . .	22
3.2	Experimental setup . . . . .	23
3.3	Functional principle of the tracking algorithm . . . . .	24
3.4	Deflection angle of the tail . . . . .	25
3.5	Tail deflection and angle extraction . . . . .	26
3.6	Mathematical descriptions for the tracking algorithm . . . . .	27
3.7	Mathematical descriptions for calculating deflection angles . . . . .	29
3.8	Graphical User Interface . . . . .	30
3.9	Operant conditioning protocol . . . . .	31
3.10	Correct and incorrect trials during operant conditioning . . . . .	32
3.11	Classification of learners and non-learners . . . . .	34
3.12	Sample routine turn . . . . .	36
3.13	Protocol of operant conditioning with odor stimulation . . . . .	37
3.14	Classical conditioning protocol . . . . .	38
3.15	Quantification for classical conditioning experiments . . . . .	40
3.16	Chamber for odor stimulation . . . . .	41
3.17	Odor-delivery setup . . . . .	42

3.18	Neuronal activity evoked by odor stimulation . . . . .	42
3.19	Sample escape behaviour . . . . .	43
3.20	Timing aspects for the classical conditioning protocol . . . . .	44
4.1	A successful training experiment . . . . .	48
4.2	Recent performance of learners . . . . .	49
4.3	Recent performance of non-learners 1 . . . . .	50
4.4	Recent performance of non-learners 2 . . . . .	50
4.5	Ratio of learners and non-learners dependent on differing experimental conditions .	51
4.6	Performances based on differing experimental conditions: with warming . . . . .	52
4.7	Performances based on differing experimental conditions: without warming . . . . .	53
4.8	Latency modulated by recent performance . . . . .	54
4.9	Operant conditioning with odor stimulation: Experiment 1 . . . . .	55
4.10	Operant conditioning with odor stimulation: Experiment 2 . . . . .	56
4.11	Operant conditioning with odor stimulation: Experiment 3 . . . . .	57
4.12	Operant conditioning with odor stimulation: Experiment 4 . . . . .	58
4.13	Learning progress for two sample experiments . . . . .	60
4.14	Training progress of animals classified into three groups . . . . .	61
4.15	Distribution of $A_{increase}$ for all experiments . . . . .	62
4.16	Reconstructed brain of zebrafish larvae . . . . .	64
4.17	Identified spatial filters by ICA . . . . .	65
4.18	Performance of learner combined with imaging . . . . .	66
4.19	Recording of neuronal activity before learning . . . . .	67
4.20	Recording of neuronal activity after learning . . . . .	68
A.1	Setup distances . . . . .	78
A.2	Photograph of setup . . . . .	79
A.3	Dimensions of holder (custom-built) . . . . .	80
A.4	Estimation of beam diameter . . . . .	81
A.5	Final conditions: measured beam diameters . . . . .	82
A.6	Measured beam diameters: initial conditions . . . . .	84
A.7	Photograph of setup during classical conditioning . . . . .	86
A.8	Duration of DAQ board signals . . . . .	87
A.9	Chamber dimensions . . . . .	88
A.10	Temperature profile: chamber with integrated IR LEDs . . . . .	89
A.11	Chamber with integrated IR LEDs . . . . .	89
A.12	Switching of odor-delivery setup . . . . .	90
A.13	Photograph of odor-delivery setup . . . . .	91
A.14	Temperature profiles measured with bimetallic strip . . . . .	92
A.15	Temperature profiles measured with thermographic camera . . . . .	93
B.1	Operating steps (GUI) . . . . .	97



---

## List of Tables

3.1	Classification of learners and non-learners . . . . .	35
A.1	Setup components . . . . .	80
A.2	Laser power settings for operant conditioning: for final conditions . . . . .	85
A.3	Laser power settings for operant conditioning: for initial conditions . . . . .	85



## **Setup Components & Preparatory Work**

This appendix contains detailed informations about setup components; photos and sketches with exact descriptions and distances are provided.

Additionally, preparative investigations and measurements for experimentation are presented.

## Details of Setup

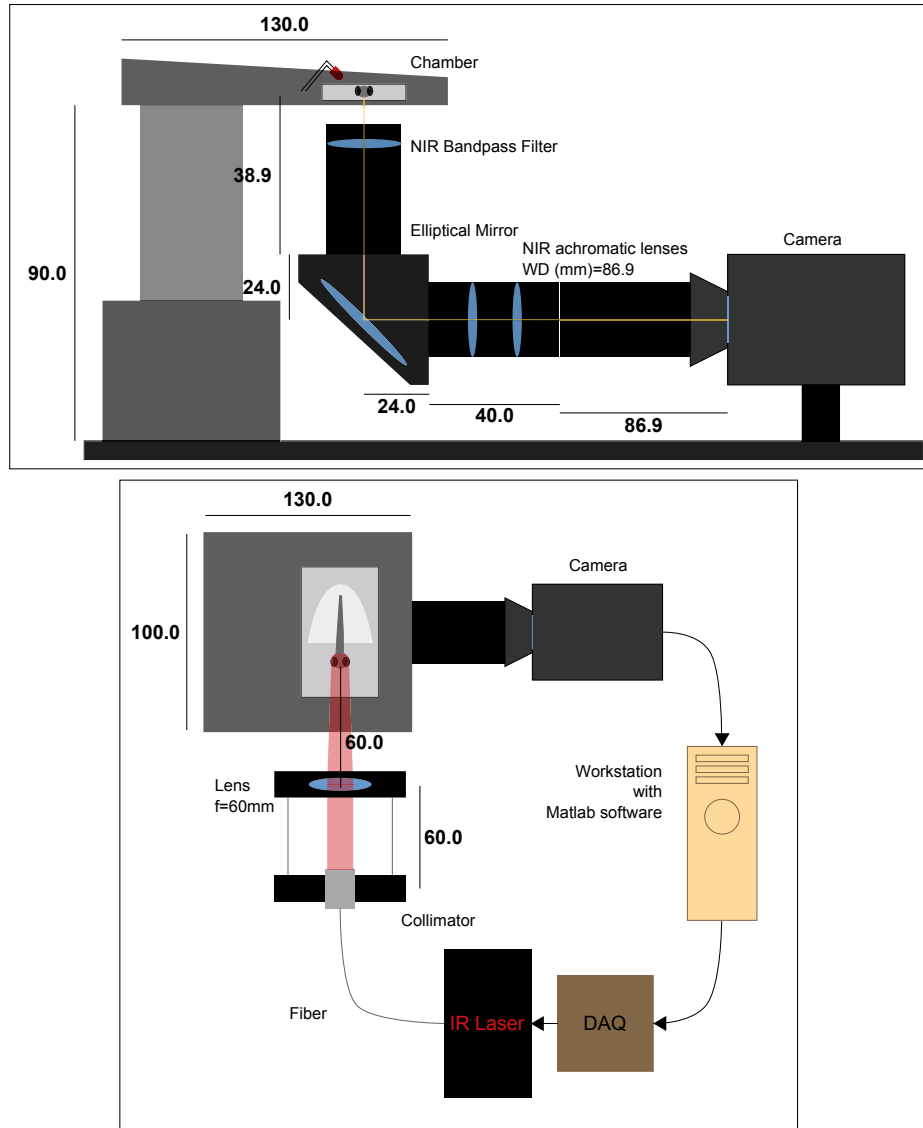


**Figure A.1: Setup distances.** Exact distances of components in the setup (cf. Figure 3.2). Sketches are not to scale.

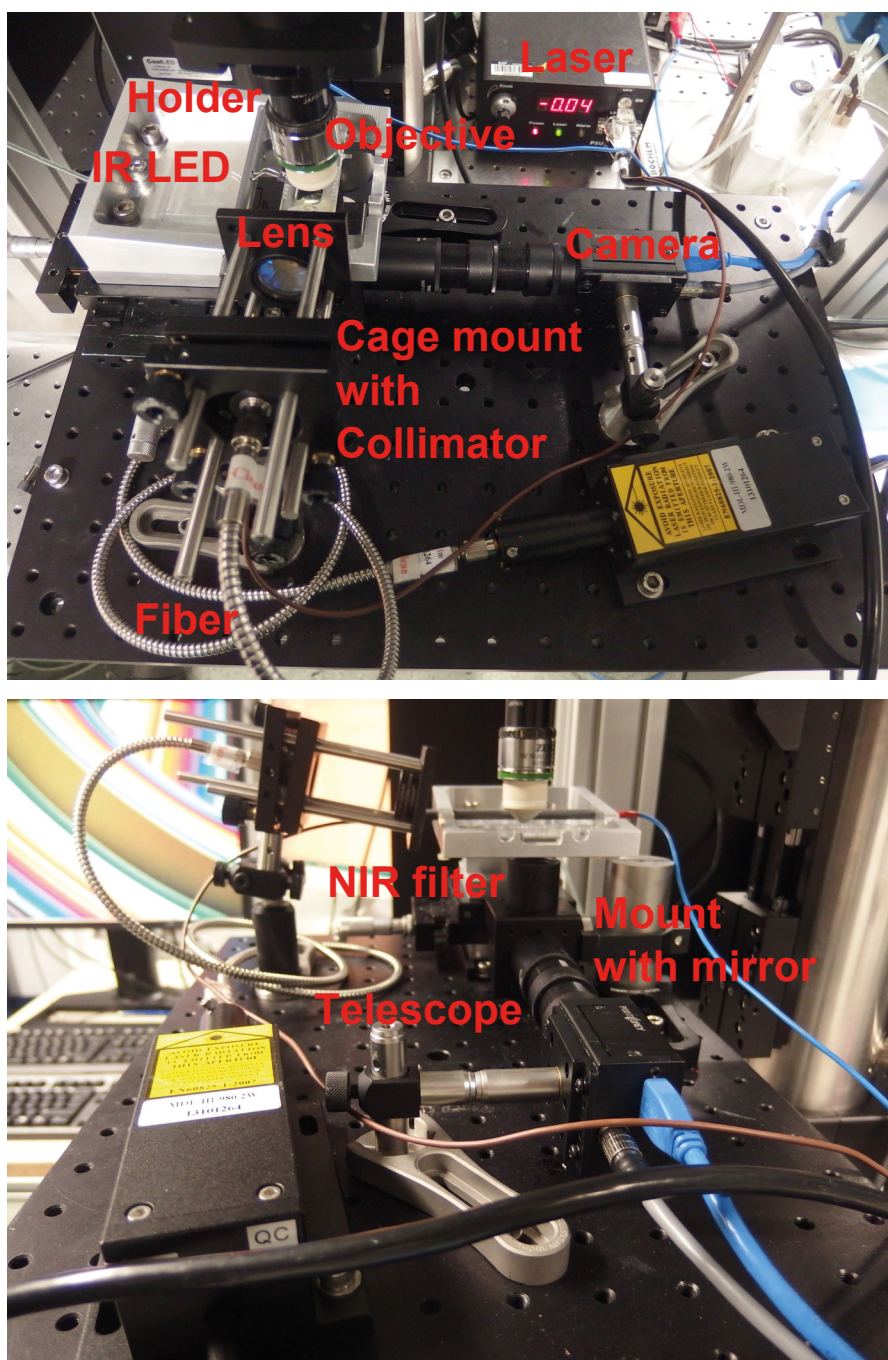


**Figure A.2: Photograph of setup.** Components are labelled and specified in Table A.1.

Label	Vendor	Part Nr.
Camera	Point Grey	GS3-U3-41C6M-C
Telescope	Thorlabs	MAP10100100-B
Mount	Thorlabs	KCB1E
Mirror	Thorlabs	PFE10-P01
NIR filter	Thorlabs	FB950-10
Laser	Roithner Lasertechnik	RLTMDL-980-2W-1
Fiber	Roithner Lasertechnik	RLTMxL FC-400
Collimator	Thorlabs	F220FC-1064
Lens	Thorlabs	AC254-060-B-ML
Cage mount	Thorlabs	KC1-T
IR LED	RS company	LD 274-3
Objective	Zeiss	420957-9900
Holder	custom-built	Figure A.3

**Table A.1:** Labels refer to those shown in Figure A.2.

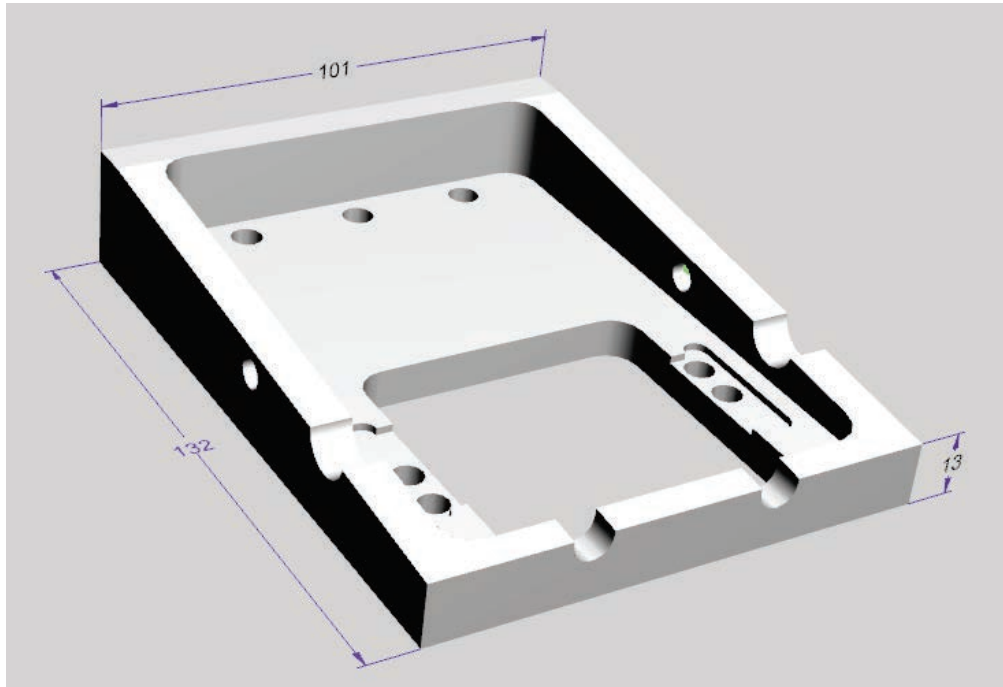


**Figure A.3:** Dimensions of holder (custom-built).

The use of different optic components for collimation and focusing of the laser beam resulted in different beam diameters. These diameters were estimated by the formula A.1 according to Figure A.4. These estimations were confirmed by measuring the actual diameters with a camera (Baumer, FWXC13c) before experimentation.

$$D_2 = D_1 \cdot \frac{f_2}{f_1} \quad (\text{A.1})$$

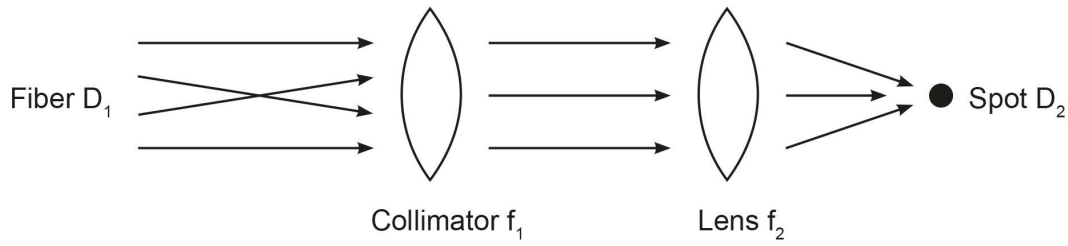


**Figure A.4: Estimation of beam diameter.** The core diameter of the fiber is denoted as  $D_1$ .  $f_1$  indicates the focal length of the collimator, whereas  $f_2$  is the focal length of the lens. The resulting beam diameter is denoted as  $D_2$ .

The components finally used for **operant conditioning**:

- FC/PC Fiber Collimator,  $f_1 = 11.17$  mm (Thorlabs, F220FC-1064)
- Lens,  $f_2 = 60$  mm (Thorlabs, AC254-060-B-ML)
- MM-Fiber,  $D_1 = 400$   $\mu\text{m}$  (Roithner Lasertechnik)

This choice of components resulted in an estimated beam diameter of:

$$D_2 = D_1 \cdot \frac{f_2}{f_1} = 400 \mu\text{m} \cdot \frac{60 \mu\text{m}}{11.17 \mu\text{m}} = 2149 \mu\text{m} \quad (\text{A.2})$$

The measured beam spot gave a diameter of 2.0 mm, shown in Figure A.5 (bottom).

The components finally used for **classical conditioning**:

- FC/PC Fiber Collimator,  $f_1 = 11.17$  mm (Thorlabs, F220FC-1064)
- Lens,  $f_2 = 40$  mm (Thorlabs)
- MM-Fiber,  $D_1 = 400$   $\mu\text{m}$  (Roithner Lasertechnik)

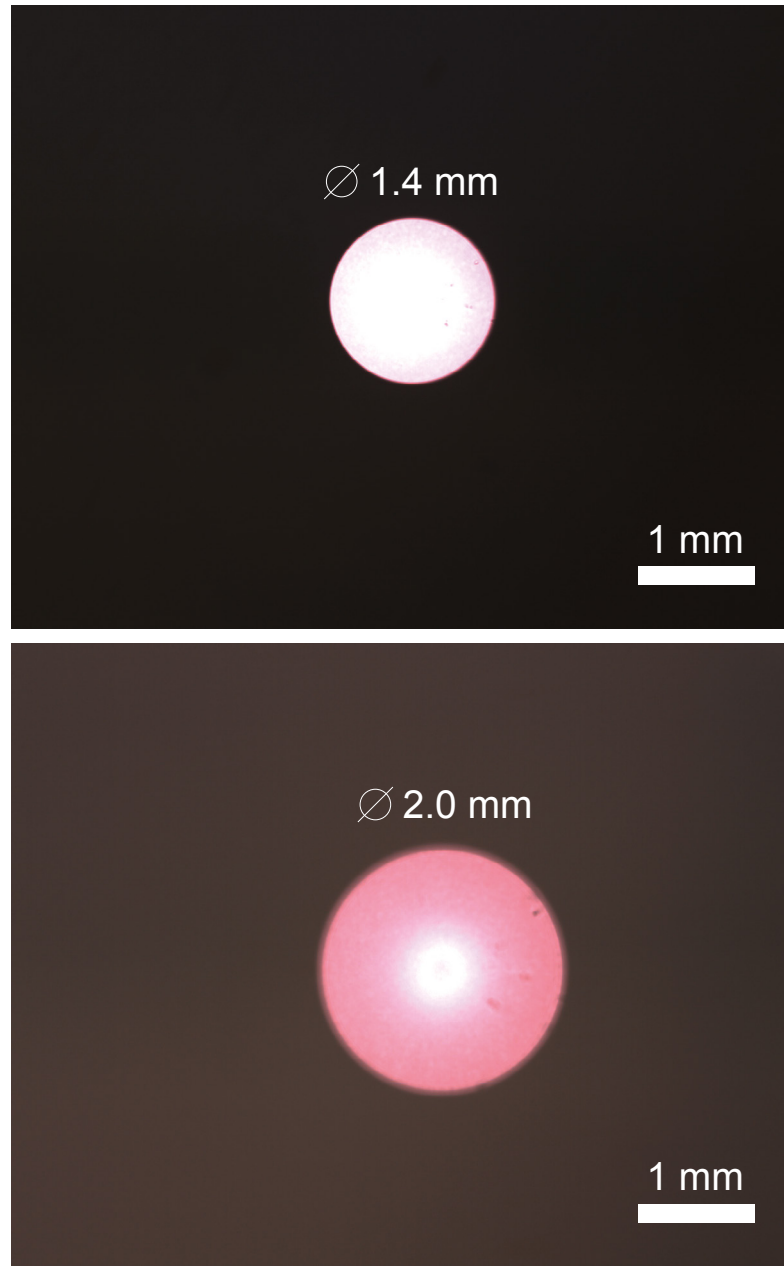


**Figure A.5: Final conditions: measured beam diameters.** Top: The beam diameter finally used during classical conditioning experiments was about 1.4 mm. Under these conditions and by heating the inward of the chamber up to 26 °C by warming the liquids with a warming bath, a laser power of around 550 – 600 mW was used. Bottom: The beam diameter finally used during operant conditioning experiments was about 2.0 mm. Depending on heat conditions and presence of pumps, various laser powers were used, see Table A.2.



These choice of components resulted in a estimated beam diameter of:

$$D_2 = D_1 \cdot \frac{f_2}{f_1} = 400 \mu\text{m} \cdot \frac{40 \text{ mm}}{11.17 \text{ mm}} = 1430 \mu\text{m} \quad (\text{A.3})$$

The measurement of the beam spot resulted in a diameter of 1.4 mm, shown in Figure A.5 (top).

When starting with **operant conditioning** experiments, a smaller beam diameter was used (according to [28]). Due to a personal hint from Florian Engert and due to my observation that a smaller diameter resulted in a more inconsistent behaviour, a bigger diameter was chosen for subsequent experiments.

Altogether, 42 out of 95 experiments included in this work, were performed with a beam diameter of around  $500 \mu\text{m}$ , received by using following optic components:

- FC/PC Fiber Collimator,  $f_1 = 4.6 \text{ mm}$  (Thorlabs, CFC-5X-B)
- Lens,  $f_2 = 50 \text{ mm}$  (Thorlabs)
- MM-Fiber,  $D_1 = 50 \mu\text{m}$  (Thorlabs)

The usage of these components resulted in a estimated beam diameter of

$$D_2 = D_1 \cdot \frac{f_2}{f_1} = 50 \mu\text{m} \cdot \frac{50 \text{ mm}}{4.6 \text{ mm}} = 540 \mu\text{m} \quad (\text{A.4})$$

and a measured one of  $530 \mu\text{m}$ , see Figure A.6.

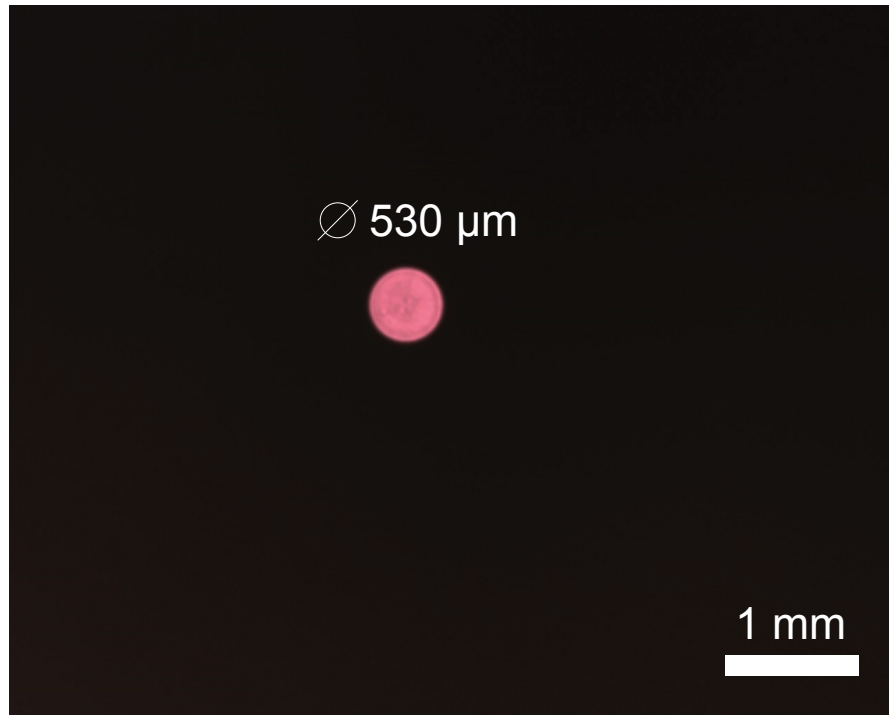


**Figure A.6: Measured beam diameters: initial conditions.** For the first 42 of 95 operant conditioning experiments, a beam diameter of about 500  $\mu\text{m}$  were chosen. Depending on heat conditions laser powers from 150 to 300 mW were chosen, see Table A.3.

#### **Laser settings during operant conditioning**

Operant conditioning experiments were performed with various settings of the laser power depending on given conditions. Depending on the presence of heating of the inward of the chamber as well as on the presence of liquid flow pumped through the chamber, laser powers from 150 up to 600 mW were used. In Table A.2 the adjusted laser powers under different conditions are summarized when using a beam diameter of about 2 mm (final). In case of an existent flow, the liquids were either heated in a warming bath (bath adjusted to  $\approx 80^\circ\text{C}$ , resulting temperature at fish chamber:  $\approx 26^\circ\text{C}$ ) (flow: yes, heating: yes), or not heated (flow: yes, heating: no). Without flow, the inward of the chamber was heated to about  $26^\circ\text{C}$  by using the chamber with integrated IR LEDs described below (flow: no, heating: yes), or not heated (flow: no, heating: no). Heating of the inward was an important factor for the success of training (cf. 4.1). The optimal conditions (with heating) are indicated in green.

		flow	
		yes	no
heating	yes	550 – 600 mW	150 – 200 mW
	no		400 – 500 mW

**Table A.2:** Laser power settings are given for operant conditioning with a beam diameter of 2 mm (final). Optimal conditions for operant conditioning (with heating) are indicated in green.

Table A.3 summarizes the used laser powers under various conditions when using a beam diameter of about 0.5 mm (in early experiments, first 42 of 95 experiments). In the case of no heating it was not possible to find appropriate laser powers in order to achieve a good learning rate. In case of no flow but heating of the inward of the chamber (with integrated LEDs), a comparatively high laser power density was used. This resulted in faster behavioural responses within a few seconds.

		flow	
		yes	no
heating	yes		200 mW
	no	150 – 250 mW	150 – 300 mW

**Table A.3:** Laser power adjustments are given for operant conditioning with a beam diameter of 0.5 mm (early experiments).

During the developmental process of operant conditioning, several experiments were made for testing specific conditions. Also the tracking algorithm needed to be tested, time for permanent modifications was needed to run in robust manner. During experimentation, it happened from time to time that animals died. Some animals could not be classified according to the classification described in Section 3.4.1, because too few trials or only the first block was performed. All experiments under these kind of conditions were ignored in this work and excluded from any statistics. Also not observed in statistics were experiments classified as undefined (cf. Section 3.4.1), 15 experiments fell into this class.

### **Laser settings during operant conditioning combined with LFM**

During operant conditioning experiments in combination with imaging, the laser was adjusted to higher power of around 450 mW due to no usage of heating (cf. Table A.2).

### **Laser settings during classical conditioning**

Classical conditioning experiments were performed with distinct laser settings. The beam diameter was adjusted to about 1.4 mm (see Figure A.5 top). The used laser power when working with warmed liquids (adjusted temperature of heat bath:  $\approx 80^\circ\text{C}$ , temperature in chamber:  $\approx 26^\circ\text{C}$ ) was around 550 – 600 mW. The laser beam impinged on the fish head from a tilted position, a photograph is shown in Figure A.7.

During the developmental process, finding the right settings for the laser power in order to avoid no or low behavioural responses as well as death due to overheating was a tricky subject.

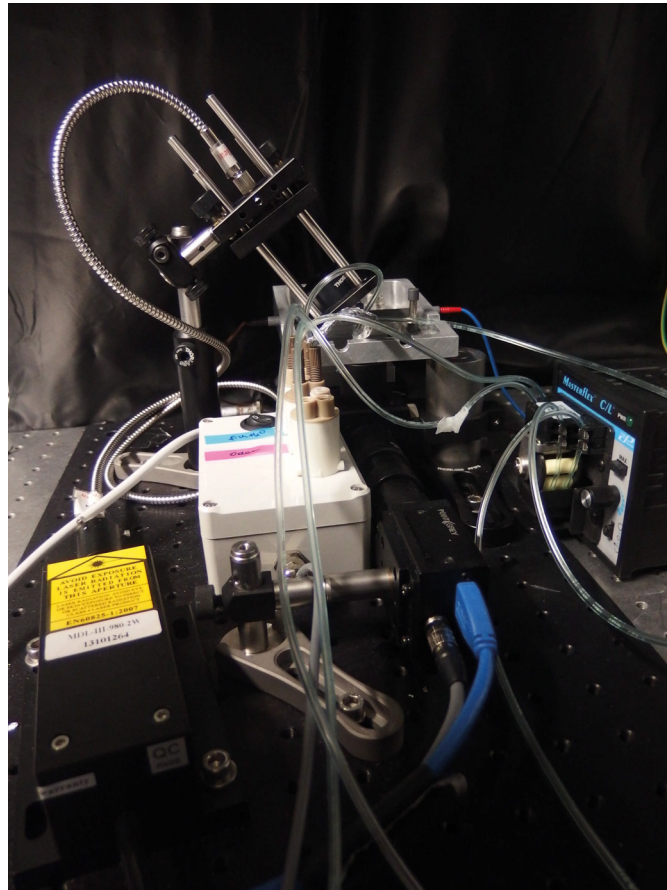


**Figure A.7:** *Photograph of setup during classical conditioning. The laser beam impinged on the fish head from a tilted position.*

### Heat stimulation by IR laser

The heat stimulation during conditioning was provided by a IR laser (Roithner Lasertechnik, RLTM DL-980-2W-1). The laser pulses were controlled by a DAQ board (National Instruments, NI USB-6008) by sending square-wave signals of 0 or 5 Volts (port "AO0") in Matlab. The duration of switching from 0 to 5 Volts or reversed was measured with an oscilloscope and resulted in 2.75 ms (see Figure A.8).

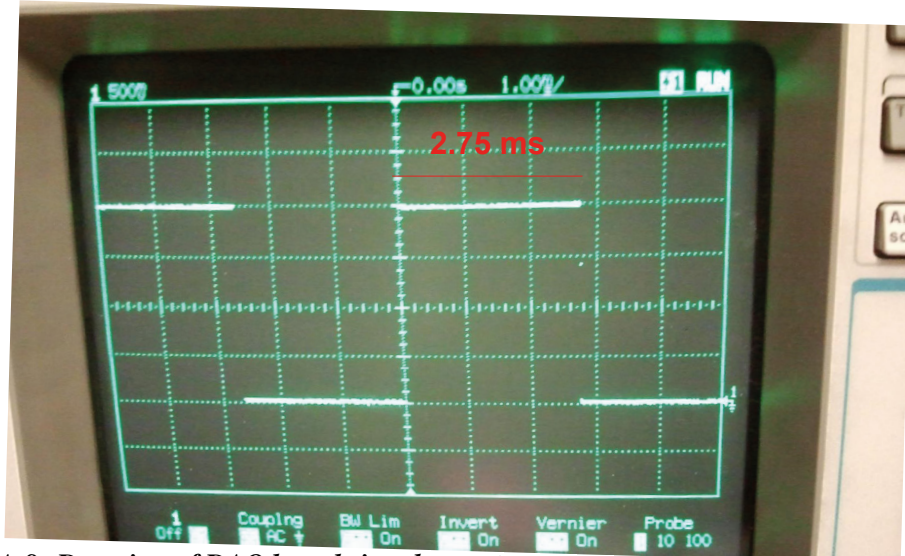


**Figure A.8: Duration of DAQ board signals.** Sending of square-wave signals of 0 or 5 Volts to the DAQ board in Matlab lasted about 2.75 ms, measured with an oscilloscope.

### Custom-built chambers for embedding

For the embedding of larval zebrafish, different chambers were custom-built and used during conditioning. The dimensions of the chambers are given in Figure A.9. For operant conditioning experiments the bigger chamber (cf. Section 3.4) was used, whereas for classical conditioning the smaller one was used (cf. Section 3.5).

The total **volume of the big chamber** could be estimated:

$$V_{\text{reservoir}} = (4 \cdot 6.5 \cdot \pi) \cdot 3 = 245 \text{ mm}^3, V_{\text{chamber}} = (4 \cdot 6 \cdot \pi + 20 \cdot 12) \cdot 3 = 946 \text{ mm}^3, \\ V_{\text{total}} = V_{\text{chamber}} + 2 \cdot V_{\text{reservoir}} = 1436 \text{ mm}^3.$$

If the half of the chamber (without reservoirs) was filled with agarose, the residual volume was:

$$V_{\text{agarose}} = \frac{V_{\text{chamber}}}{2} + 2 \cdot V_{\text{reservoir}} = 963 \text{ mm}^3.$$

The total **volume of the small chamber** could be estimated:

$$V_{\text{total}} = (10 \cdot 10 + 10 \cdot 5) \cdot 3 = 450 \text{ mm}^3.$$

With the half chamber filled with agarose:

$$V_{\text{agarose}} = \frac{V_{\text{total}}}{2} = 225 \text{ mm}^3.$$

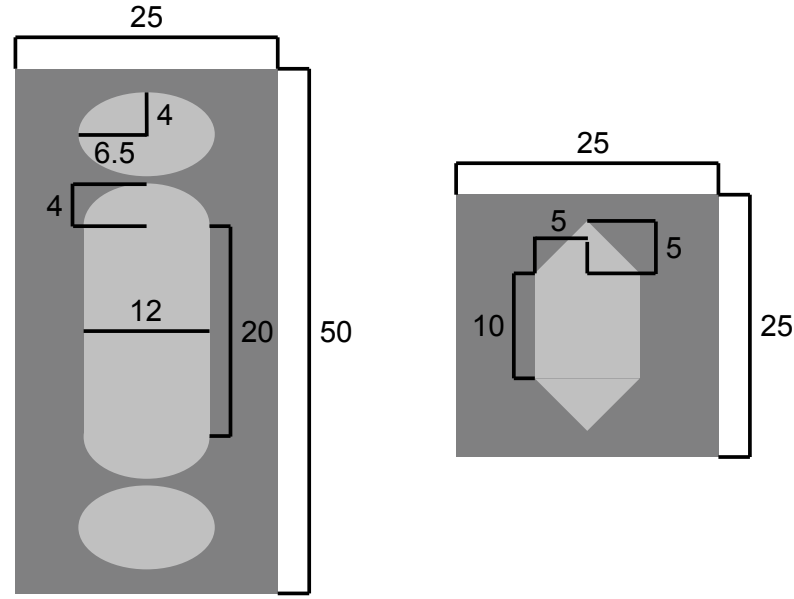


**Figure A.9: Chamber dimensions.** Left: Dimensions of the big chamber, used for operant conditioning experiments. Right: Dimensions of the small chamber, used for classical conditioning. Dimensions are given in mm. The height of both chambers was 3 mm.

With a flow rate of  $60 \mu\text{l/s}$ , the time of fluid exchange for the big chamber amounts to:

$$t = \frac{V_{\text{agarose}}}{\text{rate}} = \frac{963 \mu\text{l}}{60 \mu\text{l/s}} \approx 16 \text{ s},$$

whereas for the small chamber the time of fluid exchange was lower:

$$t = \frac{V_{\text{agarose}}}{\text{rate}} = \frac{225 \mu\text{l}}{60 \mu\text{l/s}} \approx 4 \text{ s}.$$

For several operant conditioning experiments a chamber with integrated IR LEDs (RS company, CQY37N) was used (cf. Section 4.1). The LEDs were originally needed for contrast purposes, but generated a temperature increase of the agarose as a side effect (see Figure A.10). During experimentation it turned out that this heating of the inward of the chamber to about  $26^\circ\text{C}$  was a crucial factor for the success of training.

A photograph of the chamber is shown in Figure A.11, the dimensions of the chamber were equal to the big chamber shown in Figure A.9 (left). Altogether 18 LEDs (with max. voltage of 1.3 V each) were affixed at the chamber, 9 at each side. The LEDs were operated at 11.7 V (serial connection).

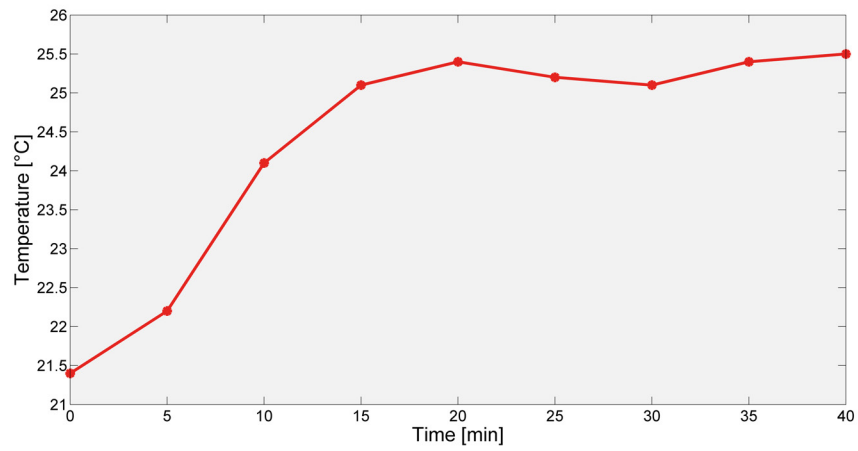


**Figure A.10: Temperature profile: chamber with integrated IR LEDs.** The temperature of the inward of the chamber increased to about 26 °C by the integrated LEDs.



**Figure A.11: Chamber with integrated IR LEDs.** Altogether 18 LEDs were affixed at the chamber, 9 at each side. Dimensions were equal to the chamber shown in Figure A.9 left.

### Odor-delivery setup

For the odor-delivery setup needed for operant conditioning with additional odor stimulation (Section 3.4.3) as well as for classical conditioning (Section 3.5), a custom-built relay consisting of three valves with three ports each (The Lee company, LFY 3-Way 156 MINSTAC Solenoid Valves) was used. For my setup only two of the three integrated valves were needed (see Figure A.12 and A.13, cf. Figure 3.17).

Each valve comprised three ports connected via tubing (Carl Roth, Tygon ID 1.6 mm): the Common Port (C) was used for the input, the Normally Open Port (NO) and the Normally Closed Port (NC) for the output depending on the applied voltage. The valves were controlled by the DAQ board (National Instruments, NI USB-6008) connected to the relay by sending square-wave signals of 0 or 5 Volts (port "AO1") in Matlab. When no voltage was applied (0 Volt) the Common Ports of the valves were connected to the Normally Open Port. When switching the valves by applying a voltage of 12 Volts (input signal amplified in the relay), the Common Ports were connected to the Normally Closed Ports. This mechanism is illustrated in Figure A.12. A photograph of the odor-delivery setup with annotations of the ports is provided in Figure A.13.

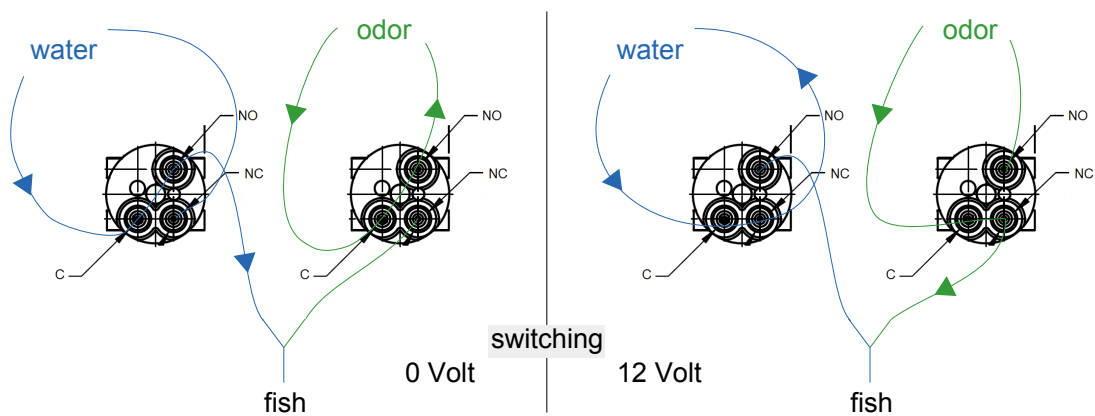


**Figure A.12: Switching of odor-delivery setup.** Each valve comprised three ports: Common Port (C), Normally Open Port (NO) and Normally Closed Port (NC). When no voltage was applied (0 Volt) the C ports were connected with the NO ports, resulting in the transportation of water to the fish (indicated in blue). The odor was circulating in the meantime (green). When switching the valves by applying a voltage of 12 Volts, the C ports were connected to the NC ports. This induced the transport of odor to the fish.



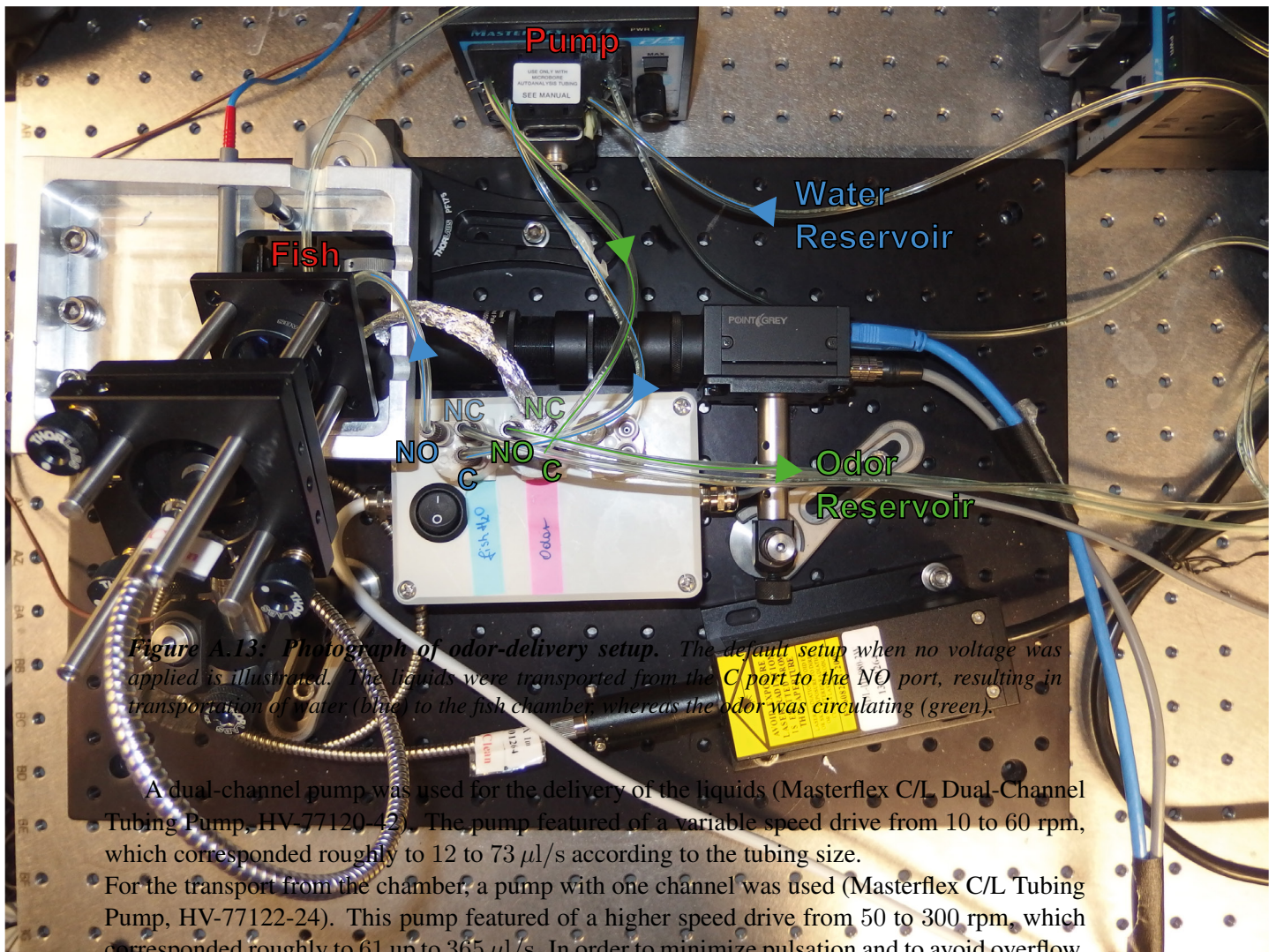


*Figure A.13: Photograph of odor-delivery setup. The default setup when no voltage was applied is illustrated. The liquids were transported from the C port to the NO port, resulting in transportation of water (blue) to the fish chamber, whereas the odor was circulating (green).*

A dual-channel pump was used for the delivery of the liquids (Masterflex C/L Dual-Channel Tubing Pump, HV-77120-42). The pump featured of a variable speed drive from 10 to 60 rpm, which corresponded roughly to 12 to 73  $\mu\text{l/s}$  according to the tubing size. For the transport from the chamber, a pump with one channel was used (Masterflex C/L Tubing Pump, HV-77122-24). This pump featured of a higher speed drive from 50 to 300 rpm, which corresponded roughly to 61 up to 365  $\mu\text{l/s}$ . In order to minimize pulsation and to avoid overflow, the smallest possible flow rate of around 60  $\mu\text{l/s}$  was chosen for experimentation.

## Investigations of generation of heat during laser stimulation

Over the course of this work, several temperature measurements were conducted to estimate the temperature arising at the head of the animals induced by laser stimulation. Investigations on the generation of heat were performed with a temperature sensor (bimetallic strip) on the one hand, and with a thermographic camera provided by the company InfraTec (model nr. PIR uc 180) on the other hand. Results gave only an indication for the resulting heat development, but did not provide complete clarification.

Figure A.14 shows the arising heat development in agarose depending on different laser powers. The generated heat was measured with the bimetallic strip dipped into the fish chamber

filled with water at position of the focused laser spot. If the heating of the metallic material itself played a role in the measurements shown in the figure is uncertain.

Experiments were performed with a beam diameter of about 0.5 mm (cf. Figure A.6).

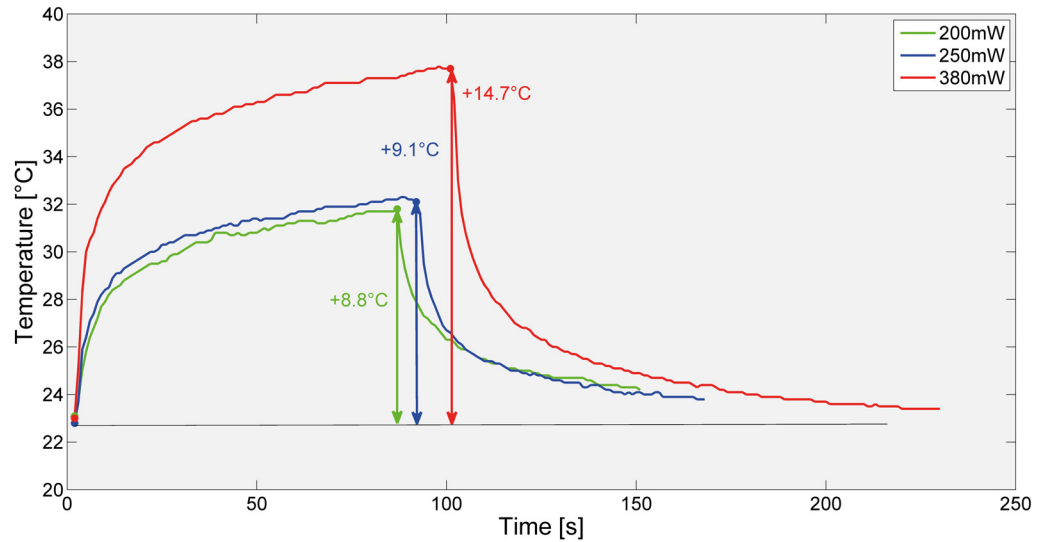
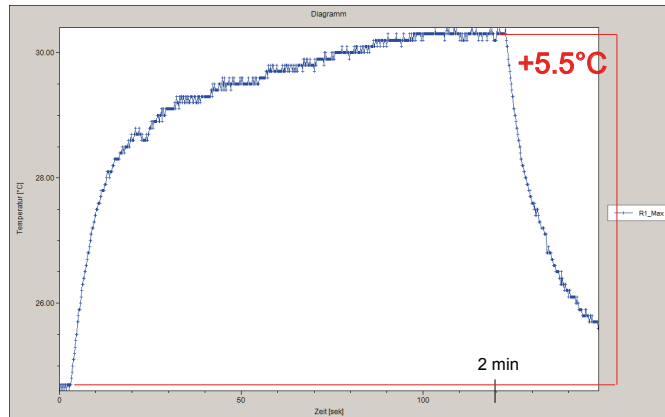


**Figure A.14: Temperature profiles measured with bimetallic strip.** With a laser stimulation of 200 mW ( $1000 \text{ mW/mm}^2$ ) the water was warmed up by  $8.8^\circ\text{C}$  (indicated in green). A power of 250 mW ( $1250 \text{ mW/mm}^2$ ) resulted in a growth of  $9.1^\circ\text{C}$  (indicated in blue), and a power of 380 mW ( $1900 \text{ mW/mm}^2$ ) generated a temperature increase of  $14.7^\circ\text{C}$  (indicated in red).

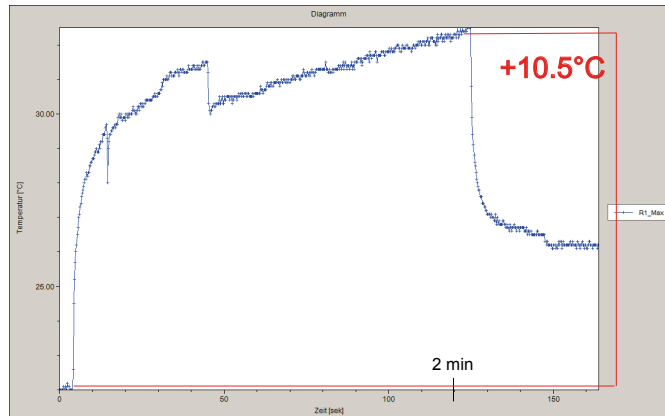
Figure A.15 shows the temperature profile when measuring the generated heat with the thermographic camera. The camera measured the generated temperature at the surface of the water layer with a height of around 1 mm on top of agarose (as well with a height of around 1 mm) wherein the fish was embedded (Figure A.15A). In Figure A.15B and C the temperature was measured directly at the head of the fish lying on an agarose layer, but without water and agarose overhead.

Experiments were performed with a beam diameter of about 2 mm (cf. Figure A.5 bottom).

A 360 mW, w/ water



B 360 mW, w/o water



C 250 mW, w/o water

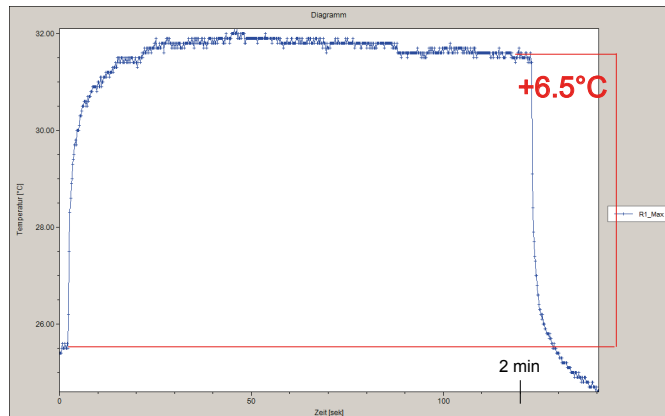


**Figure A.15: Temperature profiles measured with thermographic camera.** (A) A laser stimulation of 360 mW ( $115 \text{ mW/mm}^2$ ) resulted in a growth of temperature of  $5.5^\circ\text{C}$ , measured at the surface of the water layer. (B) When measuring directly at the head of the fish without liquids overhead, a laser power of 360 mW ( $115 \text{ mW/mm}^2$ ) generated an increase of  $10.5^\circ\text{C}$ . (C) A power of 250 mW ( $80 \text{ mW/mm}^2$ ) measured directly at the head induced a growth of  $6.5^\circ\text{C}$ .



---

## Experimental Procedures

This appendix contains detailed descriptions of procedures during experimentation. Preparation progresses before the actual execution of the experiment are explained and subsequent statements guide through an experiment in a step by step manner.

### Get started

#### Embedding:

Agarose in liquid state must be heated up to 40 °C. Soak up the fish with a pipette and fill the chamber with agarose to halfway. Position the fish in the middle of the chamber as parallel as possible to the long side of the chamber. Position the ventral side downward. Leave the agarose to cool and dry up. Cut free the tail with a scalpel, for odor experiments cut free the nose additionally. Fill up the chamber with E3 medium and wait a few hours before experimentation. For overnight incubation, immerse the chamber into water to avoid drying out.

#### Settings:

For laser settings, switch on the main power of the power supply (red LED "Power" is on). Turn on the key switch to "ON" state (green LED "Laser" is on). Note the warming up time of about 15 minutes. Adjust the Toggle Switch at the back panel of the power supply to CW mode. Adjust the desirable power by turning the knob and measuring the effective power with a power meter. Turn off the key switch to "OFF" state.

Place the chamber into the holder and fixate it with magnets. Turn on the power supply of the IR LED for contrast and adjust it to about 1.3 Volt. Ensure proper contrast by moving and altering the position.

Start the Point Grey camera software (FlyCapture 2). Open "camera control dialog", select the field "Custom Video Modes", select Mode 2 ( $\hat{=}$  2 × 2 binning) and the Pixel Format "Raw 8". Choose a ROI with width of 480 and height of 380. Center ROI, click "Apply" and ensure achieving a frame rate of 178 fps.

Translate the stage in lateral direction to position the fish in the field of view of the camera. The position from laser beam to camera should remain constant from experiment to experiment. Use

the infrared viewer for exact alignment of the laser beam (lower the power by turning the knob, choose CW mode at back panel), position the laser beam to the head of the fish. Adjust the Toggle Switch at the back panel to Modulation Mode in order to operate with external signals (leads need to be connected to the DAQ board at port "AO0"). Adjust the desirable power by turning the knob.

When performing experiments with odor stimulation, ensure the realy of the odor-delivery setup is switched on (leads need to be connected to the DAQ board at port "AO1").

Open Matlab (important: only after above settings, camera settings are adopted automatically by Matlab) and run the main file "myGUI.m" in order to open the GUI.

### **Operating steps (GUI), compare Figure B.1:**

1. Click the button "Take test image" to capture a snap shot of the embedded fish. Ensure that the fish does not move.
- 2a. Click the button "set anchor point".
- 2b. Click once in the image to define the anchor point. Place the anchor point on the trunk of the body, at the level of the border between agarose and the removed part. The anchor point defines the starting point for the algorithm.
- 3a. Click the button "set reference line".
- 3b. Define the first point of the reference line by clicking in the image. Place the point near the anchor point. The position of this point affects the calculation of the deflection angle.
- 3c. Define the second point of the reference line by clicking in the image. Place the point at the tip of the tail.
4. Choose one of the protocols, depending on conditioning experiment (described below). Optional: change the length of one trial (default: 120 s) and the angle threshold for defining a turn (default: 45°).
5. Optional: Tick the checkbox "capture movie" to save single frames of camera in workspace (3D array). In order to reduce data size, frames are kept only until the laser is terminated plus a risk buffer of 500 frames.
6. Click the button "start trial". A trial of the length of 2 min is initiated.
7. Click the button "save trials" (at least) before closing the GUI in order to save data in a struct file in the workspace (important, otherwise data is getting lost).
8. Optional: in case of necessity laser and valves can be controlled manually during execution of trials. Clear the workspace (after saving potentially saved frames manually) in order to avoid slowing down of algorithm.

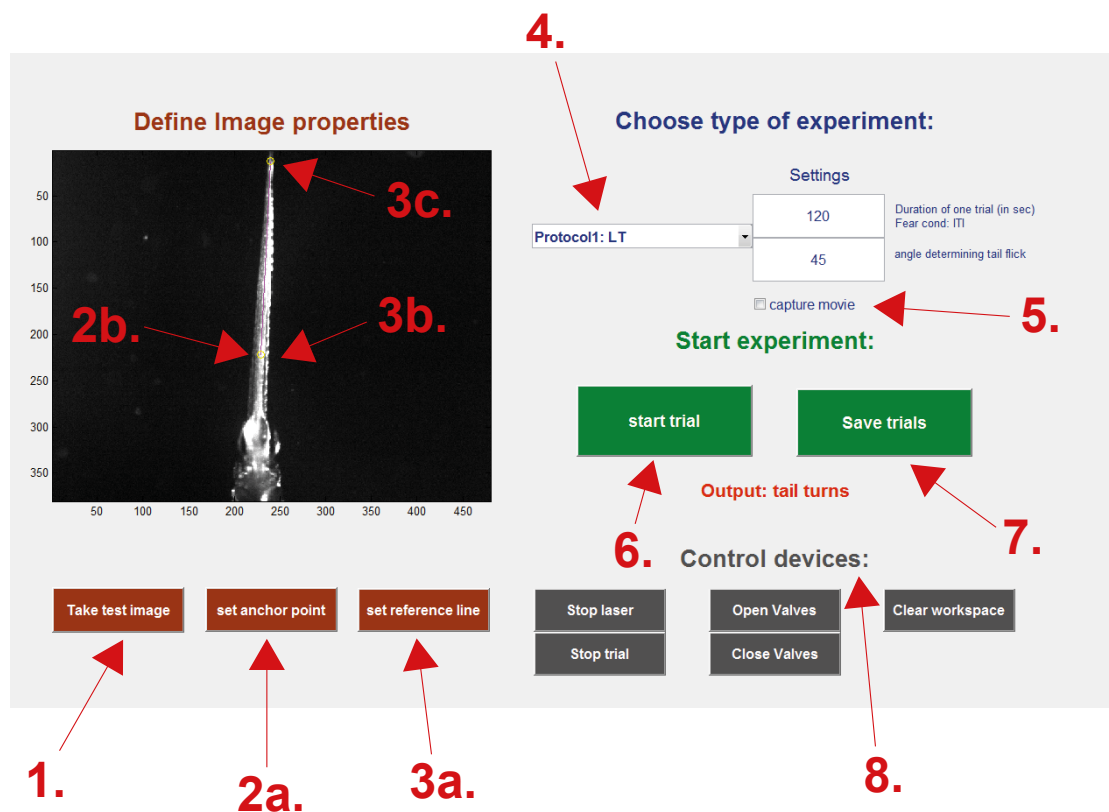


*Figure B.1: Operating steps (GUI).*

## Operant Conditioning

### Ad 4.: Choose a conditioning protocol

For **operant conditioning** different protocols can be chosen in the GUI. "Protocol 1" and "Protocol 2" differ only in respect of odor stimulation. "Protocol 1" is outdated and was used for an older version of the odor-delivery setup containing three valves with longer afflux to the chamber (pause of 5 seconds precedes the start of laser power-up and tail tracking). Valves needed to be closed manually. Protocols counted among "Protocol 1" are ignored in further description. Following protocols can be chosen in the GUI:

- "Bias determination": a potential turn direction preference is determined. Laser is terminated by the first turn. At the end of the trial, bias direction is displayed in the GUI. Choose opposite direction for training.
- "Protocol 1: LT": outdated
- "Protocol 1: RT": outdated
- "Protocol 1: test Reaction": outdated

- "Protocol 2: LT": protocol for left training, laser is terminated by a turn to the left. A pause of 2 seconds precedes the start of laser power-up and tail tracking for additional odor stimulation.
- "Protocol 2: RT": protocol for right training, laser is terminated by a turn to the right. A pause of 2 seconds precedes the start of laser power-up and tail tracking for additional odor stimulation.
- "Protocol 2: test Reaction": Only for experiments with additional odor stimulation. Valves are opened 2 seconds before laser power-up and tail tracking. Laser is terminated by the first turn.

#### **Execution of experiment: operant conditioning (without odor and imaging)**

- Choose the chamber with integrated LEDs for experimentation (see Figure A.11). Note the warming up time of the inward of the chamber of about 15 minutes (see Figure A.10). Note evaporation and fill up chamber with E3 medium whenever necessary, or use a cover slip on top.
- Execute the protocol "Bias determination" once (results e.g. in "LEFT"). If no definite turn direction can be identified, perform another trial.
- For training choose opposite direction of bias (e.g. "Protocol 2: RT"). Perform 25 – 30 trials. If asymptotic recent performance  $\geq 0.5$ , perform second training block in inverse direction ((e.g. "Protocol 2: LT"). Perform 25-30 trials.
- Save trials.
- Classify experiment according to classification described in Section 3.4.1.

#### **Execution of experiment: operant conditioning with odor stimulation**

- So far bigger chamber was used for experimentation (see Figure A.9 left). Smaller chamber could be used potentially (note higher pulsation).
- Warm up warming bath to  $\approx 80^\circ\text{C}$ , put in two reservoirs: one filled with E3 medium, one with odor. Adjust flow rates of pumps (minimal flow rate for outflow, adjust inflow in order to keep constant level). Measure the temperature of  $\approx 26^\circ\text{C}$  at end of tubing/in chamber. Open valves to fill tubing with odor without attachment at chamber. Close valves.
- Turn off valve relay. Execute the protocol "Bias determination" (without odor).
- Turn on valve relay. Execute first training block.
- Turn off valve relay. Execute first training block (without odor).
- If classified as a learner, turn on valve relay and execute protocol "Protocol 2: test Reaction" for ten times.



### **Execution of experiment: operant conditioning with imaging**

- Choose the bigger chamber or better chamber with integrated LEDs for experimentation. Change the pause to 10 seconds in Matlab codes ("lefttraining\_odor\_circles.m" and "right-training\_odor\_circles.m"). Adjust parameter for imaging in Andor Solis software: 5 Hz, 150 or 300 frames. Adjust intensity of blue excitation LEDs in order to achieve maximal count number of around 2500.
- Execute the protocol "Bias determination".
- Choose the first training protocol. Turn on excitation light about 10 seconds before starting the trial in order to achieve calming and familiarization of the animal. Start the trial and imaging software manually at the same time. Imaging starts 10 seconds before Matlab code to obtain baseline activity without stimulation. After completion of image capturing (Andor Solis) turn off excitation LEDs. Repeat for three trials.
- Complete next 19 – 24 trials of first block without imaging.
- Perform last three trials of the block with imaging as described before).
- Choose the second training protocol. Perform the second training block similar as described for first training block.
- Save trials.
- Stitch together frames of three consecutive trials each (four times). Perform reconstruction and ICA on combined trials.

## **Classical Conditioning**

### **Ad 4.: Choose a conditioning protocol**

Choose following protocol for **classical fear conditioning** in the GUI:

- "Protocol 3: Fear Cond": protocol for pre-trials, training as well as test trials.

### **Execution of experiment: classical conditioning**

- Choose the small chamber for experimentation (see Figure A.9 right).
- Warm up warming bath to  $\approx 80^\circ\text{C}$ , put in two reservoirs: one filled with E3 medium, one with odor. Adjust flow rates of pumps (minimal flow rate for outflow, adjust inflow in order to keep constant level). Measure the temperature of  $\approx 26^\circ\text{C}$  at end of tubing/in chamber. Open valves to fill tubing with odor without attachment at chamber. Close valves.
- Choose protocol "Protocol 3: Fear Cond" in GUI.

- Change the length of one trial in GUI to 330 seconds to provide ITI of  $\approx 5$  minutes (ITI  $\approx$  trial length  $-26.5$  ).
- Trials start with baseline interval of 18.5 seconds without stimuli. Valves open 6 seconds before laser power-up (2 s afflux, 4 s IS). Laser exposure lasts 2 seconds, valves are closed 3 seconds before laser termination.
- For optional pre-trials (0 – 3), turn off the key switch of the laser.
- For training trials (7 – 15), turn on key switch of laser.
- For test trials (3), turn off the key switch of the laser.

## Matlab Codes

This appendix contains the most important parts of the conditioning protocols implemented in Matlab.

### C.1 Graphical User Interface (GUI)

Run the main mat-file 'myGUI.m' in order to start the GUI with implemented codes for different conditioning protocols. Corresponding mat-files for conditioning protocols are presented in section C.2 and C.3.

```

1
2
3 function varargout = myGUI(varargin)
4 % MYGUI MATLAB code for myGUI.fig
5 %     MYGUI, by itself, creates a new MYGUI or raises the existing
6 %     singleton*.
7 %
8 %     H = MYGUI returns the handle to a new MYGUI or the handle to
9 %     the existing singleton*.
10 %
11 %     MYGUI('CALLBACK',hObject,eventData,handles,...) calls the local
12 %     function named CALLBACK in MYGUI.M with the given input arguments.
13 %
14 %     MYGUI('Property','Value',...) creates a new MYGUI or raises the
15 %     existing singleton*. Starting from the left, property value pairs are
16 %     applied to the GUI before myGUI_OpeningFcn gets called. An
17 %     unrecognized property name or invalid value makes property application
18 %     stop. All inputs are passed to myGUI_OpeningFcn via varargin.
19 %
20 %     *See GUI Options on GUIDE's Tools menu. Choose "GUI allows only one
21 %     instance to run (singleton)".
22 %
23 % See also: GUIDE, GUIDATA, GUIHANDLES
24 % Edit the above text to modify the response to help myGUI
25 % Last Modified by GUIDE v2.5 07-Aug-2014 11:38:09
26
27 % Begin initialization code - DO NOT EDIT
28 gui_Singleton = 1;
29 gui_State = struct('gui_Name',       mfilename, ...
30                   'gui_Singleton',   gui_Singleton, ...

```

```

31         'gui_OpeningFcn', @myGUI_OpeningFcn, ...
32         'gui_OutputFcn', @myGUI_OutputFcn, ...
33         'gui_LayoutFcn', [] , ...
34         'gui_Callback', []);
35 if nargin && ischar(varargin{1})
36     gui_State.gui_Callback = str2func(varargin{1});
37 end
38
39 if nargin
40     [varargout{1:nargout}] = gui_mainfcn(gui_State, varargin{:});
41 else
42     gui_mainfcn(gui_State, varargin{:});
43 end
44 % End initialization code — DO NOT EDIT
45
46 %%%%%%%%%%%%%%%%%%%%%%%%%%%%%%%%%%%%%%%%%%%%%%%%%%%%%%%%%%%%%%%%%%%%%%%%%%%%%%%
47 %opening function for initializing
48 %%%%%%%%%%%%%%%%%%%%%%%%%%%%%%%%%%%%%%%%%%%%%%%%%%%%%%%%%%%%%%%%%%%%%%%%%%%%%%%
49 % ——— Executes just before myGUI is made visible.
50 function myGUI_OpeningFcn(hObject, eventdata, handles, varargin)
51
52 %initialize opening parameters in GUI
53 handles.seconds = 120;
54 handles.NumberTrials=2;
55 handles.threshangle=45;
56 handles.thresframes=1;
57 handles.BiasNumber=3;
58
59 %save data in struct file with fields...
60 field_names = {'name','result','angvel','laserooff','resultlast','resultlast_frame',
61               'tailpoints','tperframe','tcompare','timevec','timeperframe','inactivestate',
62               'inactivecount','output'}; % Cell with field names
61 empty_cells = repmat(cell(1),1,numel(field_names));
62 entries = {field_names{:} ; empty_cells{:}};
63 s = struct(entries{:});
64 trials=repmat(s,100,1);
65 handles.trials=trials;
66 handles.kk=0;
67 set(handles.edit_trialtime, 'String', handles.seconds);
68 set(handles.edit_trialnumber, 'String', handles.NumberTrials);
69 set(handles.edit_angle, 'String',handles.threshangle);
70 set(handles.edit_frames, 'String',handles.thresframes);
71 set(handles.edit_biasnumber, 'String',handles.BiasNumber);
72
73 %read in point grey camera
74 info=imaqhwinfo('winvideo');
75 vid=imaq.VideoDevice('winvideo', info.DeviceInfo.DeviceID);
76 set(vid,'ReturnedDataType','uint8','ReturnedColorSpace','grayscale');
77 pixelsize=get(vid, 'ROI');
78 vert_res=pixelsize(end);
79 hor_res=pixelsize(end-1);
80 preview(vid);
81
82 %define parameters for tracking algorithm
83 f=800/vert_res;
84 veclength=100; %
85 if rem(veclength,2)==1 %ungerade
86     veclength=veclength+1;
87 end
88 t=(-veclength/2):(veclength/2);
89 e=[0,-1];
90

```

```

91 % load camera properties in workspace
92 FrameRateDevice=vid.DeviceProperties.FrameRate;
93 assignin('base','FrameRateDevice',FrameRateDevice);
94
95 %daq-board acquisition
96 daq.getVendors;
97 device=daq.getDevices;
98 get(device) %get info of device = clicking on device. then get info of subsystems,
    channelNames...
99 mydaq=daq.createSession('ni');
100 valvdaq=daq.createSession('ni');
101 mydaq.addAnalogOutputChannel('Dev1','ao0','Voltage');
102 valvdaq.addAnalogOutputChannel('Dev1','ao1','Voltage');
103 mydaq.outputSingleScan(0);
104 valvdaq.outputSingleScan(0);
105
106 handles.mydaq=mydaq;
107 handles.valvdaq=valvdaq;
108 handles.vid=vid;
109 handles.FrameRate=str2double(FrameRateDevice);
110 handles.f=f;
111 handles.t=t;
112 handles.e=e;
113 handles.r=20;
114 handles.veclength=veclength;
115 handles.vert_res=vert_res;
116 handles.hor_res=hor_res;
117 %opening parameter in GUI:
118 handles.experiment = 0; %bias determination
119 handles.movie=0; %no movie capturing
120 handles.everytrial=0; %counting every trial (not only correct trials)
121 handles.output = hObject;
122 release(vid);
123 clear vid;
124 % update handles structures
125 guidata(hObject, handles);
126
127 % — Outputs from this function are returned to the command line.
128 function varargout = myGUI_OutputFcn(hObject, eventdata, handles)
129
130 varargout{1} = handles.output;
131
132 %%%%%%%%%%%%%%%%%%%%%%%%%%%%%%%%%%%%%%%%%%%%%%%%%%%%%%%%%%%%%%%%%%%%%%%%%%%%%%%
133 %take test image
134 %%%%%%%%%%%%%%%%%%%%%%%%%%%%%%%%%%%%%%%%%%%%%%%%%%%%%%%%%%%%%%%%%%%%%%%%%%%%%%%
135 % — Executes on button press in testimage.
136 function testimage_Callback(hObject, eventdata, handles)
137
138 handles.snap = step(handles.vid);
139 axes(handles.axes1);
140 imagesc(handles.snap); colormap(gray)
141 guidata(hObject, handles);
142
143 %%%%%%%%%%%%%%%%%%%%%%%%%%%%%%%%%%%%%%%%%%%%%%%%%%%%%%%%%%%%%%%%%%%%%%%%%%%%%%%
144 %set anchor point in test image
145 %%%%%%%%%%%%%%%%%%%%%%%%%%%%%%%%%%%%%%%%%%%%%%%%%%%%%%%%%%%%%%%%%%%%%%%%%%%%%%%
146 % — Executes on button press in anchorpoint.
147 function anchorpoint_Callback(hObject, eventdata, handles)
148
149 axes(handles.axes1);
150 [x,y]=ginput(1);
151 x=round(x);

```

```

152 y=round(y);
153 imagesc(handles.snap); colormap(gray)
154 hold on;
155 plot(x,y,'m',x,y,'yo')
156 handles.x=x;
157 handles.y=y;
158
159 guidata(hObject, handles);
160
161 %%%%%%%%%%%%%%%%%%%%%%%%%%%%%%%%%%%%%%%%%%%%%%%%%%%%%%%%%%%%%%%%%%%%%%%%%%%%%%%
162 %set reference line in test image and calculate parameters for tracking
163 %%%%%%%%%%%%%%%%%%%%%%%%%%%%%%%%%%%%%%%%%%%%%%%%%%%%%%%%%%%%%%%%%%%%%%%%%%%%%%%
164 % — Executes on button press in referenceline.
165 function referenceline_Callback(hObject, eventdata, handles)
166
167 r=handles.r;
168 axes(handles.axes1);
169 [x,y]=ginput(2);
170 x=round(x);
171 y=round(y);
172 imagesc(handles.snap); colormap(gray)
173 hold on;
174 plot(x,y,'m',x,y,'yo')
175 handles.c=[x(2)-x(1),y(2)-y(1)];
176 handles.M=[x(1),y(1)];
177 taillength=norm([x(2)-x(1),y(2)-y(1)]);
178 handles.n=round(taillength./r);
179 n=handles.n;
180 assignin('base','n',n);
181
182 guidata(hObject, handles);
183
184 %%%%%%%%%%%%%%%%%%%%%%%%%%%%%%%%%%%%%%%%%%%%%%%%%%%%%%%%%%%%%%%%%%%%%%%%%%%%%%%
185 %button to start trial, dependent on protocol
186 %%%%%%%%%%%%%%%%%%%%%%%%%%%%%%%%%%%%%%%%%%%%%%%%%%%%%%%%%%%%%%%%%%%%%%%%%%%%%%%
187 % — Executes on button press in startbutton.
188 function startbutton_Callback(hObject, eventdata, handles)
189
190 %commit parameters
191 movie=handles.movie;
192 trials=handles.trials;
193 kk=handles.kk;
194 kk=kk+1;
195 everytrial=handles.everytrial;
196 thresh_angle=handles.threshangle;
197 thres_frames=handles.thresframes;
198 biasnumber=handles.BiasNumber;
199 n=handles.n;
200 intens_thresh=handles.intensthresh;
201 veclength=handles.veclength;
202 t=handles.t;
203 e=handles.e;
204 r=handles.r;
205 x=handles.x;
206 y=handles.y;
207 c=handles.c;
208 M=handles.M;
209 NumberTrials=handles.NumberTrials;
210 FrameRate=handles.FrameRate;
211 vid=handles.vid;
212 mydaq=handles.mydaq;
213 valvdaq=handles.valvdaq;

```

```

214 seconds=handles.seconds;
215 vert_res=handles.vert_res;
216 hor_res=handles.hor_res;
217 axes(handles.axes1);
218 axes(handles.axes3);
219 cla
220 set(handles.outputtext, 'String', 'Output: direction');
221 minutes=0;
222
223 %define global variable for manual laser termination during trial
224 global stop stoplaser
225 stop=false;
226 stoplaser=false;
227
228 %run mat-file dependent on defined protocol (compare pop-up menu)
229 if handles.experiment==0 %'Bias determination'
230     biasdetermination_new_2
231     a=0;
232     handles.a=a;
233     assignin('base', 'a', a);
234 elseif handles.experiment==1 %'Protocol1: LT'
235     lefttraining_new_2%_loop
236     a=1;
237     handles.a=a;
238     assignin('base', 'a', a);
239 elseif handles.experiment==2 %'Protocol1: RT'
240     righttraining_new_2%_loop
241     a=2;
242     handles.a=a;
243     assignin('base', 'a', a);
244 elseif handles.experiment==3 %'Protocol1: test Reaction'
245     testreaction_new_2
246     a=3;
247     handles.a=a;
248     assignin('base', 'a', a);
249 elseif handles.experiment==4 %'Protocol2: LT'
250     lefttraining_odor_circles%_loop
251     a=4;
252     handles.a=a;
253     assignin('base', 'a', a);
254 elseif handles.experiment==5 %'Protocol2: RT'
255     righttraining_odor_circles
256     a=5;
257     handles.a=a;
258     assignin('base', 'a', a);
259 elseif handles.experiment==6 %'Protocol2: test Reaction'
260     testreaction_odor_circles
261     a=6;
262     handles.a=a;
263     assignin('base', 'a', a);
264 elseif handles.experiment==7
265     fearconditioning_trials_timernew %'Protocol3: Fear Cond'
266     a=7;
267     handles.a=a;
268     assignin('base', 'a', a);
269 end
270
271 handles.result=result; %only last result vector is memorized and can be plotted (in GUI
    )!
272 handles.counter=counter;
273 guidata(hObject, handles);
274

```

```

275 %%%%%%%%%%%%%%%%%%%%%%%%%%%%%%%%%%%%%%%%%%%%%%%%%%%%%%%%%%%%%%%%%%%%%%%%%%
276 %optional but not visible in GUI, ignore
277 %%%%%%%%%%%%%%%%%%%%%%%%%%%%%%%%%%%%%%%%%%%%%%%%%%%%%%%%%%%%%%%%%%%%%%%%%%
278 % — Executes on button press in plotbutton.
279 function plotbutton_Callback(hObject, eventdata, handles)
280
281 trials=handles.trials;
282 kk=handles.kk;
283 trial=trials(1:kk);
284 axes(handles.axes3);
285 resultplot
286
287 guidata(hObject, handles);
288
289 %%%%%%%%%%%%%%%%%%%%%%%%%%%%%%%%%%%%%%%%%%%%%%%%%%%%%%%%%%%%%%%%%%%%%%%%%%
290 %delete data when closing GUI
291 %%%%%%%%%%%%%%%%%%%%%%%%%%%%%%%%%%%%%%%%%%%%%%%%%%%%%%%%%%%%%%%%%%%%%%%%%%
292 % — Executes when user attempts to close figure1.
293 function figure1_CloseRequestFcn(hObject, eventdata, handles)
294
295     delete(hObject);
296
297 %%%%%%%%%%%%%%%%%%%%%%%%%%%%%%%%%%%%%%%%%%%%%%%%%%%%%%%%%%%%%%%%%%%%%%%%%%
298 %define time of one trial in edit field
299 %%%%%%%%%%%%%%%%%%%%%%%%%%%%%%%%%%%%%%%%%%%%%%%%%%%%%%%%%%%%%%%%%%%%%%%%%%
300 function edit_trialtime_Callback(hObject, eventdata, handles)
301 seconds = str2double(get(hObject, 'String'));
302 handles.seconds = seconds;
303 guidata(hObject, handles)
304
305 % — Executes during object creation, after setting all properties.
306 function edit_trialtime_CreateFcn(hObject, eventdata, handles)
307
308 if ispc && isequal(get(hObject,'BackgroundColor'), get(0,'
    defaultUicontrolBackgroundColor'))
309     set(hObject,'BackgroundColor','white');
310 end
311
312 %%%%%%%%%%%%%%%%%%%%%%%%%%%%%%%%%%%%%%%%%%%%%%%%%%%%%%%%%%%%%%%%%%%%%%%%%%
313 %stop trial manually
314 %%%%%%%%%%%%%%%%%%%%%%%%%%%%%%%%%%%%%%%%%%%%%%%%%%%%%%%%%%%%%%%%%%%%%%%%%%
315 % — Executes on button press in stopbutton.
316 function stopbutton_Callback(hObject, eventdata, handles)
317
318 global stop
319 stop=true;
320 guidata(hObject, handles)
321
322 %%%%%%%%%%%%%%%%%%%%%%%%%%%%%%%%%%%%%%%%%%%%%%%%%%%%%%%%%%%%%%%%%%%%%%%%%%
323 %define pop-up menu for various protocols
324 %%%%%%%%%%%%%%%%%%%%%%%%%%%%%%%%%%%%%%%%%%%%%%%%%%%%%%%%%%%%%%%%%%%%%%%%%%
325 % — Executes on selection change in popupmenu1.
326 function popupmenu1_Callback(hObject, eventdata, handles)
327
328 str = get(hObject, 'String');
329 val = get(hObject, 'Value');
330 % Set current data to the selected data set.
331 switch str{val};
332 case 'Bias determination' % User selects 'Bias determination'
333     handles.experiment = 0;
334 case 'Protocol1: LT'
335     handles.experiment = 1;

```



```

336 case 'Protocol1: RT'
337     handles.experiment = 2;
338 case 'Protocol1: test Reaction'
339     handles.experiment = 3;
340 case 'Protocol2: LT'
341     handles.experiment = 4;
342 case 'Protocol2: RT'
343     handles.experiment = 5;
344 case 'Protocol2: test Reaction'
345     handles.experiment = 6;
346 case 'Protocol3: Fear Cond'
347     handles.experiment = 7;
348 end
349 % Save the handles structure.
350 guidata(hObject, handles)
351
352 % — Executes during object creation, after setting all properties.
353 function popupmenu1_CreateFcn(hObject, eventdata, handles)
354
355 if ispc && isequal(get(hObject,'BackgroundColor'), get(0,'
    defaultUicontrolBackgroundColor'))
356     set(hObject,'BackgroundColor','white');
357 end
358
359 %user defines threshold value for angle (defined as turn)
360 %user defines threshold value for angle (defined as turn)
361 %user defines threshold value for angle (defined as turn)
362 function edit_angle_Callback(hObject, eventdata, handles)
363
364 thresangle = str2double(get(hObject, 'String'));
365 handles.threshangle = thresangle;
366 guidata(hObject, handles)
367
368 % — Executes during object creation, after setting all properties.
369 function edit_angle_CreateFcn(hObject, eventdata, handles)
370
371 if ispc && isequal(get(hObject,'BackgroundColor'), get(0,'
    defaultUicontrolBackgroundColor'))
372     set(hObject,'BackgroundColor','white');
373 end
374
375 %user defines if movie (single frames) saved to the
376 %workspace
377 %user defines if movie (single frames) saved to the
378 %workspace
379 % — Executes on button press in checkbox1.
380 function checkbox1_Callback(hObject, eventdata, handles)
381
382 if (get(hObject,'Value') == get(hObject,'Max'))
383     handles.movie=1;
384 else
385     handles.movie=0;
386 end
387 guidata(hObject, handles)
388
389 %button clears workspace
390 %button clears workspace
391 %button clears workspace
392 % — Executes on button press in clear_pushbutton.
393 function clear_pushbutton_Callback(hObject, eventdata, handles)
394
395 evalin('base','clear ');

```

```

396 set(handles.outputtext, 'String', 'Output: direction');
397 guidata(hObject, handles)
398
399 %%%%%%%%%%%%%%%%%%%%%%%%%%%%%%%%%%%%%%%%%%%%%%%%%%%%%%%%%%%%%%%%%%%%%%%%%%
400 %button stops laser during one trial
401 %%%%%%%%%%%%%%%%%%%%%%%%%%%%%%%%%%%%%%%%%%%%%%%%%%%%%%%%%%%%%%%%%%%%%%%%%%
402 % — Executes on button press in stoplaser_button.
403 function stoplaser_button_Callback(hObject, eventdata, handles)
404
405 global stoplaser
406 stoplaser=true;
407 guidata(hObject, handles)
408
409 %%%%%%%%%%%%%%%%%%%%%%%%%%%%%%%%%%%%%%%%%%%%%%%%%%%%%%%%%%%%%%%%%%%%%%%%%%
410 %optional but not visible in GUI: define intensity threshold dependent on image values
    (rect) or
411 %fixed
412 %%%%%%%%%%%%%%%%%%%%%%%%%%%%%%%%%%%%%%%%%%%%%%%%%%%%%%%%%%%%%%%%%%%%%%%%%%
413 % — Executes on button press in rect_button.
414 function rect_button_Callback(hObject, eventdata, handles)
415
416 axes(handles.axes1);
417 rect=getrect;
418 aa=handles.snap(rect(2):(rect(2)+rect(4)), rect(1):(rect(1)+rect(3)));
419 %handles.intensthresh=mean(mean(aa))+0.04*mean(mean(aa)); %double: 0.04
420 %insthresh=max(max(aa));
421
422 insthresh=125; %define fixed value as threshold
423 assignin('base', 'insthresh', insthresh);
424 handles.intensthresh=insthresh;
425 imagesc(handles.snap); colormap(gray)
426
427 figure;
428 imagesc(step(handles.vid)); colormap(gray)
429 guidata(hObject, handles)
430
431 %%%%%%%%%%%%%%%%%%%%%%%%%%%%%%%%%%%%%%%%%%%%%%%%%%%%%%%%%%%%%%%%%%%%%%%%%%
432 %save struct file with data in workspace
433 %%%%%%%%%%%%%%%%%%%%%%%%%%%%%%%%%%%%%%%%%%%%%%%%%%%%%%%%%%%%%%%%%%%%%%%%%%
434 % — Executes on button press in save_trials_button.
435 function save_trials_button_Callback(hObject, eventdata, handles)
436
437 trials=handles.trials;
438 kk=handles.kk;
439 trial=trials(1:kk);
440 time=handles.time;
441 assignin('base', 'trial', trial);
442 pathdirtr='E:\data';
443 save(fullfile(pathdirtr, [num2str(time(1)) '_' num2str(time(2)) '_' num2str(time(3)) '_'
    num2str(time(4)) '_' num2str(time(5)) '_' num2str(time(6)) '.mat']), 'trial');
444
445 guidata(hObject, handles)
446
447 %%%%%%%%%%%%%%%%%%%%%%%%%%%%%%%%%%%%%%%%%%%%%%%%%%%%%%%%%%%%%%%%%%%%%%%%%%
448 %button clears data for new experiment
449 %%%%%%%%%%%%%%%%%%%%%%%%%%%%%%%%%%%%%%%%%%%%%%%%%%%%%%%%%%%%%%%%%%%%%%%%%%
450 % — Executes on button press in newexp_button.
451 function newexp_button_Callback(hObject, eventdata, handles)
452
453 clear all;
454 handles.trials=struct;
455 handles.kk=0;

```

```

456 handles.snap = step(handles.vid);
457 axes(handles.axes1);
458 imagesc(handles.snap); colormap(gray)
459
460 guidata(hObject,handles)
461
462 %%%%%%%%%%%%%%%%%%%%%%%%%%%%%%%%%%%%%%%%%%%%%%%%%%%%%%%%%%%%%%%%%%%%%%%%%
463 %button closes valves manually during trial
464 %%%%%%%%%%%%%%%%%%%%%%%%%%%%%%%%%%%%%%%%%%%%%%%%%%%%%%%%%%%%%%%%%%%%%%%%%
465 % — Executes on button press in valvesoff_button.
466 function valvesoff_button_Callback(hObject, eventdata, handles)
467
468 valvdaq=handles.valvdaq;
469 valvdaq.outputSingleScan (0);
470 guidata(hObject,handles)
471
472 %%%%%%%%%%%%%%%%%%%%%%%%%%%%%%%%%%%%%%%%%%%%%%%%%%%%%%%%%%%%%%%%%%%%%%%%%
473 %button opens valves manually during trial
474 %%%%%%%%%%%%%%%%%%%%%%%%%%%%%%%%%%%%%%%%%%%%%%%%%%%%%%%%%%%%%%%%%%%%%%%%%
475 % — Executes on button press in valveson_button.
476 function valveson_button_Callback(hObject, eventdata, handles)
477
478 valvdaq=handles.valvdaq;
479 valvdaq.outputSingleScan (5);
480 guidata(hObject,handles)
481
482 % — Executes on button press in save_video_button.
483 function save_video_button_Callback(hObject, eventdata, handles) %ignore, not working
484
485 videoframes=handles.videoframes;
486 time=handles.time;
487 assignin('base', ['BD_' num2str(time(1)) '_' num2str(time(2)) '_' num2str(time(3)) '_'
    num2str(time(4)) '_' num2str(time(5)) '_' num2str(time(6)) '_videoframes'],
    videoframes);
488 a=handles.a;
489 movie=handles.movie;
490 set(handles.outputtext, 'String', 'BUSY: save');
491 pathdir='E:\data\fish behaviour';
492 if a==0 %bias
493     if movie==1
494         save( fullfile(pathdir,[ num2str(time(1)) '_' num2str(time(2)) '_' num2str(time(3))
            '_' num2str(time(4)) '_' num2str(time(5)) '_' num2str(time(6)) '
            _BD_videoframes.mat' ]) ,...
            'videoframes','-v7.3');
495     end
496 elseif a==1 %left
497     if movie==1
498         save( fullfile(pathdir,[ num2str(time(1)) '_' num2str(time(2)) '_' num2str(time(3)) '
            '_' num2str(time(4)) '_' num2str(time(5)) '_' num2str(time(6)) '_LT_videoframes
            .mat' ]) ,...
500         ['LT_' num2str(time(1)) '_' num2str(time(2)) '_' num2str(time(3)) '_' num2str(
            time(4)) '_' num2str(time(5)) '_' num2str(time(6)) '_videoframes'], '-v7.3'
            );
501     end
502 elseif a==2 %right
503     if movie==1
504         save( fullfile(pathdir,[ num2str(time(1)) '_' num2str(time(2)) '_' num2str(time(3)) '
            '_' num2str(time(4)) '_' num2str(time(5)) '_' num2str(time(6)) '_RT_videoframes
            .mat' ]) ,...
505         ['RT_' num2str(time(1)) '_' num2str(time(2)) '_' num2str(time(3)) '_' num2str(
            time(4)) '_' num2str(time(5)) '_' num2str(time(6)) '_videoframes'], '-v7.3'
            );

```

```

506     end
507 elseif a==3
508     if movie==1
509         save( fullfile( pathdir ,[ num2str(time(1)) '_' num2str(time(2)) '_' num2str(time(3)) '_'
                    num2str(time(4)) '_' num2str(time(5)) '_' num2str(time(6)) '_tR_videoframes
                    .mat' ]) ,...
510             ['tR_' num2str(time(1)) '_' num2str(time(2)) '_' num2str(time(3)) '_' num2str(
                    time(4)) '_' num2str(time(5)) '_' num2str(time(6)) '_videoframes' ],'-v7.3'
                    );
511     end
512 end
513 set(handles.outputtext , 'String' , '');

```

## C.2 Operant Conditioning Protocol

Matlab code for left training of the operant conditioning protocol with additional odor stimulation ('Protocol2: LT') is presented as an example.

```

1  %%%%%%%%%%%%%%%%%%%%%%%%%%%%%%%%%%%%%%%%%%%%%%%%%%%%%%%%%%%%%%%%%%%%%%%%%%
2  %code for 'Protocol2: LT' in GUI (left training with odor stimulation)
3  %%%%%%%%%%%%%%%%%%%%%%%%%%%%%%%%%%%%%%%%%%%%%%%%%%%%%%%%%%%%%%%%%%%%%%%%%%
4
5  %initialization
6  frames=round(seconds*FrameRate)+2;
7  assignin('base', 'movie', movie); %display variables in workspace
8  resultlast=cell(1,50);
9  resultlast_frame=cell(1,50);
10 counter=2; %start to write in 2nd entry of arrays for calculation of angel
11 counter3=0;
12 inactive=0.2; %for definition of turn event: tail needs to be inactive for 200ms
13 inactivecount=0;
14 result=zeros(1,frames); %array of angles
15 inactivestate=result; %for calculation of time without turn event
16 tperframe=result; %processing time per frame
17 tcompare=result; %ignore
18 tailpoints=zeros(n,2,frames); %coordinates of points representing the tail
19 if movie==1
20     videoframes=zeros(vert_res , hor_res , frames , 'uint8'); %save captured frames of cam in
        3D array
21 end
22 laseroff=zeros(1,frames); %keep frame# when events (valves switching , laser off)
23 counteroff=0;
24
25 %valves on
26 set(handles.outputtext , 'String' , 'PAUSE');
27 pause on;
28 valvdaq.outputSingleScan (5); %valve switch for odor pulse
29 pause(2); %estimated time to reach fish , change pause to 10sec for operant with imaging
        !
30 set(handles.outputtext , 'String' , '');
31 %laser on
32 mydaq.outputSingleScan (5);
33
34 %time definition of one trial
35 S = datestr(clock);
36 time=datevec(S);
37 finalTime = datenum(clock + [0, 0, 0, 0, minutes , seconds]); %time of one trial ,
        defined by user
38 finalTimeVec=datevec( datestr( finalTime));

```

```

39  tstart=tic;
40  while datenum(clock) < finalTime && ~stop % tail tracking runs defined time
41
42  ts=tic; %set timestamp
43  frame=step(vid); %frame capturing
44
45  %tracking algorithm, cf. section 'Automated Tail Tracking—Mathematical description' and
      figure 3.6.
46  points=zeros(n,2); %P_0–P_last
47  pos=zeros(n-1,1);
48  maxval=pos;
49  circ=zeros(veclength+1,3); %for pixel coordinates and intensities of B_1–B_last
50  points(1,:)=[x,y]; %anchor point P_0, x,y according to image coordinates
51  %-----
52  k=2; %seperate case: find P_1
53  rr=e; %vertical vector
54  circ(:,1)=round(points(k-1,1)+r*rr(1)-t*(-rr(2))); %pixel coordinates of B_1
55  circ(:,2)=round(points(k-1,2)+r*rr(2)-t*rr(1));
56  for i=1:veclength+1
57      if (circ(i,2)<=0) || (vert_res<=circ(i,2)) || (circ(i,1)<=0) || (hor_res<=circ(i,
          1)) %B_1 at image boarder
58          break
59      end
60      circ(i,3)=frame(circ(i,2),circ(i,1)); %intensity values of B_1
61  end
62  [maxval(k-1),pos(k-1)]=max(circ(:,3)); %maximal intensity value
63  points(k,:)=[circ(pos(k-1),1), circ(pos(k-1),2)]; %P_1
64
65  for k=3:n %find P_2–P_last
66  rr=(points(k-1,:)-points(k-2,:))./(norm(points(k-1,:)-points(k-2,:))); %directional
      vectors r_P
67  circ(:,1)=round(points(k-1,1)+r*rr(1)-t*(-rr(2))); %pixel coordinates of B_i
68  circ(:,2)=round(points(k-1,2)+r*rr(2)-t*rr(1));
69  for i=1:veclength+1
70      if (circ(i,2)<=0) || (vert_res<=circ(i,2)) || (circ(i,1)<=0) || (hor_res<=circ(
          i,1)) %B_i at image boarder
71          break
72      end
73      circ(i,3)=frame(circ(i,2),circ(i,1)); %intensity values of B_i
74  end
75  [maxval(k-1),pos(k-1)]=max(circ(:,3)); %maximal intensity value
76  if maxval(k-1)<intens_thresh || (circ(i,2)<=0) || (vert_res<=circ(i,2)) || (circ(i,
      1)<=0) || (hor_res<=circ(i,1)) %if intensity value below threshold: P_last
77      break
78  end
79  points(k,:)=[circ(pos(k-1),1), circ(pos(k-1),2)]; %P_i
80  end
81  %calculating deflection angle
82  index=find(points(:,1));
83  last=[points(index(end),1),points(index(end),2)]; %P_last
84  a=last-M; %M is R_1 of reference line
85  alpha=acosd(dot(a,c)/(norm(a)*norm(c))); %positive deflection angle
86  if det([a;c])<0 %det<0 if a right of c in image
87      alpha=-alpha; %negative angle for right, positive for left
88  end
89  %-----
90  %read out data
91  result(counter)=alpha;
92  tps=toc(ts);
93  tcompare(counter)=toc(ts);
94  inactive=inactive+tcompare(counter);
95  inactivecount=inactivecount+1;

```

```

96  inactivestate(counter)=inactive;
97
98  if alpha < -thresh_angle && inactive > 0.2 && k-1 >= 5 %right turn (counted only when
    inactive > 0.2)
99      counter3=counter3+1;
100     inactive=0;
101     resultlast{counter3}=result(counter); %read out angles of turns
102     resultlast_frame{counter3}=counter-1; %read out frame# of turns
103     set(handles.outputtext, 'String', 'right');
104 elseif alpha > thresh_angle && inactive > 0.2 && k-1 >= 5 %left turn (counted only when
    inactive > 0.2) -> laser off
105     counteroff=counteroff+1;
106     laseroft(counteroff)=counter-1; %read out frame# when laser off, -1 because counter
        =2
107     mydaq.outputSingleScan (0); %laser off
108     valvdaq.outputSingleScan (0); %valves close
109     counter3=counter3+1;
110     inactive=0;
111     resultlast{counter3}=result(counter); %read out angles of turns
112     resultlast_frame{counter3}=counter-1; %read out frame# of turns
113     set(handles.outputtext, 'String', 'LEFT -> OFF');
114 elseif abs(alpha) > thresh_angle && k-1 >= 5 %left or right turn during 0.2 pause (not
    counted)
115     inactive=0;
116 end
117
118 if stoplaser==true
119     %laser off
120     mydaq.outputSingleScan (0);
121 end
122 if movie==1
123     videoframes(:, :, counter)=frame;
124 end
125 tailpoints(:, :, counter)=points;
126 tperframe(counter)=toc(ts); %timestamp
127 toc(ts)
128 counter=counter+1;
129 end
130 twhole=toc(tstart);
131 frameNumber = counter-1; %number of captured frames
132 timeperframe=twhole/(frameNumber-1); %averaged processing time
133 %laser off if no correct turn
134 mydaq.outputSingleScan (0);
135 %valves off if no correct turn
136 valvdaq.outputSingleScan (0);
137 %calculate angular velocity
138 angvel=zeros(1, length(result));
139 for i=2:length(result)
140     angvel(i)=abs(result(i)-result(i-1))./(tperframe(i)*1000);
141 end
142 laseroft=laseroft(1); %frame# when laser off
143 vidend=laseroft+500; %keep limited frames for video
144 if stop==true || laseroft==0
145     laseroft=frameNumber-1;
146     vidend=laseroft;
147 end
148 %arrays pruning (counter=2)
149 result=real(result(2:frameNumber));
150 angvel=angvel(2:frameNumber);
151 tperframe=tperframe(2:frameNumber);
152 tailpoints=tailpoints(:, :, 2:frameNumber);
153 inactivestate=inactivestate(2:frameNumber);

```

```

154 tcompare=tcompare(2:frameNumber);
155 %calculate time axis according to tperframe
156 timevec=zeros(1,length(result));
157 timevec(1)=tperframe(1);
158 for i=2:length(result)
159 timevec(i)=timevec(i-1)+tperframe(i);
160 end
161 %save captured frames in workspace
162 if movie==1
163 videoframes=videoframes(:,2:vidend);
164 assignin('base',[ 'LT_' num2str(time(1)) '_' num2str(time(2)) '_' num2str(time(3)) '_'
    num2str(time(4)) '_' num2str(time(5)) '_' num2str(time(6)) '_videoframes'],
    videoframes);
165 assignin('base','time',time);
166 assignin('base','finalTimeVec',finalTimeVec);
167 assignin('base','movie',movie);
168 end
169 resultlast=cell2mat(resultlast(1:(counter3)));
170 resultlast_frame=cell2mat(resultlast_frame(1:(counter3)));
171 %save parameters in struct file
172 trials(kk).name=[ 'LT_' num2str(time(1)) '_' num2str(time(2)) '_' num2str(time(3)) '_'
    num2str(time(4)) '_' num2str(time(5)) '_' num2str(time(6)) ];
173 trials(kk).result=result;
174 trials(kk).angvel=angvel;
175 trials(kk).laseroff=laseroff;
176 trials(kk).resultlast=resultlast;
177 trials(kk).resultlast_frame=resultlast_frame;
178 trials(kk).tailpoints=tailpoints;
179 trials(kk).tperframe=tperframe;
180 trials(kk).tcompare=tcompare;
181 trials(kk).timevec=timevec;
182 trials(kk).timeperframe=timeperframe;
183 trials(kk).inactivestate=inactivestate;
184 trials(kk).inactivecount=inactivecount;
185 if numel(resultlast)==0 %no turn at all
186     trials(kk).output='incorrect';
187 elseif resultlast(1)<0 %first turn was to the right
188     trials(kk).output='incorrect';
189 elseif resultlast(1)>0 %first turn was to the left
190     trials(kk).output='correct';
191 end
192 %commit variables
193 handles.trials=trials;
194 handles.time=time;
195 handles.kk=kk;

```

### C.3 Classical Conditioning Protocol

Matlab code of the classical fear conditioning protocol ('Protocol3: Fear Cond') is presented.

```

1
2 %%%%%%%%%%%%%%%%%%%%%%%%%%%%%%%%%%%%%%%%%%%%%%%%%%%%%%%%%%%%%%%%%%%%%%%%%%
3 %code for 'Protocol3: Fear Cond' in GUI (classical fear conditioning)
4 %%%%%%%%%%%%%%%%%%%%%%%%%%%%%%%%%%%%%%%%%%%%%%%%%%%%%%%%%%%%%%%%%%%%%%%%%%
5
6 %timing aspects of valves
7 odorstart=18.5; %time of valve opening
8 laserstart=(odorstart+2)+4; %time of laser on (t_1=2)
9 laserend=laserstart+2; %duration of laser

```

```

10 odorend=laserend-3; %time of valve closing (t_2=3)
11 %initialization
12 frames=round((seconds+laserend)*FrameRate)+2;
13 assignin('base','movie',movie);
14 resultlast=cell(1,50);
15 resultlast_frame=cell(1,50);
16 counter=2; %start to write in entry 2, because of angvel
17 counter3=0;
18 inactive=0;
19 inactivecount=0;
20 result=zeros(1,frames);
21 inactivestate=result;
22 tperframe=result;
23 tcompare=result;
24 tailpoints=zeros(n,2,frames);
25 if movie==1
26     videoframes=zeros(vert_res, hor_res, frames, 'uint8');%!!! single
27 end
28 %keep frame# of events
29 markerodon=zeros(1,frames);
30 markerodoff=markerodon;
31 markerlason=markerodon;
32 markerlasoff=markerodon;
33 counterodon=0;
34 counterodoff=0;
35 counterlason=0;
36 counterlasoff=0;
37
38 %time definitions within one trial
39 S = datestr(clock);
40 time=datevec(S);
41 %set timer for events
42 odoron=timer('TimerFcn', @(~,~) valvdaq.outputSingleScan(5)); %valves open
43 laseron = timer('TimerFcn', @(~,~) mydaq.outputSingleScan(5)); %laser on
44 odoroff=timer('TimerFcn', @(~,~) valvdaq.outputSingleScan(0)); %valves close
45 laseroftimer('TimerFcn', @(~,~) mydaq.outputSingleScan(0)); %laser off
46 nowtime=clock;
47 odoron_time = datenum(nowtime + [0, 0, 0, 0, 0, odorstart]);
48 odoroff_time = datenum(nowtime + [0, 0, 0, 0, 0, odorend]);
49 laseron_time = datenum(nowtime + [0, 0, 0, 0, 0, laserstart]);
50 laseroft_time = datenum(nowtime + [0, 0, 0, 0, 0, laserend]);
51 finalTime = datenum(nowtime + [0, 0, 0, 0, minutes, seconds + laserend]);
52 finalTimeVec=datevec(datestr(finalTime));
53 %start timer
54 startat(odoron, odoron_time);
55 startat(odoroff, odoroff_time);
56 startat(laseron, laseron_time);
57 startat(laseroft, laseroft_time);
58 tstart=tic;
59 %tail tracking runs for defined time
60 while datenum(clock) < finalTime && ~stop
61     ts=tic;
62     frame=step(vid);
63     points=zeros(n,2);
64     pos=zeros(n-1,1);
65     maxval=pos;
66     circ=zeros(veclength+1,3);
67     points(1,:)=[x,y];
68     %
69     k=2;
70     rr=e;
71     circ(:,1)=round(points(k-1,1)+r*rr(1)-t*(-rr(2)));

```



```

72 circ(:,2)=round(points(k-1,2)+r*rr(2)-t*rr(1));
73 for i=1:veclength+1
74     if (circ(i,2)<=0) || (vert_res<=circ(i,2)) || (circ(i,1)<=0) || (hor_res<=circ(i
75         ,1))
76         break
77     end
78     circ(i,3)=frame(circ(i,2),circ(i,1));
79 end
80 [maxval(k-1),pos(k-1)]=max(circ(:,3));
81 points(k,:)=[circ(pos(k-1),1), circ(pos(k-1),2)];
82 for k=3:n
83     rr=(points(k-1,:)-points(k-2,:))./(norm(points(k-1,:)-points(k-2,:)));
84     circ(:,1)=round(points(k-1,1)+r*rr(1)-t*(-rr(2)));
85     circ(:,2)=round(points(k-1,2)+r*rr(2)-t*rr(1));
86     for i=1:veclength+1
87         if (circ(i,2)<=0) || (vert_res<=circ(i,2)) || (circ(i,1)<=0) || (hor_res<=circ(i
88             ,1))
89             break
90         end
91         circ(i,3)=frame(circ(i,2),circ(i,1));
92     end
93     [maxval(k-1),pos(k-1)]=max(circ(:,3));
94     if maxval(k-1)<intens_thresh || (circ(i,2)<=0) || (vert_res<=circ(i,2)) || (circ(i
95         ,1)<=0) || (hor_res<=circ(i,1))
96         break
97     end
98     points(k,:)=[circ(pos(k-1),1), circ(pos(k-1),2)];
99 end
100 index=find(points(:,1));
101 last=[points(index(end),1),points(index(end),2)];
102 a=last-M;
103 alpha=acosd(dot(a,c)/(norm(a)*norm(c)));
104 if det([a;c])<0
105     alpha=-alpha;
106 end
107 %-----
108 result(counter)=alpha;
109 tps=toc(ts);
110 tcompare(counter)=toc(ts);
111 inactive=inactive+tcompare(counter);
112 inactivecount=inactivecount+1;
113 inactivestate(counter)=inactive;
114
115 if abs(alpha) > thresh_angle && k-1>=5 % defined as turn
116     counter3=counter3+1;
117     inactive=0;
118     resultlast{counter3}=result(counter);
119     resultlast_frame{counter3}=counter-1;
120     set(handles.outputtext,'String','turn');
121 else
122     set(handles.outputtext,'String','');
123 end
124
125 if datenum(clock)>=laserooff_time %read out frame# when laser off
126     counterlasoff=counterlasoff+1;
127     markerlasoff(counterlasoff)=counter-1;
128 elseif datenum(clock)>=laseron_time %read out frame# when laser on
129     counterlason=counterlason+1;
130     markerlason(counterlason)=counter-1;
131 elseif datenum(clock)>=odoroff_time %read out frame# when valves close
132     counterodoff=counterodoff+1;

```

```

131     markerodoff(counterodoff)=counter-1;
132 elseif datenum(clock)>=odoron_time %read out frame# when valves open
133     counterodon=counterodon+1;
134     markerodon(counterodon)=counter-1;
135 end
136
137 if stoplaser==true
138     mydaq.outputSingleScan (0); %laser off
139 end
140 if movie==1
141     videoframes(:, :, counter)=frame;
142 end
143 tailpoints(:, :, counter)=points;
144 tperframe(counter)=toc(ts);
145 toc(ts)
146 counter=counter+1;
147 end
148 twhole=toc(tstart);
149 frameNumber = counter-1;
150 timeperframe=twhole/(frameNumber-1);
151
152 %laser off
153 mydaq.outputSingleScan (0);
154 %valves off
155 valvdaq.outputSingleScan (0);
156
157 angvel=zeros(1,length(result));
158 for i=2:length(result)
159     angvel(i)=(result(i)-result(i-1))/(tperframe(i)*1000);
160 end
161
162 laseroff=zeros(1,4); %array laseroff contains frame# of events
163 laseroff(1)=markerodon(1); %valves open
164 laseroff(2)=markerodoff(1); %valves close
165 laseroff(3)=markerlason(1); %laser on
166 laseroff(4)=markerlasoff(1); %laser off
167 vidend=laseroff(4)+500;
168 if stop==true || laseroff(4)==0
169     laseroff=frameNumber-1;
170     vidend=laseroff;
171 end
172 result=real(result(2:frameNumber));
173 angvel=angvel(2:frameNumber);
174 tperframe=tperframe(2:frameNumber);
175 tailpoints=tailpoints(:, :, 2:frameNumber);
176 inactivestate=inactivestate(2:frameNumber);
177 tcompare=tcompare(2:frameNumber);
178
179 timevec=zeros(1,length(result));
180 timevec(1)=tperframe(1);
181 for i=2:length(result)
182     timevec(i)=timevec(i-1)+tperframe(i);
183 end
184
185 if movie==1
186     videoframes=videoframes(:, :, 2:vidend); %alle frames
187 assignin('base', ['FC_' num2str(time(1)) '_' num2str(time(2)) '_' num2str(time(3)) '_'
188                 num2str(time(4)) '_' num2str(time(5)) '_' num2str(time(6)) '_videoframes'],
189         videoframes);
188 assignin('base','time',time);
189 assignin('base','finalTimeVec',finalTimeVec);
190 assignin('base','movie',movie);

```

```

191 end
192 resultlast=cell2mat(resultlast(1:(counter3)));
193 resultlast_frame=cell2mat(resultlast_frame(1:(counter3)));
194
195 trials(kk).name=[ 'FC_' num2str(time(1)) '_' num2str(time(2)) '_' num2str(time(3)) '_'
    num2str(time(4)) '_' num2str(time(5)) '_' num2str(time(6)) ];
196 trials(kk).result=result;
197 trials(kk).angvel=angvel;
198 trials(kk).laserooff=laserooff;
199 trials(kk).resultlast=resultlast;
200 trials(kk).resultlast_frame=resultlast_frame;
201 trials(kk).tailpoints=tailpoints;
202 trials(kk).tperframe=tperframe;
203 trials(kk).tcompare=tcompare;
204 trials(kk).timevec=timevec;
205 trials(kk).timeperframe=timeperframe;
206 trials(kk).inactivestate=inactivestate;
207 trials(kk).inactivecount=inactivecount;
208 if numel(resultlast)==0
209     trials(kk).output='';
210 elseif resultlast(1)<0
211     trials(kk).output='';
212 elseif resultlast(1)>0
213     trials(kk).output='';
214 end
215
216 handles.trials=trials;
217 handles.time=time;
218 handles.kk=kk;

```



---

## Abbreviations

<b>CS</b>	conditioned stimulus
<b>US</b>	unconditioned stimulus
<b>CR</b>	conditioned response
<b>GECI</b>	genetically encoded calcium indicator
<b>LFM</b>	light-field microscopy
<b>LFDM</b>	light-field deconvolution microscopy
<b>dpf</b>	days post fertilization
<b>OE</b>	olfactory epithelium
<b>OB</b>	olfactory bulb
<b>Hb</b>	habenula
<b>Tel</b>	telencephalon
<b>Teo</b>	optic tectum
<b>Cb</b>	cerebellum
<b>Md</b>	medulla
<b>GFP</b>	green fluorescent protein
<b>fps</b>	frames per second
<b>IR</b>	infrared
<b>NIR</b>	near-infrared

**DAQ** data acquisition  
**GUI** graphical user interface  
**AA** amino acid  
**ITI** inter-trial interval  
**IS** inter-stimulus interval  
**ICA** Independent Component Analysis  
**rpm** rounds per minute

---

## Bibliography

- [1] Divid A Agard. Optical sectioning microscopy: cellular architecture in three dimensions. *Annual review of biophysics and bioengineering*, 13(1):191–219, 1984.
- [2] Masakazu Agetsuma, Hidenori Aizawa, Tazu Aoki, Ryoko Nakayama, Mikako Takahoko, Midori Goto, Takayuki Sassa, Ryunosuke Amo, Toshiyuki Shiraki, Koichi Kawakami, et al. The habenula is crucial for experience-dependent modification of fear responses in zebrafish. *Nature neuroscience*, 13(11):1354–1356, 2010.
- [3] Misha B Ahrens, Jennifer M Li, Michael B Orger, Drew N Robson, Alexander F Schier, Florian Engert, and Ruben Portugues. Brain-wide neuronal dynamics during motor adaptation in zebrafish. *Nature*, 485(7399):471–477, 2012.
- [4] Misha B Ahrens, Michael B Orger, Drew N Robson, Jennifer M Li, and Philipp J Keller. Whole-brain functional imaging at cellular resolution using light-sheet microscopy. *Nature methods*, 10(5):413–420, 2013.
- [5] Mark Aizenberg and Erin M Schuman. Cerebellar-dependent learning in larval zebrafish. *The Journal of Neuroscience*, 31(24):8708–8712, 2011.
- [6] Jasper Akerboom, Tsai-Wen Chen, Trevor J Wardill, Lin Tian, Jonathan S Marvin, Sevinç Mutlu, Nicole Carreras Calderón, Federico Esposti, Bart G Borghuis, Xiaonan Richard Sun, et al. Optimization of a gcamp calcium indicator for neural activity imaging. *The Journal of Neuroscience*, 32(40):13819–13840, 2012.
- [7] GV Anrep and Ivan Petrovitch Pavlov. *Conditioned reflexes: An investigation of the physiological activity of the cerebral cortex*. 1927.
- [8] Tazu Aoki, Masae Kinoshita, Ryo Aoki, Masakazu Agetsuma, Hidenori Aizawa, Masako Yamazaki, Mikako Takahoko, Ryunosuke Amo, Akiko Arata, Shin-ichi Higashijima, et al. Imaging of neural ensemble for the retrieval of a learned behavioral program. *Neuron*, 78(5):881–894, 2013.

- [9] Kazuhide Asakawa and Koichi Kawakami. Targeted gene expression by the gal4-uas system in zebrafish. *Development, growth & differentiation*, 50(6):391–399, 2008.
- [10] Wikimedia Commons (Azul). A female specimen of a zebrafish (danio rerio) breed with fantails, 2005.
- [11] Herwig Baier and Ethan K Scott. Genetic and optical targeting of neural circuits and behaviorzebrafish in the spotlight. *Current opinion in neurobiology*, 19(5):553–560, 2009.
- [12] Jeroen Bakkers. Zebrafish as a model to study cardiac development and human cardiac disease. *Cardiovascular research*, 91(2):279–288, 2011.
- [13] Isaac H Bianco, Adam R Kampff, and Florian Engert. Prey capture behavior evoked by simple visual stimuli in larval zebrafish. *Frontiers in systems neuroscience*, 5, 2011.
- [14] Joseph Bilotta, Michael L Risner, Erin C Davis, and Steven J Haggblom. Assessing appetitive choice discrimination learning in zebrafish. *Zebrafish*, 2(4):259–268, 2005.
- [15] Martina Blank, Laura D Guerim, Reinaldo F Cordeiro, and Monica RM Vianna. A one-trial inhibitory avoidance task to zebrafish: rapid acquisition of an nmda-dependent long-term memory. *Neurobiology of learning and memory*, 92(4):529–534, 2009.
- [16] Rachel Blaser and Robert Gerlai. Behavioral phenotyping in zebrafish: comparison of three behavioral quantification methods. *Behavior Research Methods*, 38(3):456–469, 2006.
- [17] Rachel E Blaser and Damien Vira. Experiments on learning in zebrafish (danio rerio): A promising model of neurocognitive function. *Neuroscience & Biobehavioral Reviews*, 42:224–231, 2014.
- [18] Oliver R Braubach, Nobuhiko Miyasaka, Tetsuya Koide, Yoshihiro Yoshihara, Roger P Croll, and Alan Fine. Experience-dependent versus experience-independent postembryonic development of distinct groups of zebrafish olfactory glomeruli. *The Journal of Neuroscience*, 33(16):6905–6916, 2013.
- [19] Oliver R Braubach, Heather-Dawn Wood, Simon Gadbois, Alan Fine, and Roger P Croll. Olfactory conditioning in the zebrafish (danio rerio). *Behavioural brain research*, 198(1):190–198, 2009.
- [20] Michael Broxton, Logan Grosenick, Samuel Yang, Noy Cohen, Aaron Andalman, Karl Deisseroth, and Marc Levoy. Wave optics theory and 3-d deconvolution for the light field microscope. *Optics express*, 21(21):25418–25439, 2013.
- [21] Seth A Budick and Donald M O’Malley. Locomotor repertoire of the larval zebrafish: swimming, turning and prey capture. *Journal of Experimental Biology*, 203(17):2565–2579, 2000.
- [22] Harold A Burgess and Michael Granato. Modulation of locomotor activity in larval zebrafish during light adaptation. *Journal of Experimental Biology*, 210(14):2526–2539, 2007.



- [23] Tsai-Wen Chen, Trevor J Wardill, Yi Sun, Stefan R Pulver, Sabine L Renninger, Amy Bao-han, Eric R Schreiter, Rex A Kerr, Michael B Orger, Vivek Jayaraman, et al. Ultrasensitive fluorescent proteins for imaging neuronal activity. *Nature*, 499(7458):295–300, 2013.
- [24] Tristan Darland and John E Dowling. Behavioral screening for cocaine sensitivity in mutagenized zebrafish. *Proceedings of the National Academy of Sciences*, 98(20):11691–11696, 2001.
- [25] Winfried Denk, James H Strickler, Watt W Webb, et al. Two-photon laser scanning fluorescence microscopy. *Science*, 248(4951):73–76, 1990.
- [26] Wikimedia Commons (derivative work: Henry Muehlfordt (talk)). Structure of a fluorescence microscope, 2008. File:FluorescenceFilters 2008-09-28.svg.
- [27] Iain A Drummond. The zebrafish pronephros: a genetic system for studies of kidney development. *Pediatric nephrology*, 14(5):428–435, 2000.
- [28] Florian Engert. Brain-wide imaging reveals lateralized neural dynamics in operant conditioning. Unpublished work.
- [29] Raymond E Engeszer, Da Barbiano, Laura Alberici, Michael J Ryan, and David M Parichy. Timing and plasticity of shoaling behaviour in the zebrafish, danio rerio. *Animal behaviour*, 74(5):1269–1275, 2007.
- [30] Kandice Fero, Tohei Yokogawa, and Harold A Burgess. The behavioral repertoire of larval zebrafish. In *Zebrafish models in neurobehavioral research*, pages 249–291. Springer, 2011.
- [31] Rainer W Friedrich, Gilad A Jacobson, and Peixin Zhu. Circuit neuroscience in zebrafish. *Current Biology*, 20(8):R371–R381, 2010.
- [32] Rainer W Friedrich and Sigrun I Korsching. Combinatorial and chemotopic odorant coding in the zebrafish olfactory bulb visualized by optical imaging. *Neuron*, 18(5):737–752, 1997.
- [33] Ethan Gahtan and Herwig Baier. Of lasers, mutants, and see-through brains: Functional neuroanatomy in zebrafish. *Journal of neurobiology*, 59(1):147–161, 2004.
- [34] David Hall and Milton D Suboski. Visual and olfactory stimuli in learned release of alarm reactions by zebra danio fish (brachydanio rerio). *Neurobiology of learning and memory*, 63(3):229–240, 1995.
- [35] Fritjof Helmchen and Winfried Denk. Deep tissue two-photon microscopy. *Nature methods*, 2(12):932–940, 2005.
- [36] Shin-ichi Higashijima, Mark A Masino, Gail Mandel, and Joseph R Fetcho. Imaging neuronal activity during zebrafish behavior with a genetically encoded calcium indicator. *Journal of Neurophysiology*, 90(6):3986–3997, 2003.

- [37] Michael J Higley and Bernardo L Sabatini. Calcium signaling in dendrites and spines: practical and functional considerations. *Neuron*, 59(6):902–913, 2008.
- [38] Maximilian Hoffmann. Light field deconvolution microscopy for optical recording of neuronal population activity. Master’s thesis, University of Vienna, 2014.
- [39] Allan V Kalueff and Jonathan M Cachat. *Zebrafish neurobehavioral protocols*. Springer, 2011.
- [40] Allan V Kalueff, Michael Gebhardt, Adam Michael Stewart, Jonathan M Cachat, Mallorie Brimmer, Jonathan S Chawla, Cassandra Craddock, Evan J Kyzar, Andrew Roth, Samuel Landsman, et al. Towards a comprehensive catalog of zebrafish behavior 1.0 and beyond. *Zebrafish*, 10(1):70–86, 2013.
- [41] Eric R Kandel, James H Schwartz, Thomas M Jessell, et al. *Principles of neural science*, volume 4. McGraw-Hill New York, 2000.
- [42] Johan Lauwereyns, Katsumi Watanabe, Brian Coe, and Okihide Hikosaka. A neural correlate of response bias in monkey caudate nucleus. *Nature*, 418(6896):413–417, 2002.
- [43] Aletheia Lee, Ajay S Mathuru, Cathleen Teh, Caroline Kibat, Vladimir Korzh, Trevor B Penney, and Suresh Jesuthasan. The habenula prevents helpless behavior in larval zebrafish. *Current biology*, 20(24):2211–2216, 2010.
- [44] Marc Levoy, Ren Ng, Andrew Adams, Matthew Footer, and Mark Horowitz. Light field microscopy. In *ACM Transactions on Graphics (TOG)*, volume 25, pages 924–934. ACM, 2006.
- [45] Jun Li, Julia A Mack, Marcel Souren, Emre Yaksi, Shin-ichi Higashijima, Marina Mione, Joseph R Fetcho, and Rainer W Friedrich. Early development of functional spatial maps in the zebrafish olfactory bulb. *The Journal of neuroscience*, 25(24):5784–5795, 2005.
- [46] University College London. Zebrafish research. <http://www.ucl.ac.uk/zebrafish-group/research/neuroanatomy.php>.
- [47] Richard L Mayden, Kevin L Tang, Kevin W Conway, Jörg Freyhof, Sarah Chamberlain, Miranda Haskins, Leah Schneider, Mitchell Sudkamp, Robert M Wood, Mary Agnew, et al. Phylogenetic relationships of danio within the order cypriniformes: a framework for comparative and evolutionary studies of a model species. *Journal of Experimental Zoology Part B: Molecular and Developmental Evolution*, 308(5):642–654, 2007.
- [48] Eran A Mukamel, Axel Nimmerjahn, and Mark J Schnitzer. Automated analysis of cellular signals from large-scale calcium imaging data. *Neuron*, 63(6):747–760, 2009.
- [49] William Norton and Laure Bally-Cuif. Adult zebrafish as a model organism for behavioural genetics. *BMC neuroscience*, 11(1):90, 2010.

- [50] Donald M O'Malley, Yen-Hong Kao, and Joseph R Fetcho. Imaging the functional organization of zebrafish hindbrain segments during escape behaviors. *Neuron*, 17(6):1145–1155, 1996.
- [51] Michael B Orger, Ethan Gahtan, Akira Muto, Patrick Page-McCaw, Matthew C Smear, and Herwig Baier. Behavioral screening assays in zebrafish. *Essential Zebrafish Methods: Genetics and Genomics: Genetics and Genomics*, page 113, 2009.
- [52] Michael B Orger, Adam R Kampff, Kristen E Severi, Johann H Bollmann, and Florian Engert. Control of visually guided behavior by distinct populations of spinal projection neurons. *Nature neuroscience*, 11(3):327–333, 2008.
- [53] Bradley W Patterson, Aliza O Abraham, Malcolm A MacIver, and David L McLean. Visually guided gradation of prey capture movements in larval zebrafish. *The Journal of experimental biology*, 216(16):3071–3083, 2013.
- [54] Ruben Portugues and Florian Engert. The neural basis of visual behaviors in the larval zebrafish. *Current opinion in neurobiology*, 19(6):644–647, 2009.
- [55] Ruben Portugues, Claudia E Feierstein, Florian Engert, and Michael B Orger. Whole-brain activity maps reveal stereotyped, distributed networks for visuomotor behavior. *Neuron*, 81(6):1328–1343, 2014.
- [56] Gabriele Pradel, Melitta Schachner, and Rupert Schmidt. Inhibition of memory consolidation by antibodies against cell adhesion molecules after active avoidance conditioning in zebrafish. *Journal of neurobiology*, 39(2):197–206, 1999.
- [57] Robert Prevedel, Young-Gyu Yoon, Maximilian Hoffmann, Nikita Pak, Gordon Wetzstein, Saul Kato, Tina Schrödel, Ramesh Raskar, Manuel Zimmer, Edward S Boyden, et al. Simultaneous whole-animal 3d imaging of neuronal activity using light-field microscopy. *Nature methods*, 2014.
- [58] Sabine L Renninger and Michael B Orger. Two-photon imaging of neural population activity in zebrafish. *Methods*, 62(3):255–267, 2013.
- [59] Adam C Roberts, Brent R Bill, and David L Glanzman. Learning and memory in zebrafish larvae. *Frontiers in neural circuits*, 7, 2013.
- [60] Ethan K Scott. The gal4/uas toolbox in zebrafish: new approaches for defining behavioral circuits. *Journal of neurochemistry*, 110(2):441–456, 2009.
- [61] Ethan K Scott, Lindsay Mason, Aristides B Arrenberg, Limor Ziv, Nathan J Gosse, Tong Xiao, Neil C Chi, Kazuhide Asakawa, Koichi Kawakami, and Herwig Baier. Targeting neural circuitry in zebrafish using gal4 enhancer trapping. *Nature methods*, 4(4):323–326, 2007.
- [62] Margarette Sison and Robert Gerlai. Associative learning in zebrafish (*danio rerio*) in the plus maze. *Behavioural brain research*, 207(1):99–104, 2010.

- [63] Burrhus F Skinner. The behavior of organisms: An experimental analysis. 1938.
- [64] Diana Smetters, Ania Majewska, and Rafael Yuste. Detecting action potentials in neuronal populations with calcium imaging. *Methods*, 18(2):215–221, 1999.
- [65] Kenneth R Spring and Michael W Davidson. Introduction to fluorescence microscopy. <http://www.microscopyu.com/articles/fluorescence/fluorescenceintro.html>, 4-December-2014.
- [66] David Sterratt, Bruce Graham, Andrew Gillies, and David Willshaw. *Principles of computational modelling in neuroscience*. Cambridge University Press, 2011.
- [67] Lin Tian, Samuel A Hires, Tianyi Mao, Daniel Huber, Eugenia Chiappe, Sreekanth H Chalasani, Leopoldo Petreanu, Jasper Akerboom, Sean A McKinney, Eric R Schreiter, et al. Imaging neural activity in worms, flies and mice with improved gcamp calcium indicators. *Nature methods*, 6(12):875–881, 2009.
- [68] André Valente, Kuo-Hua Huang, Ruben Portugues, and Florian Engert. Ontogeny of classical and operant learning behaviors in zebrafish. *Learning & Memory*, 19(4):170–177, 2012.
- [69] Wikipedia. Classical conditioning — wikipedia, the free encyclopedia, 2014. [Online; accessed 21-November-2014].
- [70] Wikipedia. Fluorescence microscope — wikipedia, the free encyclopedia, 2014. [Online; accessed 5-December-2014].
- [71] Wikipedia. Learning — wikipedia, the free encyclopedia, 2014. [Online; accessed 6-November-2014].
- [72] Wikipedia. Lernen — wikipedia, die freie enzyklope, 2014. [Online; Stand 19. November 2014].
- [73] Wikipedia. Operant conditioning — wikipedia, the free encyclopedia, 2014. [Online; accessed 21-November-2014].
- [74] Xiaojuan Xu, Theodora Scott-Scheiern, Leah Kempker, and Katie Simons. Active avoidance conditioning in zebrafish (danio rerio). *Neurobiology of learning and memory*, 87(1):72–77, 2007.
- [75] Emre Yaksi, Benjamin Judkewitz, and Rainer W Friedrich. Topological reorganization of odor representations in the olfactory bulb. *PLoS biology*, 5(7):e178, 2007.
- [76] Sarah M Zala and Ilmari Määttänen. Social learning of an associative foraging task in zebrafish. *Naturwissenschaften*, 100(5):469–472, 2013.